Single Droplet Ignition: Theoretical Analyses and Experimental Findings

Suresh K Aggarwal (ska@uic.edu)
Department of Mechanical & Industrial Engineering
University of Illinois at Chicago

Abstract

Spray ignition represents a critical process in numerous propulsion and energy conversion devices. Compared to a gaseous mixture, ignition in a spray is significantly more complex, as the state of ignition in the latter case can be defined by three distinct ignition modes namely, droplet ignition, droplet cluster ignition, and spray ignition. Ignition for an individual droplet represents the appearance of a flame surrounding the droplet or in the wake region, with a dimension on the order of droplet diameter. The cluster or group ignition refers to the ignition around or inside a droplet cloud, while the spray ignition implies the appearance of a global flame with a characteristic dimension few orders of magnitude larger than a droplet. In all three modes, ignition is preceded by the evaporation of fuel droplets, formation of a combustible gaseous fuel-air mixture, and initiation of chemical reactions producing sufficient radical species. The identification of the dominant ignition mode for given two-phase properties represents a problem of significant fundamental and practical importance. Research dealing with laminar and turbulent spray ignition has been reviewed by Aggarwal [1] and Mastorakos [2], respectively, while Annamalai and Ryan [3] have provided a review of droplet group combustion/ignition. In the present review, we discuss experimental, theoretical, and computational research dealing with individual droplet ignition. Topics include the quasi-steady and unsteady models for the ignition of a fuel droplet in a stagnant environment, the droplet ignition in a high-pressure environment, the convective effects on droplet ignition, and multicomponent fuel droplet ignition. Studies dealing with the two-stage and NTC ignition behavior for a droplet are also discussed. Finally, relationship between the droplet ignition mode to droplet cluster and spray ignition modes is briefly described. Potential topics for further research are outlined.

Key words: Droplet ignition, quasi-steady, transient model, two-stage ignition, multicomponent

Nomenclature:

a_F fuel exponent
a_O oxygen exponent
B' preexponential factor in Arrhenius rate expression
c_p specific heat
d_0 initial droplet diameter

E' activation energy
Le Lewis number
M non-dimensional burning rate
p non-dimensional pressure
Q' heat release per unit mass of fuel consumed
r non-dimensional radial coordinate= r'/r'_s
r_s instantaneous droplet radius= r'_s/r'_{so}
R_u universal gas constant
t non-dimensional time
T non-dimensional temperature= c'_pT'/Q'
T_s non-dimensional surface temperature
T'_a activation temperature (^{0}K)
W molecular weight
X mole fraction
Y mass fraction

Greek Letters

λ thermal conductivity
ν Stoiciometric coefficient
ρ density
σ Stoiciometric oxidizer/fuel ratio

Subscripts

f fuel
L liquid phase
o oxidizer
p product
s droplet surface
∞ ambient (at infinity)

Superscripts

′ dimensional variable

1. Introduction

Liquid spray combustion is employed in industrial furnaces, boilers, gas turbines, diesels, spark-ignition, and rocket engines. Ignition represents a crucial event in the operation of these systems. It is followed by the appearance of a flame, which then propagates at the local flame speed into the spray or two-phase mixture or gets stabilized depending upon the mixture conditions. Ignition of a fuel spray in a jet engine combustor is an important process due to the desirability of fast and reliable ignition under a wide range of conditions, and its relation to the

issues of flame stabilization and transient combustion. Similar considerations apply to direct-injection spark ignition engines, in which a fast, well-controlled ignition is important to engine efficiency and emissions. In a diesel engine, the self-ignition of fuel sprays injected into a high-temperature and high-pressure environment represents a critical event in their operation. Spray ignition research is also motivated by the safety considerations in various systems, in which the ignition must be avoided. Examples include explosions in mines and industrial settings, fire safety in earth and space environments, and prevention of autoignition in the mixture delivery system of prevaporized-premixed gas turbine combustors.

Compared to a gaseous mixture, the ignition process in a spray is significantly more complex, as the state of ignition in the latter case can be defined by three distinct ignition modes, namely, droplet ignition, droplet cluster ignition, and spray ignition. In all three modes, ignition is preceded by the evaporation of fuel droplets, formation of a combustible gaseous fuel-air mixture, and initiation of chemical reactions producing sufficient radical species. These processes are determined by the local and global spray properties, which include temperature, pressure, overall and local equivalence ratios, and other gas and dispersed phase properties. The ignition of an individual droplet represents the appearance of a flame surrounding the droplet or in the wake region, with a dimension on the order of droplet diameter. An ignition event for a droplet distinguishes the state of pure vaporization from that of a diffusion flame around the droplet. This has implications for spray combustion with regard to flame stability and amount of pollutants formed. In spray combustion modeling, the identification of this event is important since it determines the amount of heterogeneous burning involved, and the rates of mass and heat transport are significantly altered following its occurrence. A common droplet ignition situation, which has received the most attention, involves the ignition or autoignition of an isolated droplet in a hot, oxidizing environment, although some experimental studies have also employed an electric spark to ignite an individual droplet. The ignition time is defined as the time from the instant a droplet is introduced into the hot environment to the instant a flame is detected in the vicinity of the droplet.

The ignition of a liquid fuel spray, on the other hand, represents the appearance of a global flame that is associated with the whole spray, and has a characteristic dimension few orders of magnitude larger than a droplet. Spray ignition may be initiated by an external source, such as an electric spark ignition in gas turbine combustors and spark-ignition engines, or without any localized ignition source, i.e. spontaneous ignition such as in a diesel engine. The introduction of an electric spark creates a localized region of intense droplet vaporization, high reactivity and heat release. This region, which is commonly referred to as an ignition kernel, involves several evaporating droplets. During the spark duration, the temperature in the ignition kernel increases sharply, but then decreases due to vaporization and heat losses to the

surrounding. As the chemical activity intensifies and the heat-releasing reactions are initiated, the temperature starts increasing again, and the inflection point in the temperature time history is often used to identify the occurrence of ignition. Spontaneous spray ignition involves introduction of a two-phase mixture into a high-pressure, high-temperature, oxidizing environment. The concept of an ignition kernel is generally not employed here though it may be applicable in several autoignition situations. The ignition delay is generally defined as the time interval between the creation of a combustible mixture and the "appearance" of a flame. In a diesel engine, it is defined by the time interval between the start of fuel injection and the appearance of a flame as detected by sharp rise in temperature or OH species concentration. In this case, the ignition location is also an important property that strongly affects flame stabilization [4, 5] and engine combustion and emissions. The ignition of a droplet cloud or cluster [3] represents an intermediate situation, and can be utilized to bridge the results of studies dealing with the other two ignition modes. Here also, a typical physical model involves a group or cloud of droplets in a specified geometric configuration, subjected to a hot, oxidizing environment. Then, depending upon the two-phase conditions, the ignition may occur outside or inside the cloud, and for the latter case, it may involve one or several droplets.

The above three ignition modes are schematically depicted in Fig. 1, which represents the ignition of a liquid fuel spray flowing over a heated wall [1]. Of the three ignition modes shown, the one likely to occur would depend upon the flow conditions, spray properties, liquid fuel loading, and wall temperature etc. Clearly, determination of the dominant ignition mode (and the development of an appropriate criteria for its occurrence) and ignition location in a two-phase mixture is of practical and fundamental importance. The ignition mode can significantly influence the ensuing spray flame structure, as well as the combustor performance, flame stability, and emission characteristics. For example, the issue of dominant spray combustion mode, dealing with whether the spray flame occurs around individual droplet, cluster of droplets or globally in the mixture, may be directly related to the determination of the dominant ignition mode. It also has implications in regards to pollutant formation and flame stability. For example, if the combustion process predominantly involves individual droplet or group burning, it may significantly influence the NOx, CO, and soot emissions. An evidence of this is provided by the experimental study of Rah et al. [6, 7], who observed that the soot and NOx emissions closely correlated with the ignition of fuel droplets and the formation of an enveloped flame around the droplet array. Substantial amount of soot was produced when an envelope flame is formed around the burning droplets. In addition to the three ignition modes, other ignition scenarios are of interest. One such scenario examined by Russo and Gomez [8] involves droplets that survive an envelope spray flame and are ignited. A critical vaporization Damköhler number, representing

the ratio of vaporization time to residence time, was used to define the ignition of these droplets. Their study indicates the possibility of all three ignition modes occurring in a spray.

The literature review reveals that all three ignition modes have been extensively studied. This paper focuses on the droplet ignition mode, since reviews of studies on spray ignition have been reported by Aggarwal [1] and Mastorakos [2], while the research on droplet cluster ignition has been reviewed by Annamalai and Ryan [3]. Ignition of an isolated droplet represents a very fundamental problem involving fluid mechanics, thermodynamics, heat and mass transport, and chemical kinetics. A fundamental study of droplet ignition is also relevant to the combustion of high-density fuels, liquid-propellant combustion, material synthesis, and fire safety.

The fundamental problem considered in this review involves the introduction of an individual droplet into a hot oxidizing environment. Due to heat transfer from the environment, the droplet surface temperature increases, and vaporization commences. The resulting fuel vapor mixes with the oxidizer forming a locally combustible mixture, and the chemical activity involving initially premixed combustion begins. As the chemical activity intensifies, partially premixed and subsequently non-premixed combustion become more prevalent as the oxygen near the droplet surface is consumed, and heat-releasing reactions are initiated. Consequently, the gas temperature in the droplet vicinity starts rising, and a flame may appear in the vicinity of the droplet. A droplet ignition delay is defined by counting the time from the instant a droplet is introduced into an hot gas environment to the instant the ignition is detected a spike in temperature or species (OH) profile, or an envelope flame* is established. The ignition delay consists of a physical delay, during which the droplet is heated and the fuel vapor diffuses outward, and a chemical delay, which is the time required for the reactions to reach a runaway condition. Determination of critical conditions of the ignition in terms of the physical and chemical processes involved is a problem of fundamental interest. So is the determination of droplet ignition delay time and parameters affecting this time. To this end, the ignitability of individual droplets and the conditions (in terms of droplet size, fuel volatility, and ambient properties such as temperature, pressure and oxygen concentrations) determining this ignitability and ignition delay time provide the fundamental information.

While the problem of droplet vaporization and combustion [9, 10] has been examined quite extensively, there are relatively fewer studies on droplet ignition. Theoretical/computational research dealing with droplet ignition can be broadly classified into two groups, namely quasi-steady analysis and transient analysis. A major objective of the quasi-steady analysis is to develop a droplet ignition criterion, based on a critical Damköhler number,

*Note that the "envelope flame" is used here in a generic sense and includes both an envelope flame surrounding a droplet or in its wake.

that can be used to identify the state of ignition for a droplet of given initial size in an environment of known temperature and other properties. Previous investigations on this aspect are discussed in Section 2.1. Experimental results on droplet ignition are summarized in Section 2.2. The transient droplet ignition analysis involves a numerical solution of relevant partial differential equations governing the processes of fluid mechanics, and heat and mass transfer in the liquid phase (droplet interior) and gas phase surrounding the droplet. This topic is reviewed in Section 2.3. Studies dealing with the effect of pressure and fuel properties on droplet ignition are discussed in Sections 2.4 and 2.5, respectively. There has also been some limited experimental and computational work on the effects of natural and forced convection on droplet ignition, which is discussed in Section 2.6. A brief summary of work dealing with droplet group ignition and spray ignition is given in Section 2.7. Concluding remarks are provided in Section 3.

2.1 Quasi-Steady Analysis of Droplet Ignition (QSDI model)

The quasi-steady analysis is based on the consideration that at moderate pressures, the gas density is two to three orders of magnitude smaller than the liquid fuel density. Consequently, the time scale associated with the gas-phase transport is small compared to that for the liquid-phase processes (droplet surface regression), and, therefore, the gas-phase processes can be assumed quasi steady. Clearly, this approach is not applicable if the system pressure is close to or above the critical pressure of the fuel [11]. The quasi-steady analysis is also not valid if the gas flow field is inherently unsteady, for example, due to fluid dynamic or combustion instability, since the analysis requires that the boundary conditions at infinity be constant. Furthermore, the quasi-steady assumption breaks down in regions far from the droplet, since the characteristic transport time becomes comparable to the surface regression time.

The basic assumptions involved in the quasi-steady droplet ignition (QSDI) model are essentially the same as those employed in the derivation of the classical d^2-law relation [9] for droplet vaporization/combustion. The assumptions include spherical symmetry, an isolated single-component fuel droplet, constant gas-phase and liquid-phase thermo-transport properties, unity gas-phase Lewis number, constant droplet surface temperature, and saturation vapor pressure at the droplet surface. One notable difference is the inclusion of finite-rate chemistry based on a global one-step mechanism in the quasi-steady ignition analysis, in contrast to the flame sheet approximation used in the classical gasification model. Some earlier studies employed ad hoc approximations to the Arrhenius term. For example, Tarifa et al. [12] represented the temperature distribution in the flame zone by an algebraic expression, while Peskin et al. [13, 14, 15] used a delta function to represent the heat-release term. The ignition condition was identified by a sudden jump in mass burning rate. Another approach, considered

by Fendell [16] and Kassoy and Williams [17], employed a perturbation technique using the Damköhler number D as a small or a large parameter. This approach can study perturbations in the droplet gasification rate and other properties, but is incapable of providing ignition and extinction conditions.

Linan [18] employed the method of large asymptotic analysis in the limit of large activation temperature to analyze the structure of counterflow diffusion flames. The entire range of Damköhler number was represented by plotting the classical S-shaped curve in terms of the maximum temperature versus D. As the maximum temperature in the flow varied from the ambient value to the adiabatic flame temperature, four regimes were defined on this curve, namely a nearly frozen regime, a partial burning regime, a premixed flame regime, and a diffusion flame regime. Law [19, 20] developed the basic quasi-steady droplet ignition (QSDI) model by extending Linan's approach to analyze the structure of diffusion flames around an evaporating droplet. The finite-rate chemistry was represented by a one-step irreversible reaction:

$$\nu_f F + \nu_o O \xrightarrow{k} \nu_p P \tag{1}$$

and the four combustion regimes were identified, as the flame temperature varied from the ambient value to the adiabatic flame temperature. The first regime, which is the nearly frozen or ignition regime was further analyzed to derive an explicit ignition criterion in terms of a critical Damköhler number for ignition. Mawid and Aggarwal [21] extended Law's analysis to include the effects of arbitrary reaction orders with respect to the fuel and oxidizer. Similar to Law's analysis, the starting point is the governing equations for gas temperature and species mass fractions, which under the quasi-steady, spherically symmetric assumptions can be written in the non-dimensional form as

$$\Omega\{Y_o / \sigma\} = \Omega\{Y_F\} = -\Omega\{T\} = \dot{w} \tag{2}$$

where the operator $\Omega\{\ \}$ and the reaction rate are given as

$$\Omega\left\{\frac{M}{r^2}\frac{d}{dr} - \frac{1}{r^2}\frac{d}{dr}\left(r^2\frac{d}{dr}\right)\right\}\{\ \} \tag{3}$$

$$\dot{w} = -D\frac{Y_o^{a_o} Y_f^{a_f}}{M^2 T^{a_o + a_f}} \exp(-T_a / T) \tag{4}$$

with the Damköhler number D as

$$D = \frac{\nu_f B' \sigma^{a_o} (W_f')^{(1-a_f)}}{\lambda_\infty' / c_{p_\infty}' (W_o')^{a_o}} \left(\frac{p' c_p'}{R' Q'} \right)^{a_o + a_f} (M' r_s')^2 \qquad (5)$$

The boundary conditions for Eqs. (2) are

at r = ∞

$$Y_o = Y_{o_\infty} / \sigma = \alpha \qquad (6)$$

$$Y_f = 0$$

$$T = T_\infty$$

at r = 1.0

$$\frac{dY_o}{dr} = M Y_{os} \qquad (7)$$

$$\frac{dY_f}{dr} = -M(1 - Y_{fs})$$

$$\frac{dT}{dr} = M H$$

$$T = T_s$$

where H (non-dimensional) is the effective latent heat of vaporization which includes the latent heat of vaporization L, and the amount of heat conducted to the droplet interior to heat up the droplet per unit mass of fuel vaporized.

As noted earlier, the above equations differ from those of Law [19] in the exponents of Y_o and Y_f in Eqs. (4-5) which accounts for the nonlinear dependence of the reaction rate on the fuel and oxidizer concentrations. Using the Shvab-Zeldovich formulation [19], the species mass fractions can be expressed in terms of T, which reduces the problem to the solution of the energy equation. The resulting energy equation can be solved numerically to examine the structure of the reaction region and thus determine the ignition/extinction states. The solution can be represented in terms of a plot of the burning rate (M) versus D, which typically yields the classical S curve for large activation energies. A representative plot from Ref. [19] is shown in Fig. 2. For D ~ 0, the flow is chemically frozen, and the solution corresponds to the pure vaporization. As D is increased along the lower branch of the S curve, the chemical activity is initiated. With continuous increase of D, the system approaches the ignition state at $D = D_I$. As D is increased beyond D_I, the system abruptly moves from the lower to the upper branch, which represents droplet combustion states, and D –>∞ corresponds to the flame sheet approximation. Consequently, increasing D above represents the ignition or thermal run away condition, and the

Damköhler number D_I can be defined as the critical ignition Damköhler number. In a similar manner, as we decrease D along the upper branch, the system approaches the extinction state and then D_E represents an extinction Damköhler number.

In order to derive an explicit ignition criterion [19, 21], the energy equation has been solved by using the large activation energy asymptotic analysis. Then, considering $\varepsilon = T_\infty/T_a$ as a small parameter, the flow field can be separated into a frozen region, where diffusion balances convection, and a narrow reaction region where diffusion balances chemical reaction. A representative solution from Ref. [21] is shown in Fig. 3, where the perturbed temperature is plotted in the reaction zone for $\beta = 0.5$ and for different values of the modified Damköhler number Δ. Here Δ, X (the stretched spatial coordinate) and β are, respectively, given by

$$\Delta = \frac{D\,\alpha^{a_o}\,\varepsilon^{-3}\,\varepsilon^{a_f}\exp(-T_a/T_\infty)}{(T_\infty)^{a_o+a_f}} \tag{8}$$

$$X = (1/\varepsilon)(1-\exp(-M/r)) \tag{9}$$

$$\beta = T_\infty - T_s + H \tag{10}$$

The lower bend of the S curve is then generated by plotting θ ($X \to \infty$) as a function of the Damköhler number. These plots for different values of β are given in Fig. 4. The vertical tangents to these curves yield the critical ignition Damköhler numbers. Figure 5 shows the critical Damköhler number plotted as a function of the parameter β for both unity and non-unity ($a_F = 0.25$) exponents of fuel concentration. From this plot, an explicit expression for the critical Damköhler number can be obtained [21] as

$$\Delta_I = 0.9865\exp(6.463\beta + 0.35) \qquad \text{for } \beta \le 0.30 \tag{11}$$

For larger values of β, it was found impractical to approximate a relation between Δ_I and β due to very large values of Δ_I. It was therefore suggested to obtain Δ_I directly from Fig. 5. However, as discussed by Law [20], the range of β relevant for the ignition phenomenon is $0 \le \beta \le 1.0$. Moreover, for most practical combustion systems involving hydrocarbon fuels, β is typically 0.1 or less. Then, an explicit criterion for droplet ignition can be written as

$$\Delta \ge \Delta_I(\beta) \tag{12}$$

where the modified system Damköhler number can be written, after combining Eqs. (5) and (8), as

$$\Delta = \left\{ \frac{B'(W'_f)^{(1-a_f)}}{\lambda'_\infty / c'_{p_\infty} (W'_o)^{a_o}} \left(\frac{p' c'_p}{R'_u Q'} \right)^{a_o + a_f} \right\} \left\{ \frac{(Y_{o\infty})^{a_o} \exp(-T'_a / T'_\infty)(M' r'_s)^2}{\left(\frac{c'_p T'_\infty}{Q'} \right)^{a_o + a_f} \left(\frac{c'_p T'^2_\infty}{T'_a Q'} \right)^{3 - a_f}} \right\} \tag{13}$$

With $a_o = a_F = 1.0$, the above equation yields the system Damköhler number of Law [20]. In spite of its limitations, the QSDI model can be extremely useful in distinguishing between evaporating and combusting droplets in a spray environment. In fact, the criterion has been employed in several investigations dealing with spray flames; for example, see Buchholtz and Tapper [22], and Seth et al. [23]. Furthermore, it has been used and subsequently modified by several researchers to predict the ignition delay time for a droplet that is suddenly introduced into a hot, oxidizing environment. The basic procedure followed by these researchers to predict the ignition delay time is as follows. A droplet is introduced into a hot oxidizing environment at time t=0. As it receives heat from the gas phase, its surface temperature starts increasing, and vaporization is initiated. The droplet surface temperature (T_s) is calculated by using an appropriate liquid-phase model, such as infinite-conductivity or conduction-limit models [24], while the instantaneous droplet radius r'_s is obtained from

$$\frac{d r'^2_s}{dt'} = -2 \frac{\rho'_\infty D'_\infty}{\rho'_L} M \tag{14}$$

The temporal history of relevant droplet properties such as r'_s, T'_s etc. is then followed, and the system and ignition Damköhler numbers are calculated at each instant to check the ignition criterion given by Eq. 12. The instant when the ignition criterion is satisfied is defined as the droplet ignition delay time. Some representative results from Ref. [21], obtained by using the above equations for the ignition of n-hexadecane droplets, are shown in Figs. 6-7. The chemical kinetic parameters, E' = 45.0 kcal/mole and B' = 1.9 x 10^9 cm^3/mole-sec, were extracted from the ignition data of Faeth and Olson [25] for $Y_{o\infty} = 0.23$, $a_o = 1.5$ and $a_F = 0.25$. The parameters T_s and H were calculated by using the conduction-limit model [24].

Figure 6 compares the predicted ignition delay time with the experimental data of Faeth and Olson [25] and Saitoh et al. [26] as a function of initial drop size. As expected, the predictions agree quite well with the measurements of Faeth and Olson, since the kinetics constants were obtained from their experimental data. There is also satisfactory agreement between the predicted ignition lags and the measured data of Saitoh et al., although minor differences in the initial conditions, T'_∞ and T'_{so}, of the present calculations and their experiments exist. In addition, the predicted ignition delay plot indicates that near the ignitable

limit (d_o = 0.7 mm), there exists an optimum droplet size corresponding to a minimum ignition delay time. For droplet sizes smaller than this optimum, the ignition delay increases as the drop size is decreased, approaching the ignitable limit. This is probably due to the decrease in the system Damkohler number near the ignition limit, since the ignition criterion indicates that ignition is favored for larger droplets. However, for droplet sizes larger than the optimum, the ignition delay increases as the droplet size is increased. This is caused by the increase in droplet heat-up time, an evidence of which is provided by several experimental and theoretical studies as discussed later. It is also important to note that the existence of an optimum droplet size corresponding to a minimum ignition delay, and the behavior near the ignition limit indicated in Fig. 6, have been observed in experimental studies as well as in numerical studies based on transient models. These are discussed in later sections in this review.

Figure 7 shows the computed and measured ignition delay times plotted versus the ambient temperature for two different droplet sizes. Again, it is indicated that smaller droplets are ignited earlier than the larger ones in the droplet-heating-controlled regime, whereas in the kinetically-controlled (lower ambient temperature) regime, they may fail to ignite as the ambient temperature is decreased. The minimum ambient temperature for ignition is seen to be a function of the droplet size. It decreases as the droplet size is increased. For the results shown in Fig. 7, the minimum temperature values are 1005 K and 900 K for r'_{so} = 0.0208 and 0.078 cm respectively. It should also be noted that a_F affects both the system (Δ) and the ignition Damköhler numbers (Δ_I), while a_o has only a weak influence on Δ_I. This can be expected since ignition occurs in the oxidizer-rich region and the oxidizer concentration in the inner reaction region is typically much greater than the stoichiometric value. This also implies that for droplet ignition in an oxidizer-lean environment, the effect of a_o on Δ_I would be stronger.

Several studies have employed the quasi-steady droplet ignition (QSDI) model to examine the effects of various parameters on droplet ignition. In some investigations, the model was further modified to extend its applicability and examine the effects of various assumptions employed in the original analysis. In some cases, expressions for the modified system Damköhler number (Δ) and ignition Damköhler number (Δ_I) were modified based on the relaxation of some assumptions. Aggarwal [27] employed the ignition criterion of Law [20] to examine the role of transient droplet heating in the ignition process. The effect of three different liquid-phase heating models, namely, infinite-conductivity, conduction-limit, and vortex models, on the droplet ignition delay was examined. Results indicated that for less volatile fuels, the droplet heating time is comparable to the ignition delay time. Consequently, for such fuels, the transient droplet heating has noticeable influence on ignition delay, especially in the vaporization-controlled (higher ambient temperature) regime. Since the conduction-limit model predicts a higher surface temperature during the droplet heating period, it yields a shorter

ignition delay compared to that predicted by the infinite-conductivity model. This effect has also been examined by Sazhin et al. [28] for n-dodecane droplets. They observed that using the effective conductivity model yielded lower ignition delays compared to those predicted using the infinite conductivity model. Note that a higher surface temperature reduces the ignition Damköhler number. Using the conduction-limit model, the ignition limits in terms of the minimum ambient temperature and the minimum droplet size were also computed and compared with the experimental results of Faeth and Olson [25], and Wood and Rosser [29]. As indicated in Fig. 8, the computed ignition limits are in good agreement with measurements. Another important observation from this figure is that the minimum droplet size for ignition increases as the ambient temperature is reduced, which is consistent with the results discussed earlier. The computed results also indicate that the effect of pressure is to extend the ignitability limits. Both the minimum ambient temperature and the minimum droplet size for ignition decrease as pressure is increased. This result is confirmed by experimental studies discussed in the next section.

Law and Chung [30] extended the QSDI model to include the presence of fuel vapor in the ambient gas. The objective was to improve the applicability of the classical ignition criterion to more realistic sprays, wherein the gas phase (droplet ambiance) is expected to contain fuel vapor. Important modifications to the QSDI model included changing the ambient boundary condition for the fuel vapor mass fraction, and moving the location of the ambient boundary from infinity to finite distance, see Eq. 6. A representative result showing the plot of Δ_I versus β for various values of the parameter γ ($=Y_{f\infty} / \varepsilon$) is presented in Fig. 9. As expected, the presence of fuel vapor reduces the ignition Damköhler number, implying enhanced droplet ignitability. The presence of fuel vapor also reduces the vaporization rate and thus affect ignitability. However, the chemical effect of fuel vapor is more dominant in most situations.

Another key assumption in the QSDI model is that of constant thermo-transport properties and unity Lewis number. Li and Renksizbulut [31] extended the QSDI model to include the effects of variable properties and arbitrary Lewis numbers. The thermo-transport properties were considered to be temperature- and concentration-dependent, and the system (reduced) and ignition Damköhler numbers were rederived using the matched asymptotic technique. It was observed that the effects of variable properties on ignition appear through the vaporization rate M' which modifies the reduced Damköhler number (Δ), and through β which influences the ignition Damköhler number (Δ_I). It was recommended that the mixture Lewis number should be defined as

$$Le = \Sigma \sum_i Le_{f,i} X_i \qquad (15)$$

Here $Le_{f,i}$ is the Lewis number of fuel vapor with respect to species i in the environment, and X_i is the mole fraction of that species. An increase in this Lewis number would enhance droplet ignitability (reduce the ignition delay time) because of the enhanced rate of heat transport to the droplet. It was also observed that the appropriate specific heat (c_p) should be that of fuel vapor rather than that of inert species in the environment. Further, the variable specific heat (c_p) would increase β and thus increase Δ_I because of its exponential dependence on β. This implies that the variable c_p would increase the ignition delay time. Li [32] further extended the above analysis to study droplet ignition in fuel-lean, oxidizer-lean, and fuel/oxidizer-lean environments. For each case, the ignition Damköhler number was obtained as a function of the parameter β. In addition, Makino [33] obtained more general correlations between the ignition Damköhler number (Δ_I) and the parameter β, Δ_I (β). This further extends the applicability of the QSDI model.

In summary, the QSDI model was first developed by Law [19, 20], based on the analysis of Linan [18]. Subsequently several investigators modified it to extend its applicability. The extensions include the general (non-unity) reaction orders with respect to fuel and oxidizer [21], transient droplet heating [27], presence of fuel vapor in the gas phase [30], and variable thermo-transport properties and non-unity Lewis numbers [31, 32]. The QSDI model is quite useful in spray computations for distinguishing the state of pure vaporization from that of combustion. In two-phase computations employing either the Eulerian or Lagrangian approach for the liquid phase, the quasi-steady droplet ignition criterion can be applied in a continuous manner, and the rates of interphase heat and mass transfer modified accordingly. The QSDI model has also been employed to predict the ignition delay time of an individual droplet, which is suddenly introduced into a hot, oxidizing droplet. By coupling the quasi-steady gas-phase analysis with the unsteady liquid-phase analysis, Law [20], Aggarwal and Mawid [21], Aggarwal [27], and Sangiovanni and Kestin [34] examined the effects of important parameters on the droplet ignition delay time. In addition, the model has been used to determine a critical droplet diameter (as a function of other parameters) below which droplets fail to ignite and undergo complete vaporization without combustion. Important limitations of the QSDI model should also be noted. Its applicability is limited to the ignition of an isolated droplet* under moderate-pressure, mildly convective conditions. Also, it cannot provide details of the ignition process, which can be obtained by using a transient analysis. For example, the transient model can analyze the detailed transition from premixed combustion to diffusion combustion, as well as the ignition location with respect to the droplet, although it requires a numerical solution of coupled, nonlinear partial

* A group of droplets may be deemed as one large droplet and then the above criterion may be used to predict the ignition delay time. This situation is akin to external group combustion.

differential equations. In addition, as discussed in later sections, the transient model can also be used to examine the effects of detailed chemical kinetics, multicomponent species diffusion, and high pressure (critical and supercritical) on the droplet ignition phenomena. It can also be employed to examine the validity and applicability of the QSDI model. This aspect is discussed in Section 2.3.

2.2 Experimental Studies on Droplet Ignition

Several researchers have reported experimental data on droplet ignition under various conditions. In addition to ignition delays, they have provided data on ignition limits in terms of minimum droplet size and ambient temperature, different ignition regimes in terms of ambient temperature and pressure, and the effects of various parameters including gravity, pressure, and fuel volatility. Two commonly employed configurations are the suspended droplet technique and the freely falling or moving droplet technique. In the first configuration, a fiber-suspended droplet is exposed to a hot, stagnant environment in a preheated furnace, and the ignition delay time is measured, based on an appropriate ignition criterion, by using an optical technique. This approach has been used by Nishiwaki [35], El-Wakil and Abdou [36], Faeth and Olson [25], Kadota et al. [37], Saitoh et al. [26], Bergeron and Hallett [38, 39], Tanabe et al. [40, 41], Marchese et al. [42, 43], and many others. The second configuration involves a freely falling droplet in a furnace or a droplet injected into a heated stream. It has been employed by Rah et al. [6], Wood and Rosser [29], Sangiovanni and Kesten [34], Satcunanathan [44] and others. Goodger and Eissa [45] reported a review of experimental studies reported prior to 1987.

El-Wakil and Abdou [36] measured ignition delay times for pure alkane droplets suspended on a filament in a furnace. Saitoh et al. [26] also used this technique for the ignition of n-heptane and n-hexadecane droplets. Their objective was also to validate the results of their numerical simulations [49]. The droplet diameter was measured photographically, and the instant of ignition was detected by a change in the intensity of infrared rays. Ignition delay times were reported for d_0 = 0.7-2.2 mm, T_a= 650-800 ˚C, and initial droplet temperature=5-35 ˚C. Representative results from this study for n-heptane and n-hexadecane are shown in Figs. 10 and 11, respectively. The ignition delay for n-heptane droplets appears to be nearly independent of initial droplet size, except near the ignition limit, where the ignition delay increases as d_0 is decreased, and eventually reaches a non-ignitable condition. In addition, the minimum droplet size for ignition increases as T_a is increased. For n-hexadecane droplets, the ignition delay exhibits stronger sensitivity to the initial size; it increases as d_0 is increased, which can be attributed to the increase in droplet heating time for larger droplets. For both fuels, the data indicate a decrease in ignition delays as T_a is increased. An important implication from the

results in Figs. 10-11 is that droplet heating is more important for larger droplets and for less volatile fuels, since heat-up time occupies a significant part of total ignition time.

Bergeron and Hallett [38] conducted a numerical-experimental investigation on droplet ignition for four n-alkanes. Simulations were based on a transient spherical-symmetric model using global one-step chemistry with non-unity reaction orders with respect to fuel and oxygen concentrations. The gas-phase model was further simplified by including the reaction terms only in the energy equation, and the droplet temperature was calculated by using the infinite-conductivity model. Note that studies employing transient models of various complexities are reviewed in Section 2.3. The experimental investigation employed a fiber-suspended droplet in a heated furnace. The fiber was 0.2 mm in diameter with a 0.6 mm bead at the tip. The droplet diameter was measured photographically, and the ignition event was detected by photodiodes. Ignition delays were measured for d_0 = 1.2-1.6 mm and T_a= 900-1100 K. Some representative results are provided in Figs. 12-13. Results are generally similar to those reported by Saitoh et al. [26] in that the ignition delay increases with the increase in d_0, and with the decrease in T_a or fuel volatility. Simulations show good agreement with measured data, as the kinetic constants were obtained by matching predictions with experiments. Further, the numerical results indicate a minimum droplet diameter below which droplets vaporize without ignition. In addition, the minimum diameter decreases as T_a is increased, which is consistent with several results discussed earlier. The existence of a minimum diameter for ignition and its dependence on the ambient temperature have been observed in previous theoretical studies based on quasi-steady models of Faeth and Olson [25], Law [20], and Mawid and Aggarwal [21], as well as in the experimental studies of Saitoh et al. [26] and Wood and Rosser [29].

Sangiovanni and Kesten [34] employed the moving droplet configuration to determine the influence of ambient temperature, oxygen content, droplet relative velocity, droplet size, and fuel type on the ignition of single fuel droplets. A monosized stream of liquid fuel droplets was injected in a hot environment provided by the post-combustion zone of lean, premixed, laminar methane-air flame on a flat flame burner. High-speed photography was used to record the time history of droplets as they enter the hot region. The ignition delay time was obtained from the ignition delay height, measured from the photographs, and the average droplet velocity. They also employed a numerical model based on the quasi-steady, gas-phase equations for the heat and mass transport in the gas film surrounding a droplet. The effect of droplet relative velocity was included by using the standard Ranz and Marshall correlation [46]. As expected, the results indicated a pronounced effect of ambient temperature, with the ignition delay time decreasing with increasing temperature in the kinetically-controlled (low ambient temperatures) regime, but a relatively weak effect in the diffusion-controlled regime. However, contrary to expectations, the effects of droplet size and fuel type were found to be more significant in the kinetically-

controlled regime. The presence of droplet relative velocity decreased the ignition delay time slightly, while the oxygen concentration (above a certain) had negligible effect. The theoretical results, however, indicated a decrease in ignition delay with decreasing oxygen concentration, which appears to be a counter-intuitive result.

Another notable study using the suspended droplet technique was reported by Tanabe et al. [40]. A distinguishing feature of this study was the investigation of two-stage ignition[1] process for a droplet by simultaneously using a fine thermocouple to measure the temperature as a function of time, and an interferometer to detect the cool (invisible) and hot flame ignition. A n-dodecane droplet of 0.7 mm diameter was suspended in a hot environment, where T_a was varied from 500 to 800 K, and pressure from 1 to 10 atm. The droplet diameter was measured using a CCD camera. Experiments were carried out under normal-gravity (1g) and microgravity conditions. Microgravity (μg) experiments were performed in the 5- and 110-m drop towers and the parabolic flights. The investigation focused on two important aspects, namely the two-stage ignition process and the effect of gravity. More details including the chemical kinetic aspects of two-stage ignition are discussed in the next section. In general, the phenomenon is characterized by the low-temperature (cool flame) oxidation at temperatures of about 500-800 K, followed by the high-temperature oxidation. The two stages are distinguished by different chain branching steps. While this phenomenon has been extensively examined for homogeneous mixtures, it was observed perhaps for the first time in the context of droplet ignition. Figure 14 from Ref. [47] illustrates the two-stage ignition process by plotting the peak temperature history in the droplet vicinity. The first temperature jump marks the onset of first-stage ignition, while the second jump represents the occurrence of second-stage ignition. The first–stage ignition or induction period involves the droplet heat-up, slow vaporization, and low-temperature oxidation, while the second period involves faster vaporization and high-temperature ignition chemistry. Increasing the ambient pressure or temperature decreases the transition period from the first to second stage, or the second induction period τ_2. This is illustrated in Fig. 15 from Ref. [40], which shows the different droplet ignition regions at 1g. In the cool flame region, characterized by low ambient temperatures and pressures (1-2 atm), only the first-stage ignition occurs; the second-stage ignition does not follow, implying that the droplet undergoes extinction or vaporizes completely prior to the occurrence of second-stage ignition. At higher pressures, the two-stage ignition is observed, and the transition from the first stage to second becomes increasingly short as pressure is increased further. The effect of gravity is shown in Fig. 16, which plots the total ignition delay as a function of ambient gas temperature for 1g and μg conditions. The presence of gravity increases both the induction periods, and thus the total

[1]The chemical kinetic aspects of the two-stage ignition phenomenon are discussed in a later section.

ignition delay time by a factor of up to 3. The buoyancy-induced flow enhances the rates of heat and mass transport, which reduce the droplet heat-up time and increase the vaporization rate, but decreases the temperature rise due to chemical reaction as it removes heat and chemical intermediates from the ignition zone. The latter effect is found to be more dominant, especially when the ambient temperature is low (kinetically-controlled regime). This effectively reduces the system Damköhler number, and increases the ignition delay at 1g. As also indicated in Fig. 16, the minimum ambient temperature for ignition was found to be lower at μg compared to that at 1g. Moreover, the effect of gravity on droplet ignitability seems to be more significant at lower ambient temperatures.

2.3 Transient Droplet Ignition Analysis

Processes associated with transient droplet ignition have been extensively investigated both computationally and experimentally. The basic computational model considers a fuel droplet that is suddenly introduced into a hot, oxidizing environment. Many of the underlying assumptions in the model are essentially the same as those used in the quasi-steady analysis. These include spherical symmetry, phase equilibrium at the interphase, transient liquid-phase heating, etc. The major difference is the retention of the transient term in the gas-phase governing equations, which requires the solution of strongly-coupled, nonlinear partial differential equations with a moving interphase. However, this allows the consideration of many important effects, including the use of detailed chemistry models, and high-pressure and multicomponent effects. It also facilitates the analysis of ignition location, the role of radical species, and the low- and high-temperature chemistry effects including the negative temperature coefficient (NTC) and zero temperature coefficient (ZTC) regions [48]. Here NTC refers to the range of temperature in which the ignition delay increases as the ambient temperature is increased, while ZTC implies the ignition delay becoming independent of the ambient temperature. Earlier studies of transient droplet ignition employed a global one-step reaction mechanism [49, 50, 51, 52, 53]. These are discussed in Section 3.1. Studies during the last two decades have used increasingly complex multi-step chemistry models, including the reduced, skeletal and detailed mechanisms. These are reviewed in Section 3.2

2.3.1 Transient Droplet Ignition Analysis with a Global One-Step Chemistry Model

Niioka et al. [49] employed a transient model for the ignition of n-heptane fuel droplets. The transient liquid-phase heating was included by using the conduction-limit model. The ignition time was determined by using a thermal ignition criterion, based on the appearance of an inflection point in the radial gas temperature profile. A representative plot showing the temporal history of the radial temperature profile, starting from the initially prescribed condition to the

state of ignition and beyond, is illustrated in Fig. 17. As the droplet is introduced into a hot, oxidizing environment, it is heated up and the vaporization is initiated, while the surrounding gas is cooled down. The ignition occurs at non-dimensional time, $t^+ = 11.5$, when the gas temperature exceeds the ambient temperature, followed by a thermal runaway characterized by a rapid rise in gas temperature. The numerical results indicated that the ignition delay time decreases as the ambient temperature, oxygen concentration, and initial droplet temperature are increased, and as the droplet initial diameter is decreased. These results are generally in concert with those from experimental and theoretical studies. The simulations also predicted ignition limits in terms of the minimum droplet diameter and the ambient temperature. Rah et al. [6] used a similar approach to study the ignition of a n-dodecane fuel droplet. However, the numerical model was considerably simplified by specifying the gasification rate using a known value of the evaporation rate constant. The droplet temperature was computed by using a rapid-mixing or infinite-conduction model. The ignition criterion was based on the appearance of an inflection point in the radial gas temperature profile. The numerical results focused on the effects of ambient temperature, oxygen concentration, and initial droplet temperature. The predicted ignition delay times were shown to be in agreement with the experimental values, obtained by injecting a stream of droplets in a burner-stabilized flame and measuring the ignition delay time from successive photographs.

Shaygan and Prakash [50] also employed a transient, spherically-symmetric numerical model to examine the ignition characteristics of a single-component fuel droplet. The transient liquid-phase heating was included by using the conduction-limit model, the thermo-transport properties were assumed to be constant, and the chemistry was represented by a global one-step mechanism. The numerical results focused on both the global behavior (ignition delay time) and the details of the ignition process. A representative result for n-heptane droplet showing the evolution of gas temperature profile prior to and at the instant of ignition is illustrated in Fig. 18. Here, the gas temperature is normalized by using the ambient temperature, the radial location by the instantaneous droplet location, and the time by the gas-phase conduction time ($c_p \rho_\infty r_{so}^2 / \lambda_g$). The curve 'label 3' corresponds to the instant of ignition, and indicates an ignition location at about 5 times the instantaneous droplet location. The ignition criterion was based on the appearance of an inflection point in the radial gas temperature profile, which occurred at a non-dimensional time t' = 14. Following ignition, the non-dimensional flame location was observed to move away from the droplet surface. In addition, it was observed that the premixed burning is important during the preignition process, and the liquid-phase transient persists throughout the ignition process, as the droplet surface remains well below the wet-bulb temperature at the instant of ignition. Consequently, it was concluded that ignition is governed by processes, such

as liquid-phase heating, phase equilibrium, and gas-phase transport, which determine the availability of fuel vapor in the droplet vicinity. Results for n-hexadecane droplets were qualitatively similar to those for n-heptane droplets, except that the ignition location was closer to the droplet surface for less volatile fuel.

Another notable study based on a one-step reaction mechanism was reported by Wong et al. [51], who examined the validity of the QSDI model by comparing its predictions with those obtained from a transient ignition model for a wide range of parameters, including the ambient temperature, fuel volatility, droplet diameter, and initial droplet temperature. The QSDI model followed the analysis of Mawid and Aggarwal [21], while the transient model employed the transient, spherically-symmetric model of Niioka et al. [49]. Thus, the thermo-transport properties and chemical kinetics parameters in the two models were identical. Note that the QSDI model ignores the fuel vapor diffusion process, since the quasi-steady distribution of gas temperature and fuel vapor mass fraction are instantaneously specified for given ambient and droplet surface conditions. Consequently, the QSDI model is expected to underpredict the ignition delay time compared to the transient model, with the difference increasing as the droplet size is decreased or the fuel volatility is increased, since both reduce the droplet heat-up or vaporization time compared to the fuel vapor diffusion time. Some representative results from the cited work showing the above behavior are given in Figs. 19-21. QSGP in these figures refers to the quasi-steady gas phase, or results for the QSDI model. In Fig. 19, the ignition delays predicted using the QSDI and transient models are plotted versus the initial droplet temperature. As hypothesized above, the QSDI model underpredicts the ignition delay time, and differences between the two models become significant for more volatile fuels (n-heptane) and higher initial droplet temperature, since both increase the fuel vapor concentration at the surface, while higher droplet temperature also reduces the droplet heat-up and vaporization time. A similar behavior is observed in Figs. 20-21, which plot the ignition delay time as a function of ambient temperature and initial droplet diameter, respectively, for the two models. Again, differences between the predictions of the two models become significant at high ambient temperatures and small droplet diameters. Another observation from Figs. 19-21 pertains to the effect of using different ignition criteria on the ignition delay prediction. One criterion is based on gas temperature exceeding the ambient temperature in the radial temperature profile, while the other is based on the appearance of an inflection point in the temporal variation of the maximum temperature. As indicated, the first criterion consistently predicts a shorter ignition delay. Wong et al. [51] also compared the ignition limits predicted by the two models in terms of the minimum droplet diameter for ignition versus the ambient temperature. Again, the QSDI model predicted a smaller minimum diameter for ignition compared to the transient model. Figure 22 presents a comparison of the predicted ignition delays with the experimental data of Faeth and Olson [25] and Takei et al.

[54]. The kinetic parameters in the models were adjusted to match with the experimental data of Faeth and Olson [25]. While both models provide 'satisfactory' results, the predictions of the transient model agree with the experimental data over a wider droplet diameter range.

In a related study, Wang et al. [52] examined the applicability of the modified quasi-steady ignition criterion of Law and Chung [30] for droplet ignition in the spray interior. As noted earlier, Law and Chung modified the original QSDI model to account for the finite gas-phase domain and the presence of fuel vapor in the environment. Wang et al. [52] compared the results obtained using the modified ignition criterion with those from a transient numerical model that simulated droplet ignition in a uniform droplet cloud. In both models, the transient liquid-phase heating was represented by the conduction-limit model. A representative result in terms of the ignition delay versus the non-dimensional inter-droplet spacing is shown in Fig. 23. For the modified QSDI model, the ignition delay (t_{ig}) decreases very sharply to a zero value as the droplet spacing is increased. This seemingly physically unrealistic result implies that for these conditions, the droplet would ignite instantaneously for $s/d_o > 12$. In addition, for $s/d_o < 6$, a state of no-ignition is predicted, apparently caused by the excessive fuel vapor accumulation at this droplet spacing. In more realistic situations, the ignition location will shift to a radial distance greater than s/do = 6. For the transient ignition model, the ignition delay decreases sharply as s/d_o increases, and eventually becomes independent of s/d_o, which is indicative of a non-dilute spray limit at $s/d_o = 18$. Further, as s/d_o is decreased from 18 to 13, the ignition delay time increases sharply until a state of no-ignition is reached at $s/d_o = 13$. This may be attributed to evaporative cooling in the inter-droplet space. In Fig. 24, the droplet ignitability is represented in terms of the minimum ambient temperature for ignition and the non-dimensional inter-droplet spacing. The modified QSDI model predicts a significantly lower minimum ignition temperature, or significantly wider ignition limits compared to the transient model. As discussed earlier, this may be due to the artificially imposed quasi-steady fuel vapor distribution, and partly due to the ignition criterion employed in the QSDI model. In summary, the modified QSDI model of Law and Chung underestimates the ignition delays and the minimum ignitable ambient temperature compared to the transient, non-dilute droplet ignition model.

2.3.2 Transient Droplet Ignition Analysis with Multi-Step Chemistry Models

Research on this topic has generally followed the development of increasingly more detailed chemical kinetic models, which have been validated using various targets for homogeneous mixtures. Much of this research has considered n-heptane droplets, although some studies have examined other fuels, including higher alkanes, bi-component fuels, and biodiesel surrogates. A major part of this work has focused on the role of low-temperature and high-temperature chemistries, including the NTC and ZTC regimes, during the transient ignition

process. Aspects dealing with high-pressure, multi-component and other effects have also been examined, and discussed in Sections 2.4 and 2.5. There have also been studies on the effect of NTC chemistry on the ignition of gaseous fuels (prevaporized n-heptane, iso-octane, jet fuels, etc.) in nonpremixed counterflow [55, 56]. A majority of work has focused on providing the critical or minimum oxidizer temperature for ignition at different strain rates. This work is not reviewed in this paper, although there are some similarities between the gaseous nonpremixed ignition and the droplet ignition.

Tanabe et al. [57] reported a computational and experimental investigation of transient droplet ignition with the objective of characterizing the various ignition regimes. Using a 12-step reduced mechanism, they were able to identify the two-stage ignition process, which has previously been well documented for homogeneous fuel-air mixtures at intermediate temperatures (≈700-900K) and moderate to high pressures (p≥10 atm). For such conditions, the two-stage ignition process is related to the temperature dependent chemistry effects. It is characterized by the appearance of cool flame, followed by reduced chemical activity for a finite time, and then by a hot flame or thermal runaway. Figure 25 illustrates this process for homogenous n-dodecane/air mixtures at p=20 atm, equivalence ratio ϕ=1.0, and three different initial temperatures. The homogenous reactor model in CHEMKIN software was used to simulate ignition under constant pressure, adiabatic conditions. The two-stage ignition is well illustrated by the OH mole fraction and temperature profiles for the intermediate temperature (T=830 K) case. The first stage ignition or cool flame is indicated by a spike in OH or temperature profile at non-dimensional time ≈ 0.4.

Tanabe et al. [57], reported extensive ignition data and characterized the two-stage ignition process for n-heptane, n-dodecane, and iso-octane droplets. Both 1g and μg experiments were performed using the suspended droplet technique, and ignition delays and temperature field were measured using interferometer images. Representative results from this study for the ignition of n-heptane droplets are presented in Fig. 26. The top figure plots the measured total ignition delay or induction time at 1g as a function of ambient temperature for different pressures. The total ignition delay corresponds to the thermal runaway condition and includes the first ignition delay corresponding to the appearance of a cool flame. For p=5 and 10 atm, results indicate the existence of a ZTC region, in which the total ignition delay is nearly independent of ambient temperature. Based on the experimental data, they developed a qualitative diagram illustrating the various ignition regimes in terms of a temperature-pressure plot. As shown in Fig. 26b, the regimes include no-ignition, single-stage ignition, two-stage ignition, cool flame, etc. Clearly, compared to the homogeneous mixture case, the diagram becomes more complex for

droplet ignition due to the presence of non-uniform temperature and species fields. Moreover, the existence and extent of various regimes are determined by the fuel and droplet properties.

The two-stage ignition phenomenon including the NTC behavior has been extensively studied for homogeneous premixed fuel-air mixtures [58]. While the phenomenon becomes significantly more complex in the case of droplet ignition, the ignition process still involves a premixed fuel-air mixture with spatially and temporally varying equivalence ratio. Therefore, it is strongly influenced by the low- and high-temperature chemistry effects [48, 59]. As discussed by Cuoci et al. [48] and others, at moderately high pressures ($p \geq 10$ atm), the decomposition of alkanes follows two different paths, and the transition between the low- and high-temperature paths is determined by reaction (R1):

$$R + O_2 \iff ROO \qquad \text{(R1)}$$

The formation of alkyl radical (R) is initiated by fuel decomposition via H-atom abstraction by HO_2, OH and O_2, depending upon temperature and fuel-air ratio. Below 900 K, the addition of O_2 to alkyl radical (R) is favored. The resulting alkyl-peroxy radical (ROO) isomerizes (reaction R2) to produce alkyl-hydroperoxy radical (QOOH), which then forms peroxy alkyl-hydroperoxy radical (OOQOOH) through reaction R3. Subsequently OOQOOH undergoes decomposition and internal isomerization to produce ketohydroperoxides (OQOOH) and OH radicals via reaction R4. OQOOH readily decomposes to form OH, alkenes and other radicals through R5

$$ROO \iff QOOH \quad \text{(isomerization)} \qquad \text{(R2)}$$

$$QOOH + O_2 \iff OOQOOH \qquad \text{(R3)}$$

$$OOQOOH \iff OQOOH + OH \qquad \text{(R4)}$$

$$OQOOH \iff OH + \text{products} \qquad \text{(R5)}$$

OH then reacts with fuel to form more alkyl radicals that feed the above chain. In the NTC region (i.e., temperatures between 700-900 K), however, this path becomes less important, while reactions R6 and R7 become more significant. Through R6, QOOH decomposes to form HO_2, while additional HO_2 is formed via R7.

$$QOOH \iff HO_2 + \text{conjugate alkene} \qquad \text{(R6)}$$

$$R + O_2 \iff HO_2 + \text{conjugate alkenes} \qquad \text{(R7)}$$

This results in the increased formation of HO_2 relative to OH, and, consequently, the ignition delay time decreases with increase in temperature in the NTC region. In summary, the path represented by reactions R2-R5 is favored at low temperatures ($T<700$ K), and responsible

for the first-stage (or cool flame) ignition for droplets, while the path represented by reactions R6-R7 becomes more significant in the NTC region, and slows down the ignition process. At higher temperatures (T>900 K), the alkyl radicals directly decompose to alkenes and smaller alkyl radicals through β-scission reactions, and the ignition process follows the high-temperature chemistry path. As mentioned earlier, compared to homogeneous systems, droplet ignition is significantly more complex due to the processes of liquid-phase transport in the droplet interior, droplet heating, gas-phase heat and mass transport, and vaporization. Coupling of these processes with the low- and high-temperature chemistry leads to different ignition regimes for a droplet. Several studies have examined these regimes by using a transient, spherically symmetric model with reduced and detailed mechanisms.

As mentioned earlier, Tanabe et al. [57] employed experimental data and a 12-step reduced mechanism to characterize the various ignition regimes and the effects of different parameters on these regimes. Schnaubelt et al. [47] reported an experimental and computational investigation on the ignition of n-heptane droplets. They employed a 62-step mechanism and compared their predictions with μg experiments at 5 atm. Various ignition regimes with respect to initial ambient temperature were illustrated by plotting the temporal evolution of the maximum gas temperature. A representative result from their study is presented in Figure 27. Cuoci et al. [48] also characterized the ignition regimes in a similar manner using a detailed reaction mechanism consisting of about 200 species and over 5000 reactions. One result from their paper, in terms of the temporal evolution of peak gas temperature, is also shown in Fig. 27. While there are differences between the two sets of results due to different fuels and reaction mechanisms, both clearly show the cool flame and two-stage ignition for T_a between 700-900 K, and single-stage (hot flame) ignition for $T_a \geq 900$ K. Based on the results presented in Figs. 25-27, the following general observations can be made.

1. For low ambient temperature ($T_a < 600$ K[2]) or for very small droplets, results (cf. Fig. 26) indicate a state of no ignition, i.e., the droplet completely evaporates before exothermic reactions lead to a temperature rise. A similar behavior has been observed using the QSDI model.
2. As the ambient temperature is increased above 600 K, the low-temperature chemistry, characterized by reactions R2-R7 involving ketohydroperoxide decomposition, becomes important. This increases the system reactivity leading to the occurrence of cool flame or first-stage ignition, as indicated by a sudden but limited temperature rise (Fig. 27). Important processes associated with first-stage ignition include the low-temperature

[2]All the temperature values mentioned for different ignition regimes are approximate values. More precise values depend upon the fuel type, reaction mechanism and other conditions used in a given study.

chemistry, droplet heat-up, vaporization, and the heat and mass transport in the gas phase. The first-stage ignition time (τ_1) can be determined from the appearance of inflection point in the radial temperature profile. It can also be detected by a spike in peak gas temperature or in a relevant hydrocarbon species profile, for example, CH_2O profile.

3. After the first-stage ignition, the ignition process is essentially controlled by the cool flame temperature. The second-stage (hot flame) ignition time then depends upon a competition between the rate of heat releasing (oxidation) reactions and the rate of heat loss from the cool flame region. Its occurrence may be detected from the temporal evolution of peak gas temperature. The total ignition time represents the time from the introduction of a droplet into hot ambient until the appearance of hot flame. As discussed earlier in the context of Fig. 14, it represents the sum of first (τ_1) and second (τ_2) ignition delays. Schnaubelt et al. [47] used specific values of the temporal temperature gradient for determining these ignition delays.
4. The first ignition delay (τ_1) includes the droplet heat-up and fuel-air mixing (mass transport) time with the implication that the first ignition depends on both physical parameters (fuel volatility, droplet size, etc.) and ambient conditions. Thus, the droplet heat-up, vaporization and transport processes play an important role during the first ignition delay. However, the second-stage ignition is mostly kinetically controlled, and thus influenced by the cool flame temperature and mixture conditions at the time of first ignition. Note that the mixture conditions are relatively well developed when the cool flame is established near the droplet.
5. For certain conditions, as determined by ambient temperature and droplet size, only the first ignition is observed, i.e., the droplet vaporizes completely prior to the occurrence of second-stage ignition. Yang and Wong [60] numerically determined a minimum diameter, below which only the first stage ignition was observed (runaway ignition was not observed), and the droplet completely vaporized due to enhanced heat transfer from the cool flame. This is illustrated in Fig. 28a, which plots the temporal evolution of peak gas temperature for different droplet diameters. Results indicate the absence of second ignition or thermal runaway for d_o=160 μm, which represents a minimum drop size for a given ambient temperature. Yang and Wong computed the minimum diameter for different T_a, and as indicated in Fig. 28b, this diameter decreases as the ambient temperature is increased.
6. For high ambient temperatures (T_a>900 K), the first ignition or two-stage ignition may not be observed, since the high-temperature chemistry becomes dominant and drives the system directly to hot flame ignition. Representative results from Refs. [47, 48] are presented in Fig. 29, which plots the first and total ignition times with respect to ambient

temperature. In the top figure, predictions for the ignition of n-heptane droplet are compared with the measurements at μg and 1g, while in the bottom figure, predictions for n-decane droplet are compared with the 1g experiments of Moriue et al. [61]. There is fairly good agreement between predictions and measurements for both cases. The results clearly indicate two-stage ignition for T_a between 650-800 K, and only hot flame ignition for $T_a > 800$ K.

7. Previous studies do not provide a clear evidence for the existence of NTC region. See, for example, Figs. 26 and 29, and Refs. [59, 60, 61], which did not report a NTC region even though two-stage ignition was observed. This may be attributed to the fact that droplet ignition involves non-homogeneous temperature and species fields, which may smoothen out the NTC behavior. In addition, the enhanced vaporization caused by the presence of cool flame can reduce the second ignition delay, and modify the NTC behavior. The surface blowing (i.e., Stefan flow) can also affect the ignition process after the first-stage ignition [60]. In general, modification of the NTC region can lead to the existence of a ZTC region in which the total ignition time becomes independent of ambient temperature. The experimental data of Tanabe et al. [57] indicated a ZTC region between 700–780 K, while the computational results of Schnaubelt et al. [47] showed a much narrower temperature region, 620–630 K. In this context, it would be of interest to compare the NTC behavior in case of droplet ignition and gaseous nonpremixed ignition [55, 56].
8. The definition of droplet ignition time has generally included the heat-up and vaporization times. While this definition is almost universally accepted, it accentuates the effect of heat-up time, especially in the droplet-heating-controlled regime. The situation is analogous to the definition of spray ignition time that also generally includes the fuel injection and atomization times. Perhaps a more appropriate definition could be based on a time starting from the instant when the fuel vapor mass fraction at the droplet surface exceeds a prescribed value. Such a definition will exclude the dependence of heat-up time on droplet size, but still include other effects, such as Stefan flow, fuel vapor transport, turbulent wake development, etc. This would also provide a more rigorous comparison between droplet ignition and gaseous nonpremixed ignition, especially with regards to the chemical kinetic effects and NTC behavior.
9. The transient computational models with a detailed reaction mechanism can also predict the first- and second-stage ignition locations. This formation may be relevant in the context of whether the ignition occurs around an individual droplet or group of droplets. Figure 30 from Stauch et al. [59] plots the ignition location with respect to initial droplet radius for different ambient temperatures. At high temperatures ($T_a > 900$ K), the ignition radius normalized by the initial droplet radius is nearly constant, with a value of about 7. Below

900 K, the normalized ignition radius decreases due to the presence of two-stage ignition. The first ignition occurs at a smaller radius, and consequently, the second ignition is located closer to the droplet surface. For instance, Yang and Wong [60] predicted the first ignition location at about r/R=3.0. The ignition location can also be strongly influenced by other properties, such as fuel molecular structure, volatility, and pressure.

10. The initial droplet size is another important parameter affecting the transient ignition process, since most combustion systems involving polydisperse sprays. Practical devices involve relatively small droplets with d_0<0.1mm, while experimental investigations have been limited to larger droplets (d_0≈1mm). Consequently, the literature does not provide extensive data on the effect of droplet size on ignition, especially for d_0<0.1mm. For large droplets, as discussed in the preceding sections, both the QSDI and transient analysis and experiments indicate an increase in ignition delay as the droplet diameter is increased. In addition, there exists a minimum droplet size below which the ignition delay increases with the decrease in droplet size or the droplet fails to ignite. Moreover, this minimum size increases as the ambient temperature is reduced. The computed results also indicate that the effect of pressure is to extend the ignitability limits. Both the minimum ambient temperature and the minimum droplet size for ignition decrease as pressure is increased. Computational studies based on both reduced and detailed reaction mechanisms confirm these observations. For T_a > 900K, the ignition process is characterized by hot flame ignition, and thus influenced by both chemical kinetic and physical effects, including droplet heat-up, vaporization (fuel volatility) and transport. Then the ignition delay increases with droplet size, since the droplet heat-up, vaporization, and transport times all scale with droplet diameter squared. At lower ambient temperatures, the chemical kinetic effects, i.e., cool flame, two-stage ignition, etc., become dominant, although the physical parameters still play an important role, especially during the first-stage ignition. As discussed above, the first ignition delay is strongly influenced by droplet size, and increases with droplet size. Consequently for two-stage ignition, the total ignition delay also increases with droplet size; see, for example, Fig. 28 discussed earlier. A similar result regarding the effect of droplet size is reported by Stauch et al. [59]; see Fig. 6 in their paper. Another important result pertains to the presence of a critical or optimum droplet size, below with the ignition delay increases as the droplet size is reduced, and below a certain size, the droplet may vaporize completely prior to ignition. As discussed earlier, several studies using both the QSDI and transient ignition models have reported this optimum size.
11. The initial droplet temperature may also play an important role in the transient ignition process, especially for less volatile and multi-component fuels. The literature indicates

relatively little work concerning this aspect. Results reported by Stauch et al. [59] for n-heptane droplets (d_0=200 μm) indicate that at high ambient temperatures, the ignition delay time is essentially independent of droplet temperature as long as its value of not too low. Clearly the droplet heat-up time becomes negligible under such conditions. However, for low droplet temperatures (≈300 K), the ignition delay time can be expected to increase noticeably as this temperature is reduced. In general, the effect of droplet temperature is related to fuel volatility and ambient pressure, with the latter affecting the liquid boiling temperature. The effect of pressure is discussed in the next section.

2.4 Effect of Pressure on Droplet Ignition

Understanding the effect of pressure on droplet ignition is of fundamental importance for gas turbine combustors, liquid-fueled rocket engines, and direct injection spark-ignition and diesel engines. Pressure in these applications can approach high subcritical to supercritical values. At such pressures, the transient gas-phase effects become important and the validity of QSDI models becomes questionable. In addition, the effect of pressure on thermo-transport properties, phase equilibrium, boiling temperature, and heat of vaporization needs to be represented accurately, especially as pressure approaches critical values. Moreover, the chemical kinetic effects including two-stage ignition are strongly pressure dependent. There is considerable literature on the effect of pressure on droplet vaporization. High pressure effects have been considered in both quasi-steady [10, 62, 63] and transient vaporization models [64, 65, 66]. Such effects include nonideal gas behavior, solubility of gases into liquid, pressure dependence of gas- and liquid-phase thermophysical properties, transient gas-phase transport, and transient liquid transport in the droplet interior. Clearly the applicability of quasi-steady models is limited to moderate pressures due to the quasi-steady gas-phase assumption. For pressures approaching transcritical and supercritical conditions, transient vaporization models have been considered. Compared to research on droplet vaporization, computational studies of droplet ignition at high pressures have been rather limited, although fairly extensive experimental data has been reported.

Kadota et al. [37] used a constant volume vessel to measure the ignition delay of a single fuel droplet. Experiments were conducted at pressures of 1 to 41 atm, and ambient gas temperature of 500 to 975 K. The ignition delay data were correlated in the Arrhenius form. Nakanishi et al. [67] used a fiber-suspended droplet to examine the ignition behavior at high-pressure conditions. A n-heptane or n-hexadecane droplet was suddenly exposed to high-pressure, high-temperature environment in an electric furnace, and the ignition delay time was measured for a droplet diameter range of 0.35-1.4 mm, ambient temperatures upto 950 K, and

pressures upto 30 atm. A representative result showing the effect of pressure and initial droplet diameter on the ignition delay is illustrated in Fig. 31. Several important observations can be made from this figure. First, at low pressure (p = 1 and 1.5 atm), the ignition delay exhibits a non-monotonic variation with droplet size, while at high pressure, it increases monotonically with droplet size. The non-monotonic behavior at low pressures, indicating a minimum droplet size, has been observed in several experimental [25, 26, 29] and theoretical/computational studies [20, 21, 27, 51]. As discussed earlier, for droplet sizes smaller than this minimum, the ignition delay time increases as droplet diameter is decreased, which may be attributed to a decrease in system Damköhler number. For droplet sizes larger than the minimum, the increase in ignition delay with diameter is due to the increase in droplet heat-up and gas-phase transport times. Second, the ignition delay decreases as the pressure is increased. This is shown more clearly in Fig. 32, which plots ignition delay as a function of pressure for different ambient temperatures. The behavior can be attributed to a reduction in chemical time (t_{chem}) which varies as p^{-1}, while the mass transfer time (or vaporization time), varies as $t_m \sim p$, since $t_m \sim d^2/D$ where d is diameter and D is diffusivity. Consequently, the system Damköhler number (Δ), which varies as $\Delta \sim p^2$, increases significantly with increasing pressure, and enhances droplet ignitability at high pressures. Third, measurements indicate that the minimum droplet diameter for ignitability decreases as the pressure is increased (cf. Fig. 31), which can be explained by the increase in system Damköhler number with pressure. Another interesting observation is that the variation of ignition delay with pressure does not exhibit any abrupt behavior as the pressure exceeds critical pressure of the fuel. This implies that the critical conditions are not reached at the droplet surface though the ambient pressure exceeds the fuel critical pressure.

Ruszalo and Hallett [46] employed a transient numerical model to study droplet ignition at high pressures. The numerical model was based on the solution of transient, spherically symmetric equations of continuity, species, and energy by using a finite-difference technique. The droplet temperature was assumed to be spatially uniform. The chemistry was modeled using a global one-step reaction scheme with non-unity exponents of fuel and oxygen concentrations, as indicated by the fuel consumption rate below:

$$\dot{w}_f = -M_f A p^{a_f + a_o} (Y_f / M_f)^{a_f} (Y_o / M_o)^{a_f} \exp(-T_a / T) \tag{16}$$

Here all the variables are in their dimensional form. Results were presented for n-heptane and n-hexadecane droplets for ambient temperatures ranging from 850 to 1100 K, and pressures ranging from 1 to 50 atm. A representative result is provided in Fig. 33, which plots the ignition delay as a function of droplet diameter for different pressures. Results are consistent with the discussion provided above regarding the effect of pressure on droplet ignition. For a given pressure, the ignition delay decreases as the diameter is decreased, approaching an ignition limit

at some minimum diameter, which decreases as the pressure is increased. In addition, the ignition delay is seen to decrease significantly as pressure is increased. In order to further examine the effect of pressure on droplet ignition, the radial profiles of gas-phase temperature and fuel vapor mass fraction at the time of ignition for two different pressures are shown in Fig. 34. At higher pressures, the fuel vapor fraction at the surface is significantly reduced compared to that for p = 1 atm. This causes the reaction zone to move closer to the droplet surface and ignition occurs earlier and in progressively leaner mixtures as pressures is increased. Thus, the overall effect is that as pressure is increased, the ignition delay time decreases, the ignition location moves closer to the droplet, and ignition limits become wider, i.e., the minimum ambient temperature and droplet diameter for ignition decrease.

Some recent studies have considered the effect of pressure on two-stage ignition [57, 59], and observed that the first ignition delay (τ_1) is relatively insensitive to pressure, although the pressure can affect the first ignition location. In contrast, the second ignition delay (τ_2) was found to decrease noticeably with increasing pressure due to its effect on cool flame temperature and high-temperature chemistry. Tanabe et al. [57] attributed this decrease to the increase in cool flame temperature at higher pressures. One representative result from Ref. [59] is shown in Fig. 35, which indicates longer (total) ignition delays at higher pressures, consistent with the experimental and computational studies discussed above. Note that these results were obtained for T_a =1200 K, and only pertained to hot flame ignition. In addition, Fig. 35 indicates that the ignition delay for a droplet is consistently higher than that for the corresponding homogeneous mixture. This difference is mainly due to the effects of droplet heating and evaporation time, while the nonhomogeneity in gas temperature and equivalence ratio is expected to decrease the ignition delay.

2.5 Fuel Properties and Multi-Components Fuel Effects on Droplet Ignition

The droplet ignition behavior may be strongly influenced by fuel properties, such as volatility, reactivity, and molecular structure. The fuel molecular structure pertains to the length and degree of unsaturation (number of double and triple bonds) of the carbon chain. In general, as the carbon chain length increases, the fuel volatility and diffusivity decrease. This would increase the droplet heat-up and fuel vapor diffusion times, and therefore the ignition delay. However, longer chain hydrocarbons are known to be more reactive, which implies shorter ignition delays, especially at low temperatures. In contrast, the fuel unsaturation mainly affects its reactivity and thus the ignition delay. In general, the effects of fuel volatility and molecular structure on ignition depend upon other parameters, such as droplet size and ambient conditions. As discussed earlier, for high ambient temperatures and large droplets, the ignition behavior is

more strongly influenced by physical processes (i.e., droplet heating, vaporization and vapor transport), while at low temperatures (Ta<900 K), it is more controlled by chemical kinetics. There have been relatively few studies, which have systematically examined these aspects.

Tanabe [57] examined the effect of fuel volatility and reactivity by performing experiments and simulations for the ignition of n-heptane, n-dodecane, and iso-octane droplets. N-heptane and n-dodecane have similar reactivity but different volatility and other physical properties. In contrast, n-heptane and iso-octane have similar physical properties but different reactivity. Results indicated that the first ignition delay is strongly influenced by the fuel properties and ambient conditions. On the other hand, the second ignition delay is mainly determined by the cool flame temperature, since high-temperature reactions are activated through this parameter, i.e., a higher cool flame temperature shortens the second ignition time. This can also be seen through the strong dependence of second ignition time on pressure, as discussed earlier. Mixture conditions at the time of first ignition also influence the second ignition. Stauch et al. [59] performed a computational study using bi-component (n-heptane/iso-octane) fuel droplets and examined the effect of fuel composition on ignition. Detailed transport and chemical kinetic (94 reactions and 614 reactions) models were employed. Since the composition of this blend mainly affects the reactivity rather than volatility, its effect on ignition delay was found to be small for T_a >1000 K, but increasingly significant as T_a was decreased below 900 K. For instance, at T_a =833 K, the ignition delay time increased by a factor of 5 as the amount of iso-octane in the blend was increased from 0% to 95%. Marchese et al. [42] also employed a detailed computational model to examine the transient ignition and combustion behavior of single (n-heptane) and multi-component (n-heptane/n-hexadecane) fuel droplets. The model included multi-component transport, non-luminous, gas phase radiative heat transfer, and a skeletal mechanism with of 51 species and 282 reactions. Since the simulations focused on high-temperature conditions (T_a>900 K), only the hot flame ignition was examined. The predicted ignition delays showed reasonably good agreement with the μg ignition data of Faeth and Olsen [25], consistent with the results obtained using the QSDI model.

Another interesting study concerning fuel properties was reported by Moriue [61], who performed experiments using bi-component fuel droplets with n-decane (ND)/1-methylnaphthalene (MN), or ND/1,2,4-trimethylbenzene (TMB) blends. The two aromatic fuels, MN and TMB, are known to be less reactive and their ignition delays do not exhibit the NTC behavior. Moreover, normal boiling points of these three fuels are 447.3 K, 517.9 K, and 442.5 K, respectively. Thus the addition of MN to ND lowers both the reactivity and volatility of the blend, while that of TMB only lowers the reactivity. As expected, results indicated that as the amount of MN or TMB in the blends is increased, both the first and second ignition delays

increase monotonically, and that the two-stage ignition region (in terms of T_a) becomes narrower and eventually vanishes. A representative result showing the effect of ambient temperature on the first and second ignition delays for different ND/MN and MD/TMB compositions is provided in Fig. 36. In addition, the increase in ignition delay was found to be higher with TMB addition than that with MN, which may be due to the higher volatility of TMB. Note that higher volatility implies that more of this fuel is vaporized. Results further indicated that the minimum ambient temperatures for the occurrence of cool and hot flames increase monotonically with the decrease of n-decane fraction in the blend, and as the amount of ND falls below 40%, the cool flame and two-stage ignition regions disappear.

Marchese et al. [43] recently reported an experimental and computational investigation on droplet ignition for a variety of neat methyl esters and commercial soy methyl ester. The neat methyl esters included methyl decanoate (C10:0), methyl dodecanoate (C12:0), methyl oleate (C18:1). The nomenclature Cx:y here denotes the carbon chain length (x) and number of double bonds (y). Ignition experiments were conducted at 1-g and μg (10^{-4} m/s^2) using a fiber-suspended droplet introduced in a furnace at one atmosphere and temperature up to 1300 K. The ignition event was monitored using OH* chemiluminescence. Computations employed a detailed model that included spectrally resolved radiative heat transfer, multi-component transport, and a skeletal reaction mechanism with 125 species and 713 reactions. Figure 37 presents ignition delay measurements at 1-g for 1.2 mm droplets of various biodiesel fuels. SE-1885 soy methyl ester (a blend of six methyl esters) exhibits ignition delay characteristics similar to those of the commercial B99 biodiesel, although the latter has slightly shorter ignition delay for the indicated temperature range. In contrast, ignition delays for the two pure components, i.e., methyl decanoate and methyl dodecanoate, are significantly different from those of soy methyl esters, while methyl oleate exhibits similar ignition delays to both soy methyl esters for the entire temperature range. Another interesting observation is that measured ignition delays for methyl dodecanoate are longer than those for methyl decanoate, especially at lower ambient temperatures. Note that the longer chain methyl esters are known to have higher reactivity at low temperatures, and therefore shorter ignition delays. However, the longer chain methyl esters also have lower volatility and lower gas phase diffusivity, which would lead to longer ignition delays. Furthermore, the computational model showed good agreement with experiments at 1200 K, but significant differences at lower temperatures, which the authors attributed to the limitations in the skeletal chemical kinetic mechanism. The experiments also indicated the limitation of fiber-suspended droplet technique, as the measured ignition delays were shown to be noticeably affected by the fiber diameter. The technique also introduces asymmetry in the ignition process.

Measured ignition delays for the microgravity experiments were much shorter than the normal gravity results, and the differences were attributed to flow effects. However, microgravity data had significant scatter.

2.6 Droplet Ignition Under Convective Conditions

An important issue here pertains to the effects of forced or buoyant convection on ignition delay and ignitability limits in terms of the minimum droplet diameter or ambient temperature for ignition. In contrast with studies under stagnant conditions, there has been limited research on droplet ignition under convective conditions. While convective effects were present in most experimental studies using the suspended droplet or freely falling droplet technique, they were either assumed to have a negligible influence on ignition delay, or their role in the ignition process was not identified. As discussed by Marchese et al. [42, 43], even in the absence of buoyancy, the insertion process for a fiber-suspended droplet introduces convective flow within and around the droplet. Furthermore, the geometry is inherently non-symmetric due to the use of a suspension fiber. In drop tower and space experiments, a suspended droplet is deployed with a small relative velocity, and the ignition is caused by an external source, such as a spark or a hot wire. The ignition conditions in this case are inherently multi-dimensional. These convective and multi-dimensionality effects cannot be accounted for in transient, spherically-symmetric computational models. Theoretical studies using the QSDI approach [27] can include the convective effect using an empirical correction, such as the Ranz and Marshall correlation [46], to the heat and mass transfer rates.

Faeth and Olson [25] measured ignition delay times for fuel droplets at zero gravity and normal gravity. Their study indicated that the ignition delay times are slightly longer and the ignition location is slightly closer to the droplet under normal gravity compared to those under zero gravity. The experimental investigation of Tanabe [39] also indicated that the ignition delay time and the minimum temperature for ignition (near the ignition limits) are reduced under microgravity conditions. Rangel and Fernandez-Pello [68] used a boundary-layer approximation to examine droplet ignition in mixed convection. The effect of local Damköhler number on ignition near the forward stagnation point was investigated. Dash and Som [69] considered the full elliptic, steady state problem in their numerical investigation of droplet ignition under forced convection. The numerical model was based on an axisymmetric flow around a spherical fuel droplet. The ignition delay times were computed as a function of the droplet Reynolds number (Re_d) and ambient temperature (T_a). Results indicated a non-monotonic variation of the ignition delay with Re_d. It first decreased reaching a minimum value as Re_d is increased, and then increased sharply until a no-ignition limit was reached. The behavior may be related to the ignition location moving from the front to the aft (and far) of the droplet as Re_d was increased.

This is also confirmed by other studies discussed below. In addition, for a given T_a, the existence of a minimum droplet temperature was observed, and this temperature was found to increase with the increasing Re_d. Yang and Tsai [70] employed a similar approach to investigate the convective ignition and flame development over a porous sphere. An important observation was that for small Lewis numbers or large Damköhler numbers, the ignition position was located at the forward stagnation point, while for large Lewis numbers or small Damköhler numbers, it was located in the wake region.

Huang and Chen [50] employed a transient, fully elliptic numerical model to examine the ignition of a n-heptane droplet subjected to both forced and mixed convection with a relatively low Reynolds number (Re_d =1). Several simplifying assumptions were made, which included approximating droplet as a porous rigid sphere with uniform but temporally varying temperature, constant thermo-transport properties, and global one-step chemistry. Ignition was observed to be initiated in the downstream region of the droplet (at a distance of about 6-10 droplet diameter) even at this low value Re_d. The effect of gravity was found to be significant, as the ignition location moved closer to droplet in the presence of gravity. However, the ignition delay was modified only slightly by gravity, changing from 0.218s at 0-g to 0.23s at 1-g.

Kim and Park [71] also employed a fully elliptic, transient, axisymmetric model for both the gas and the liquid phase to investigate droplet ignition in convective, high-temperature environment. The chemistry was represented by a one-step mechanism. The ignition criterion was based on the appearance of an inflection point in the temporal plot of the maximum gas temperature. One representative result is shown in Fig. 38, which plots the temporal variation of peak gas temperature for droplet Reynolds number Re_D =1, 10 and 40. These results indicate that the effect of convection is to decrease the ignition delay time. This may be attributed to the convective enhancement in mass and heat transfer rates. Regarding ignition location, their results indicated that the ignition occurs in the aft of the droplet, except for the lowest number case (Re_D = 1) for which the ignition location is in the fore of the droplet. As the ambient temperature was lowered and/or the droplet Reynolds number was increased, the ignition location moved farther away from the droplet. For Re_D = 40, and T_a = 1500 K, the ignition occurred in the wake region at a downstream location more than five times the droplet radius. Based on the location of the ensuing flame, three distinct flame regions, namely, envelope flame, wake flame, and spray flame, were identified in terms of Re_D and T_∞. A representative result showing the three flame regimes is illustrated in Fig. 39. As Re_D is increased, or T_a is decreased, or the activation energy is increased, the flame type changes from envelope flame to wake flame, and then to spray flame. Finally, their results indicated that the effect of internal circulation on the ignition delay is

negligible, implying that for the conditions investigated, the droplet heating does not play a significant role in the ignition process.

Whang et al. [72] conducted an experimental study of the ignition of a suspended droplet in the convective post-flame environment of a flat-flame burner. The ignition delay and location were measured for n-heptane and n-hexadecane droplets for a range of ambient temperatures, droplet diameters, and Re_D between 10-30. Their results indicated that the minimum ambient temperature for ignition increases significantly due to forced convection. No ignition was observed for T_a less than 1050 K. As the ambient temperature was increased, the ignition first appeared in the far wake region of the droplet, and the ignition point moved upstream. At T_a = 1270, the ignition occurred near the rear stagnation point, and an envelope flame formed soon afterwards. At T_a = 1350, the ignition location moved to the front stagnation point. One representative result showing the normalized ignition location as a function of T_a is illustrated in Fig. 40. It is interesting to note that the normalized ignition location is essentially independent of the initial diameter. In addition, it was observed that while the ignition delay time increased significantly from n-heptane to n-hexadecane, the ignition location was nearly independent of fuel volatility. The plot of ignition delay time versus initial droplet diameter for the two fuels is given in Fig. 41. Similar to the non-convective case, the ignition delay time increases with increasing diameter, and exhibits significantly higher sensitivity to diameter for less volatile fuels. Also, the minimum diameter for the ignition of n-heptane droplet is about 1.1 mm, which is significantly higher compared to the non-convective case. Figure 42 shows the measured ignition time versus ambient temperature for n-hexadecane droplets. Again, similar to the non-convective case, the ignition delay increases as the ambient temperature is reduced, approaching a nonignitable state. As indicated, the minimum ignition temperature is 1050 K, which is significantly higher than that under natural convection. Thus, the results indicate that the droplet ignitability is adversely affected by forced convection.

Wong et al. [73] also reported a companion numerical investigation of droplet ignition under forced convection. The physical model was greatly simplified by assuming that the ignition occurred in the wake region far downstream of the droplet. Analytical expressions were employed for the far-wake isothermal velocity field, and the boundary layer approximation was used for the species and energy equations. Some representative results for the ignition of n-hexadecane droplets are given in Figs. 43-45. Consistent with the results of others, the ignition delay time decreases while the ignition location progressively moves upstream closer to the droplet, as the ambient temperature is increased. While the numerical and experimental results indicate similar trends, they exhibit significant differences. The effects of initial droplet diameter on the ignition delay and location are illustrated in Fig. 44. As discussed earlier, the ignition delay increases with increasing diameter. The normalized ignition location is essentially

independent of the initial diameter for d_0>800 μm. However, for smaller diameters, the location moves further downstream as the diameter is decreased, indicating that for smaller droplets, ignition is not likely to occur near the droplet. The dependence of the ignition delay and ignition location on the gas velocity is depicted in Fig. 45. Results indicate that the ignition delay decreases as the velocity is increased, implying that the forced convection has a beneficial effect on droplet ignitability. However, the ignition location moves further downstream with increasing free stream velocity, indicating reduced ignitability.

Stauch and Mass [74] performed numerical simulations for the ignition of methanol droplets in an axisymmetric laminar flow using detailed chemistry and transport models. The ambient gas temperature ranged between 1300-1500 K and Re_D between 0.5-80. As indicated in Fig. 46, with increasing Reynolds number, the ignition delay decreases. As Re_D is increased, the ignition location gradually moves around the droplet to the wake of the droplet with upstream flame propagation. At some value of Re_D, which varies with T_a, the ignition was not detected in the computational domain.

2.7 Cluster Ignition and External Spray Ignition

It is important to address the role of droplet ignition in a spray environment, in which ignition may also occur through the droplet group ignition or external spray ignition modes. Which ignition mode is dominant in a given spray depends upon the prevailing conditions, including fuel type, overall and local equivalence ratios, ambient temperature, pressure, and mean inter-droplet spacing relative to diameter. The dominant ignition modes may be viewed in the context of droplet group combustion, which has received considerable attention during the last three decades [3, 75, 76, 77, 78, 79, 80]. Chiu and co-workers [75, 76] developed a group combustion model based on a non-dimensional group number G, which represents the ratio of gas phase transport time to vaporization time. For a droplet cloud, it is defined as

$$G = 3(1 + 0.276\,\mathrm{Re}_d^{0.5}\,Sc^{0.33})LeN^{2/3}\frac{d_0}{s} \qquad (17)$$

Here Sc and Le are the gas Schmidt number and Lewis number, respectively, N is the number of droplets in the cloud, and s is the mean droplet spacing. As indicated in Fig. 47, based on the value of G, the three combustion regimes may be defined as external group combustion (G>>1), internal group combustion (G≈1), and droplet combustion (G<<1). Thus in the external combustion mode, droplets are closely spaced, individual droplets simply vaporize without any envelope or wake flame, and chemical reactions occur over a length scale that is much larger than droplet scales. Droplets then act as sources of fuel vapor but sinks of energy for the gas

phase. On the other hand, the third limit, G<<1, corresponds to a highly dilute spray in which the individual droplet combustion is favored. The internal group combustion or droplet cluster mode represents an intermediate situation with regions of both spray combustion and droplet combustion. Several researchers have analyzed these combustion modes. For example, Chen and Gomez [78] observed the internal group combustion mode for G between 16 and 50 in their experimental study of laminar spray flames. They also provided experimental evidence of transition from group combustion to individual droplet burning through oxygen enrichment of the oxidizer stream, which effectively decreased G. Beck et al. [81] analyzed individual droplet combustion mode with either an envelope flame or a wake flame in lean turbulent two-phase mixtures.

Since spray combustion and ignition processes are closely linked, one may define the dominant ignition modes in an analogous manner to characterize different ignition regimes. While there is no systematic investigation of the transition between the three ignition regimes, there is sufficient experimental and computational evidence for their existence. Aggarwal [1] and Mastorakos [2] provide reviews of research dealing with external spray ignition in laminar and turbulent flows, respectively. As discussed in these reviews, there have been a number of studies focusing on both autoignition and ignition induced by external source. For instance, Pickett [4] performed an experimental study of laser-induced spray ignition in a constant volume combustor. Boileau et al. [82] employed LES (large eddy simulations) approach to investigate spray ignition using a hot vitiated jet in a gas turbine combustor. Neophytou et al. [83] performed direct numerical simulations (DNS) of spark-induced ignition in turbulent droplet-laden mixing layers, and observed that the external spray ignition was followed by the formation of a tribrachial flame. Their conditions corresponded to Group numbers [75] of 100 and 200.

Kang et al. performed a computational investigation on autoignition in turbulent sprays using a single-step chemistry model [84]. Som and Aggarwal [5] employed a reduced chemistry model to examine autoignition and flame liftoff in a constant volume combustor. External spray ignition mode was observed in these studies. Moreover, the results reported by Som and Aggarwal were in qualitative agreement with the experimental investigation of O'Loughlin and Masri [85], who observed external spray ignition followed by a lifted flame. Wang and Rutland [86] employed a DNS approach with a reduced chemistry model to examine autoignition in turbulent spray jets. Ignition was observed to occur in the spray ignition mode at the edge of the jet, characterized by fuel lean conditions and low scalar dissipation rate. Borghesi [87] performed DNS of autoignition in turbulent sprays and observed the development of several ignition kernels in regions where the mixture fraction was close to the most reactive value, determined from homogenous autoignition calculations, and the scalar dissipation rate was low.

This aspect should also be investigated in the context of droplet ignition by examining the development of mixture fraction and scalar dissipation rate fields during ignition.

The droplet group ignition mode has also been investigated [3, 88, 89, 90, 91, 92, 93, 94, 95]. Annamalai and coworkers [3, 90, 92] provide a review of research dealing with droplet clusters and particle clusters. Mawid and Aggarwal [88] examined numerically the probability of droplet ignition versus spray ignition for pure and bi-component fuels in dilute sprays. Results indicated that for most of the conditions considered, the individual droplet ignition was favored over the external ignition. Only for diameter less than 30 μm, the ignition delay was smaller for the spray than that for the droplet. As expected, the value of minimum diameter was determined by spray properties, such as overall equivalence ratio, fuel type, oxygen concentration, and ambient temperature. Results were shown to be consistent with the group combustion theory, as the Group number was typically less than 0.01. The numerical study of Bellan and Harstad [94] concerning the autoignition of droplet clusters in convective flows indicated that ignition may occur around individual droplets or around the cluster depending on the inter-droplet spacing relative to the droplet diameter. This observation has subsequently been confirmed by experimental results for droplet clusters [96]. Dwyer et al. [97] performed numerical simulations of ignition in a 3-D droplet array and observed external cluster ignition for the conditions investigated. Moriue et al. [98] reported μg experiments on the droplet-interaction effect on the ignition of fiber-suspended n-decane droplet pair suddenly inserted into hot air at temperatures where the low-temperature oxidation reactions are active. At atmospheric pressure, cool-flame ignition delay and cool-flame temperature were found to increase with decreasing inter-droplet spacing. At pressure of 3 atm, where two-stage ignition was detected, cool-flame ignition delay and cool-flame temperature again increased with decreasing inter-droplet distance. In addition, due to the higher cool-flame temperature, the second ignition delay decreased with decreasing inter-droplet distance. More research is needed along these lines, focusing on the effects of inter-droplet spacing and other properties, and on the transition between the three ignition modes, using different droplet group and spray configurations.

3.0 Concluding Remarks

Research dealing with the ignition of a fuel droplet in a hot, oxidizing environment has been reviewed. A majority of work on this topic has focused on droplet ignition in a stagnant environment. Some limited experimental and computational studies have also examined the effects of natural and forced convection on droplet ignition. Important observations from various theoretical/computational and experimental investigations are as follows:

1. Most of the theoretical/computational research can be classified into two groups, quasi-steady analysis and transient analysis. Both of these approaches consider a spherically-

symmetric configuration, in which a fuel droplet is suddenly exposed to a hot oxidizing stagnant environment (except for the Stefan flow resulting from droplet vaporization). Due to heat transfer from the environment, the droplet surface temperature increases, and vaporization commences. The resulting fuel vapor mixes with the oxidizer forming a locally combustible mixture, and the chemical activity begins, initially involving premixed combustion and then transitioning to partially premixed combustion. As the chemical activity intensifies, heat-releasing reactions are initiated, and the gas temperature in the droplet vicinity starts rising. The state of ignition in the quasi-steady model (QSDI) is defined when the system Damköhler number exceeds a critical Damköhler number, while in the transient model, it is defined by a suitable ignition criterion based on a spike or an inflection point in the gas temperature or species profile. The droplet ignition delay is computed by counting the time from an instant the droplet is introduced into the hot environment to the instant the ignition criterion is satisfied. This ignition delay can be divided into a physical delay and a chemical delay. The physical delay involves droplet heat-up, vaporization and outward diffusion of fuel vapor, while the chemical delay represents the time required for chemical reactions to reach a thermal runaway condition.

2. The major difference between the QSDI and transient models is due to the assumptions of single-step chemistry and quasi-steady gas phase in the former. The QSDI model yields an ignition criterion based on a critical Damköhler number, which can be used to identify the state of droplet ignition in a given spray environment. Originally developed by Law et al. [19, 20], the QSDI model has been extensively studied and modified by several investigators with the objective of relaxing various assumptions used in its formulation, and extending its applicability. These include the use of non-unity reaction orders with respect to fuel and oxidizer, transient liquid-phase processes, presence of fuel vapor in the gas phase, and variable thermo-transport properties. This model has been extensively used to predict ignition delays for an isolated droplet, and examine the effects of various parameters, such as fuel properties, droplet size, ambient temperature and pressure, on droplet ignitability. It has also been employed in spray computations for distinguishing the state of pure vaporization from that of combustion for an individual droplet.
3. Due to the quasi-steady gas phase assumption, the use of QSDI model becomes questionable at high pressures, especially near critical and supercritical conditions. Moreover, it cannot provide many details of the ignition process, which can be obtained using a transient analysis. For example, the transient model can analyze transition from premixed to partially premixed combustion and then to diffusion combustion, and also predict ignition location with respect to droplet surface. In addition, it has been used to examine effects pertaining to low- and high-temperature chemistry including two-stage ignition and NTC/ZTC behavior,

non-dilute sprays, multicomponent fuel, and high pressure. However, the transient model requires solving numerically a system of strongly coupled, nonlinear partial differential equations along with a validated chemistry model and interphase boundary conditions at the droplet surface.

4. While the QSDI model is useful in characterizing droplet ignition for a wide range of conditions, and for distinguishing between evaporating and combusting droplets, it overpredicts fuel vapor concentration in the droplet vicinity due to the artificially imposed quasi-steady fuel vapor distribution. Consequently, it predicts shorter ignition delays and wider ignition limits, in terms of the minimum droplet size and ambient temperature, compared to the transient model, and the differences become more pronounced for volatile fuels, high ambient temperatures, small droplet diameters, and high initial droplet temperatures. The QSDI model is also not applicable for non-dilute sprays, as the droplet spacing is reduced relative to its droplet.
5. The experimental research has mainly employed two configurations, a fiber-suspended droplet in a preheated furnace, and a freely falling droplet in a furnace or a moving droplet in a heated stream or the post-combustion region of a laminar flame. A majority of the work has considered n-alkane (heptane, dodecane, and hexadecane) droplets, and reported ignition delays for a range of droplet sizes, ambient temperatures and pressures under normal- and micro-gravity conditions. Some recent work has also reported ignition delay measurements for other fuels including multicomponent and biodiesel fuels. In addition, experimental investigations have focused on two-stage ignition including the NTC/ZTC behavior, and reported data on the first and second-stage ignition delays. While the experimental studies have provided significant insight on droplet ignition, and extensive ignition data for model validation, they have inherently been limited to large droplet sizes ($d_o \approx 1$ mm or larger). Moreover, measurements have been influenced by convection and multi-dimensional flow effects that are present in both the fiber-suspended and freely moving droplet techniques. Even in μg experiments, the insertion process for a fiber-suspended droplet introduces convective flow within and around the droplet. Furthermore, the geometry becomes inherently non-symmetric due to the use of a suspension fiber, which induces capillary flow and affect liquid-phase transport in the droplet interior [99].
6. An important observation from experimental and theoretical/computational investigations is the existence of an optimum droplet size corresponding to a minimum ignition delay time, and a minimum size below which droplets fail to ignite. For droplets larger than the optimum, the first-stage ignition delay and thus the total ignition delay increases with the droplet size. This can be attributed to the increase in droplet heating and vapor transport times as the diameter is increased. For droplets smaller than the optimum, the ignition delay

increases and reaches a nonignitable state as the diameter is decreased. A probable explanation for this behavior is that the system Damköhler number decreases as the diameter is decreased, or the droplet heat-up and vaporization time becomes negligibly small compared to the chemical time. In addition, both the optimum and minimum droplet sizes decrease as fuel volatility, ambient temperature and pressure are increased. There also exists a minimum ambient temperature for ignition, which decreases as the pressure, droplet diameter, or fuel volatility is increased. Another important result from computational studies pertains to liquid-phase transport, which influences the droplet surface temperature and consequently the ignition delay. For instance, the use of finite-diffusivity model leads to higher surface temperature and shorter ignition delay. This effect is found to be more signficant for less volatile fuels, larger droplets, and lower ambient temperatures, since the droplet heat-up time becomes comparable to the ignition delay time for such conditions.

7. The literature indicates paucity of research on droplet ignition under convective conditions. While convective effects are present in most experimental studies performed under 'stagnant' conditions, their role in the ignition process has not been identified. In the experimental work at 1g, the effect of natural convection on the ignition behavior has not been discussed. Similarly in μg experiments, the introduction of a droplet into an oxidizing environment generates flow relative to droplet, which has not been characterized. Some limited experimental and numerical studies have been reported on this topic, but provide conflicting results. For example, experiments performed at 1g and μg [25, 40], and under forced convection [72], indicate that the ignition delay and the minimum droplet size and ambient temperature for ignition are higher in the presence of convection. In contrast, numerical studies [69, 73, 74] based on 2-D axisymmetric simulations report opposite trends. However, some of the results consistently indicate that the ignition location and flame development are strongly influenced by the droplet Reynolds number (Re_D) and ambient temperature (T_a). As Re_D is increased or as T_a is decreased, the ignition location moves from front to aft (wake) of the droplet, and correspondingly an envelope flame changes to a wake flame. Further increase in Re_D leads to either no ignition or flame extinction.
8. The literature review also highlights gaps in our current understanding of droplet ignition phenomenon, and the need for further research on a number topics, including the effect of convection, ignition of more realistic single- and multi-component fuels including petroleum-based and biologically derived fuel surrogates, and droplet ignition under high-pressure conditions. Future numerical and experimental studies should focus on characterizing the effects of natural and forced convection on ignition. To this end, computational capabilities with detailed chemistry and transport models now exist to perform transient 3-D simulations of droplet ignition in laminar and turbulent flows. While various approaches, such as RANS

(Reynolds Averaged Navier Stokes), LES, and DNS, have been employed to investigate the ignition of turbulent sprays, no such study has been reported for droplet ignition. Here the effects of turbulent characteristics, including turbulent scales relative to drop size, on droplet ignition will be of interest. New experiments should focus on producing freely suspended droplets using techniques such as acoustic levitation [100], and droplets in well-characterized laminar or turbulent flows [101]. One such study on the combustion of single droplets in isotropic, homogeneous turbulence is reported by [102]. Further research is also needed to characterize droplet ignition over a wider range of pressures and temperatures, and to investigate two-stage ignition and identify NTC and ZTC regions for practical fuel surrogates. Here the research should also focus on developing computational capabilities for examining droplet ignition at transcritical and supercritical conditions. Last but not the least, more comprehensive studies are needed to examine issues related to the dominant ignition modes in sprays. Relatively few studies have focused on the ignition of dense sprays, examining conditions for internal and external group ignition.

References

1. S. K. Aggarwal, A review of spray ignition phenomenon: present status and future research. Prog Energy Combust Sci 1998;24:565-600.
2. E. Mastorakos, Ignition of turbulent non-premixed flames. Prog Energy Combust Sci 2009;35: 57-97.
3. K. Annamalai and W. Ryan, Interactive processes in gasification and combustion. Part I: liquid drop arrays and clouds. Prog. Energy Combust. Sci. 1992;18:221-95.
4. L.M. Pickett, S. Kook, H. Persson, and O. Andersson, Diesel fuel jet lift-off stabilization in the presence of laser-induced plasma ignition, Proc. Combust. Inst. 2009;32:2793-2800.
5. S. Som, and S. K. Aggarwal, Effects of primary breakup modeling on spray and combustion characteristics of compression ignition engines, Combust. Flame, 2010;157:1179-1193.
6. S.-C. Rah, A. F. Sarofim, and J. M. Beer, Ignition and combustion of liquid fuel droplets. Part I: impact on pollutant formation, Combust. Sci. and Tech. 1986;48:273-284.
7. S.-C. Rah, A. F. Sarofim, and J. M., Beer, Ignition and combustion of liquid fuel droplets. Part II: ignition studies, Combust. Sci. and Tech., 1986;49:169-184.
8. S. Russo and A. Gomez, Physical characterization of laminar spray flames in the pressure range 0.1–0.9 MPa, Combust. Flame. 2006;145:339-356.
9. C. K. Law, Recent advances in droplet vaporization and combustion. Prog. Energy Combus. Sci. 1982;8(30):169-199.
10. S. S. Sazhin, Advanced models of fuel droplet heating and evaporation. Prog. Energy Combus. Sci. 2006;32:162–214.
11. S. K. Aggarwal, G. Zhu, and R. D. Reitz, Quasi-steady high-pressure droplet model for diesel Sprays. SAE Transactions, J. of Engines, 2000;109(3):734-743.
12. S. C. Tarifa, P. D. N. Perez Del Nota, and G. F. Moreno, Proc Combust Inst, Combustion of liquid monopropellants and bipropellants in droplets. Eighth Symposium (International) on Combustion, William and Wilkins, Baltimore, 1962, pp. 1035-1053.

13. R. L. Peskin and H. Wise, Ignition and deflagration of fuel drops. AIAA J. 4, 1646-1650 (1966).
14. R. L. Peskin, G.E., Polymeropoulos, and P. S. Yeh, Results from a theoretical study of fuel drop ignition and extinction. AIAA J. 1967;5(12):2173-2178.
15. G.E. Polymeropoulos, and R. L. Peskin, Ignition and extinction of liquid fuel drops - numerical computations. Combust Flame 1969;13:166-172.
16. F. E. Fendell, Ignition and extinction on combustion of initially unmixed reactants. J. Fluid Mech. 1965;21:293-303.
17. D.R. Kassoy and F. A. William, Effects of chemical kinetics on near equilibrium combustion in nonpremixed systems. The Physics of Fluids 1968;11(6):1343-1351.
18. A. Linan, The asymptotic structure of counterflow diffusion flames for large activation energies. Acta Astronautica 1974;1(7-8):1007.
19. C. K., Law, Asymptotic theory for ignition and extinction in droplet burning, Combust Flame 1975;26:89-98.
20. C. K., Law, Theory of thermal ignition in fuel droplet burning. Combust Flame 1978;31: 285.
21. M. Mawid and S. K. Aggarwal, Chemical kinetics effects on the ignition of a fuel droplet. Combust Sci. and Technol 1989; 65: 137-146.
22. E. K. Buchholtz and M. L. Tapper, Time to extinction of liquid hydrocarbon fuel droplets burning in a transient diesel-like environment. Combust Flame 1978;31:161-172.
23. B. Seth, S. K. Aggarwal, and W.A. Sirignano, Flame propagation through an air-fuel spray mixture with transient vaporization. Combust Flame 1980;39:149-168.
24. S. K. Aggarwal, A. Tong, and W. A. Sirignano, A comparison of vaporization models for spray calculations. AIAA J 1984 ;22(10):1448-1457.
25. G. M. Faeth and D. R. Olson, The ignition of hydrocarbon fuel droplets in air, SAE Transaction 1968;77:1793.
26 T. Saitoh, S. Ishiguro, and T. Niioka, An Experimental study of droplet ignition characteristics near the ignitable limit, Combust Flame 1982;48:27.
27. S. K. Aggarwal, Effects of internal heat transfer models on the ignition of a fuel droplet, Combust. Sci. and Tech. 1985;42:325-34.
28. S.S. Sazhin, W. A. Abdelghaffar, E. M. Sazhina, M. R. Heikal, Models for droplet transient heating: Effects on droplet evaporation, ignition, and break-up. Int J Thermal Sciences 2005;44:610–622.
29. B. J. Wood and W. A. Rosser, An experimental study of fuel droplet ignition, AIAA J. 1989;7 (12): 2288-92.
30. C. K. Law and S. H. Chung, An ignition criterion for droplets in sprays, Combust. Sci. and Technol. 1980;22 (1, 2):17-26.
31. X. Li and M. Renksizbulut, Droplet ignition with variable properties and distinct binary diffusion coefficients, AIAA Journal 1991;29 (7):1131-35.
32. Li, X., Droplet autoignition in a reactive oxidant/fuel-vapor/inert environment, J. Propulsion and Power 1997;13 (1):89-96.
33. A. Makino, Ignition criterion for a fuel droplet expressed in explicit form, Combust. Sci. and Technol. 1991;80:305-317.
34. J. J. Sangiovanni and A. S. Kesten, A theoretical and experimental investigation of the ignition of fuel droplets, Combust. Sci. and Tech. 1977;16:59-70.

35. N. Nishiwaki, Kinetics of liquid combustion processes; evaporation and ignition lag of fuel droplets, Proc. Combust. Inst. 1955;5:148-58.
36. M. M. El-Wakil, and M. I. Abdou, The self ignition of fuel drops in heated air streams. I-experimental data, Fuel 1966;45, 177.
37. T. Kadota, H. Hiroyasu, and H. Oya, Spontaneous ignition delay of a fuel droplet in high pressure and high temperature gaseous environments, Bulletin of the JSME 1976;19:130.
38. C. A, Bergeron, and W. L. H., Hallett, Ignition characteristics of liquid hydrocarbons as single droplets, Canadian J. of Chemical Eng. 1989;67:142-49.
39. C. A, Bergeron, and W. L. H., Hallett, Autoignition of single droplets of two-component liquid fuels, Sci. and Technol. 1989;65 (4-6):181-94.
40. M. Tanabe, M. Kono, J. Sato, J. Koenig, C. Eigenbrod, and H. J. Rath, Effects of natural convection on two-stage ignition of an n-dodecane droplet, Proc. Combust. Inst. 1994;25:933-40.
41. M. Tanabe, M. Kono, J. Sato, J. Koenig, C. Eigenbrod, F. Dinkelacker, and H. J. Rath, Two Stage Ignition of n-Heptane Isolated Droplets, Combust Sci Tech 1995;108:103-19
42. A. J. Marchese, F. L. Dryer, and V. Nayagam, Numerical modeling of isolated n-Alkane droplet flames: initial comparisons with ground and space-based microgravity experiments. Combust. Flame 1999;116:432-59.
43. A. J. Marchese, T. L. Vaughn, K. Kroenlein, and F. L. Dryer, Ignition delay of fatty acid methyl ester fuel droplets: Microgravity experiments and detailed numerical modeling Proc. Combust. Inst. 2011;33:2021-30
44. S. Satcunanathan, Spontaneous ignition of liquid fuel droplets falling through a hot air column, Ind. Eng. Chem Process Des. Develop. 1970;9:359-362.
45. E. M. Goodger, and A. F. M. Eissa, Spontaneous ignition review, review of experimental data, J. Inst. Energy 1987;60:84-94.
46. W. E. Ranz and W. R. Marshall, Evaporation from drops, Parts I and II, Chemical Engineering Prog. 1952;48:141-146 and 173-180.
47. S. Schnaubelt, O. Moriue, T. Coordes, C. Eigenbrod, H. J. Rath, Detailed numerical simulations of the multistage self-ignition process of n-heptane, isolated droplets and their verification by comparison with microgravity experiments, Proc. Combust. Inst. 2000;28: 953–960.
48. A. Cuoci, M. Mehl, G. Buzzi-Ferraris, T. Faravelli, D. Manca, and E. Ranzi, Autoignition and burning rates of fuel droplets under microgravity. Combust Flame 2005;143:211–226.
49. T. Niioka, S. Ishiguro, T. and Saitoh, A numerical approach to fuel droplet ignition, Technical Report of National Aerospace Laboratory, NAL TR-628T, Tokyo, Japan, 1980.
50. N. Shaygan and S. Prakash, Droplet ignition and combustion including liquid-phase heating. Combust. Flame 1995;102:1-10.
51. S.-C. Wong, T.-S. Hsu, and J.-C. Chang, Validity of droplet ignition criterion derived assuming gas-phase quasisteadiness, J. Propulsion and Power 1996;12(1):18-25.
52. S.-H. Wang, C.-C. Chiu, and S.-C. Wong, Validity of quasi-steady gas-phase ignition criterion for droplets in sprays, 16th ICDERS, August 1997.
53. P. Botros, C. K. Law, and W. A. Sirignano, Combust. Sci. and Tech. 1980;21:123-30.
54. M. Takei, T. Tsukamoto, and T. Niioka, Ignition of blended-fuel droplet in high-temperature atmosphere. Combust. Flame 1993;93:149-56.

55. U. Niemann, R. Seiser, and K. Seshadri, Ignition and extinction of low molecular weight esters in nonpremixed flows, Combustion Theory & Modelling, 2010; 14(6):875-891.
56. C. K. Law and P. Zhao, NTC-affected ignition in nonpremixed counterflow. Combust Flame 2012;159:1044–1054.
57. M. Tanabe, T. Bolik, C. Eigenbrod, H.J. Rath, J. Sato, and M. Kono, Spontaneous ignition of liquid droplets from a view of nonhomogeneous mixture formation. Proc. Combust. Inst. 1996;26: 1637-1643.
58. H. J. Curran, W. J. Pitz, C. K. Westbrook, C. V. Callahan, and F. L. Dryer, Oxidation of automotive primary reference fuels at elevated pressures, Proc. Combust. Inst. 1998;27:379-87.
59. R. Stauch, S. Lipp, and U. Maas, Detailed numerical simulations of the autoignition of single n-heptane droplets in air. Combust Flame 2006;145:533–542.
60. J.-R. Yang, S.-C. Wong, On the suppression of negative temperature coefficient (NTC) in autoignition of n-heptane droplets, Combust Flame 2003;132:475–91.
61. O. Moriue, C. Eigenbrod. H. J. Rath, J. Sato, K. Okai, M. Tsue, and M. Kono, Effects of dilution by aromatic hydrocarbons on staged Ignition behavior of n-decane droplets, Proc. Combust. Inst. 2000;28: 969–975.
62. S. K. Aggarwal and H. Mongia, Multicomponent and high-pressure effects on droplet vaporization, ASME J. Eng. Gas Turbines Power. 2002;124:248–257.
63. S. K. Aggarwal, C. Yan, and G. Zhu, On the transcritical vaporization of a liquid fuel droplet in supercritical ambient, Combust. Sci. Technol. 2002;174 (9):103-130, 2002.
64. G. Zhu and S. K. Aggarwal, Transient supercritical droplet evaporation with emphasis on the effects of equation of state, Int. J. Heat Mass Transfer. 2000;43:1157–1171.
65. G. Zhu, R. D. Reitz, and S. K. Aggarwal, Gas-phase unsteadiness and its influence on droplet vaporization in sub- and super-critical environments, Int. J. of Heat & Mass Transfer. 2001;44(16):3081-3093.
66. G. Zhu and S. K. Aggarwal, Fuel droplet evaporation in a supercritical environment, ASME-J. Eng. for Gas Turbines and Power. 2002;124 (10):762-770.
67. R. Nakanishi, H. Koyabashi, S. Kato, and T. Niioka, Ignition experiment of a fuel droplet in high-pressure, high-temperature ambient, Proc. Combust. Inst. 1994;25:447-53.
68. R. H. Rangel and A. C. Fernandez-Pello, Prog. Aero. & Astro. 1986;105:239-248.
69. S. K. Dash and S. K. Som, Ignition and combustion of liquid fuel droplet in a convective medium, ASME J. Energy Resources Technology. 1991;113 (3):165-170.
70. J. T. Yang, and G. T. Tsai, Combust. Sci. and Technol. 1994;96:1-14.
71. J. H. Kim, and S. H. Park, Numerical study on combustion of a liquid fuel droplet, Numerical Heat Transfer Part A. 1996;29:843-858.
72. J.-J. Whang, C.-Y. Yukao, J.-T. Ho, and S.-C., Wong, Experimental study of the ignition of single droplets under forced convection, Combust. Flame. 1997;110:366-376.
73. S.-C., Wong, X.-X. Liao, and J.-R. Yang, A simplified theory of the ignition of single droplets under forced convection, Combust. Flame. 1997;110:319-334.
74. R. Stauch and U. Maas, The ignition of methanol droplets in a laminar convective environment, Combust. Flame. 2008;153:45-57.
75. Chiu, H. H., and Liu, T. M., Group combustion of liquid droplets, Combust. Sci. Technol. 1977;17 (3-4):127-142.

76. Chiu, H. H., Kim, H. Y., and Croke, E. J., Internal group combustion of liquid droplets, Proc. Combust. Inst. 1982;19 (1):971-980.
77. S. M., Correa and M. Sichel, The group combustion of a spherical cloud of monodisperse fuel droplets, Proc. Combust. Inst. 1982;19 (1):981-991.
78. G. Chen and A. Gomez, Dilute laminar spray diffusion flames near the transition from group combustion to individual droplet burning, Combust. Flame. 1997;110 (3):392-404.
79. M. Mikami, K. Yamamoto, O. Moriue, and N. Kojima, Combustion of partially premixed spray jets, Proc. Combust. Inst. 2005;30;2021–2028.
80. R. T. Imaoka and W. A. Sirignano. Transient vaporization and burning in dense droplet arrays. Int. J. Heat Mass Transfer. 2005;48:4354–4366.
81. C.H. Beck, R. Koch, H.-J. Bauer, Identification of droplet burning modes in lean, partially prevaporized swirl-stabilized spray flames, Proc. Combust. Inst. 2009;32;2195–2203.
82. M. Boileau, G. Staffelbach, B. Cuenot, T. Poinsot, C. Bérat, LES of an ignition sequence in a gas turbine engine, Combust. Flame. 2008;154:2-22.
83. A. Neophytou, E. Mastorakos, R.S. Cant, DNS of spark ignition and edge flame propagation in turbulent droplet-laden mixing layers, Combust. Flame. 2010;157:1071–1086.
84. S. H. Kang, S. W. Baek, and J. H. Choi, Autoignition of Sprays in a cylindrical combustor, J. Heat Mass Transfer. 2001;44:2413–2422.
85. W. O'Loughlin and A. R. Masri, A new burner for studying auto-ignition in turbulent dilute sprays, Combust. Flame. 2011;158:1577-1590.
86. Y. Wang and C. J. Rutland, Direct numerical simulation of ignition in turbulent n-heptane liquid-fuel spray jets, Combust. Flame. 2007;149:353-365.
87. G. Borghesi, E. Mastorakos, and R. S. Cant, Complex chemistry DNS of n-heptane spray autoignition at high pressure and intermediate temperature conditions, Combust. Flame. 2013;160:1254-1275.
88. S. K. Aggarwal and W. A. Sirignano, Ignition of fuel sprays: deterministic calculations for idealized droplet arrays. Proc. Combust. Inst. 1985;20:1773–80.
89. M. Mawid And S. K. Aggarwal, Analysis of dropwise ignition versus external ignition for dilute muiticomponent fuel sprays, Combust. Flame. 1990;81:59-72.
90. R. H. Rangel and G. Continillo. Theory of vaporization and ignition of a droplet cloud in the field of a vortex. Proc. Combust. Inst. 1992;24:1493–15012.
91. K. Annamalai W. Ryan, Interactive processes in gasification and combustion-II: isolated carbon/coal and porous char particles, Prog. Energy Combust. Sci. 1993;19:383-446.
92. K. Annamalai, W. Ryan and S. Dhanapalan, Interactive processes in gasification and combustion, part iii: coal particle arrays, streams and clouds," Prog. Energy Combust. Sci. 1994;20:487-618.
93. S.-C. Wong, J.-C. Chang, and J.-C. Yang. Autoignition of droplets in nondilute monodisperse clouds, Combust. Flame. 1993;94:397-406.
94. J. Bellan and K. Harstad, Ignition of a binary-fuel (solvent-solute) cluster of drops, Combust. Sci. Technol. 1995;8:531-548.
95. J. Bellan and K. Harstad, Ignition of nondilute clusters of drops in convective flows. Combust. Sci. Technol. 1987;53:75–87.
96. D. Segawa, M. Yoshida, S. Nakaya, T Kadota, Autoignition and early flame behavior of a spherical cluster of 49 monodispersed droplets, Proc. Combust. Inst. 2007;31:2149–56.

97. H. A. Dwyer, P. Stapf, R. Maly, Unsteady vaporization and ignition of a three-dimensional droplet array. Combust. Flame. 2000;121:181–94.
98. O. Moriue, Y. Nishiyama, Y. Yamaguchi, H. Hashimoto, E. Murase, Effects of droplet interaction on spontaneous ignition of an n-decane droplet pair, Proc. Combust. Inst. 2013;34:1585–92.
99. D. Shringi, H.A. Dwyer, B.D. Shaw, Influences of support fibers on vaporizing fuel droplets, Computers & Fluids. 2013;77(1):66-75.
100. D. Foresti, M. Nabavi, M. Klingauf, A. Ferrari, D. Poulikakos, Acoustophoretic contactless transport and handling of matter in air, PNAS. 2013, doi: 10.1073/pnas.1301860110 .
101. M. Birouk, I. Gökalp, Current status of droplet evaporation in turbulent flows, Prog. Energy Combust. Sci. 2006;32 (4):408-423.
102. M. Birouk, C. Chauveau, and I. Gökalp, Turbulence effects on the combustion of single hydrocarbon droplets, Proc. Combust. Inst. 2000;28:1015–1021.

Figure Captions

Fig. 1: A schematic of a two-phase mixture ignited in the thermal boundary layer of a heated surface. Three different ignition modes, namely, the droplet ignition, droplet cluster ignition, and spray ignition are illustrated. From Ref. 1.

Fig. 2: Characteristic S-curve showing all possible modes of droplet gasification, including pure vaporization ($D \sim 0$), ignition ($D = D_I$), pure combustion ($D = \infty$) and extinction ($D = D_E$). From Ref. 19.

Fig. 3: Variation of the perturbed temperature in the reaction zone as a function of the stretched variable for $\beta = 0.5$ and different Damköhler numbers. From Ref. 21.

Fig. 4: Maximum perturbed temperature (corresponding to X —>∞ in Fig. 3) versus D for different values of β. From Ref. 21.

Fig. 5: Variation of ignition Damköhler number with β. From Ref. 21.

Fig. 6: Computed and measured ignition delays plotted as a function of the initial drop size for n-hexadecane droplets. From Ref. 21.

Fig. 7: Computed and measured ignition delays plotted versus ambient temperature for n-hexadecane droplets. From Ref. 21.

Fig. 8: Computed and measured ignition limits for n-hexadecane droplets. Curve A: C_{pl} = 0.69 cal/gm/K, p = 1 atm, B: C_{pl} = 0.52 cal/gm/K, p = 1 atm, C: Same as curve A but activation energy reduced by 12 percent, D: C_{pl} = 0.69 cal/gm/K, p = 10 atm. From Ref. 27.

Fig. 9: Ignition Damköhler number as function of heat transfer parameter (β) and fuel concentration parameter (γ). From Ref. 30.

Fig. 10: Measured ignition delay time versus droplet diameter for n-heptane droplets for different ambient gas temperatures. From Ref. 26.

Fig. 11: Measured ignition delay time versus droplet diameter for n-hexadecane droplets for two different ambient temperatures. From Ref. 26.

Fig. 12: Predicted and measured ignition delay times for n-hexadecane droplets as a function of droplet diameter. From Ref. 38.

Fig. 13: Predicted and measured ignition delay times plotted as a function of droplet diameter for different fuels. From Ref. 38.

Fig. 14: Two-stage ignition process for a n-heptane droplet illustrated by the temporal variation of the peak gas temperature. The droplet diameter=0.7 mm, Ta= 650 K, and p= 5 atm. The first (τ_1), second (τ_2), and total ignition times are indicated. From Ref. 47.

Fig. 15: Various ignition regions mapped in terms of ambient temperature and pressure under normal-gravity conditions. From Ref. 39.

Fig. 16: Comparison of ignition delays plotted as a function of ambient temperature under normal and microgravity conditions. Solid symbols: μg data and open symbols: 1g data. From Ref. 40.

Fig. 17: Temporal history of the (nondimensional) radial temperature profiles showing the ignition event. From Ref. 49.

Fig. 18: Predicted gas temperature profiles at different times before and at the instant of ignition for n-heptane fuel droplet in air at a temperature of 1000 K. From Ref. 50.

Fig. 19: Ignition delay time predicted using the QSDI and transient models and plotted versus the initial droplet temperature for (a) n-heptane, and (b) n-hexadecane droplets. From Ref. 51.

Fig. 20: Ignition delay time predicted using the QSDI and transient models and plotted versus ambient temperature for (a) n-heptane, and (b) n-hexadecane droplets. From Ref. 51.

Fig. 21: Ignition delay time predicted by using the QSDI and transient models and plotted versus initial droplet diameter for (a) n-heptane, and (b) n-hexadecane droplets. From Ref. 51.

Fig. 22: Comparison of the measured and computed ignition delays using the QSDI and transient models. Here QSGP and TR denote quasi-steady gas phase, and transient models, respectively. From Ref. 51.

Fig. 23: Comparison of ignition delays versus inter-droplet spacing obtained by using the quasi-steady and transient gas-phase models for n-heptane droplets. Here TR and QSGP refer to the transient and quasi-steady models respectively. From Ref. 52.

Fig. 24: Predicted droplet ignitability in terms of the minimum ambient temperature for ignition plotted as a function of the non-dimensional inter-droplet spacing. Predictions are based on the QSDI and transient (TR) models. From Ref. 52.

Fig. 25: Temporal variation of OH mole fraction and temperature for the ignition of homogeneous n-dodecane/air mixture for three different initial temperatures. Two-stage ignition is clearly indicated for the 830 K case. Here τ is the ignition delay time.

Fig. 26: (a) Total ignition delay (or induction time) versus ambient temperature at different pressures; (b) Various ignition regimes for the ignition of a n-heptane droplet with initial diameter of 0.7-0.75 mm. From Ref. 60.

Fig. 27: Various ignition regimes shown in terms of the temporal evolution of the maximum gas temperature. Top figure from Schnaubelt et al. [47] is for n-heptane droplet, while the bottom figure from Cuoci et al. [48] is for n-decane droplet.

Fig. 28: (a) Temporal evolution of peak gas temperature for different droplet diameters (top). (b) Ignition delay plotted versus initial diameter for different ambient temperatures. From Ref. 60.

Fig. 29: Comparison of predicted and measured first and total ignition times. Droplet diameter is 0.7 mm. Top figure from Schnaubelt et al. [47] is for n-heptane at p=5 atm, and bottom figure from Couci et al. [48] for n-decane at p=3 atm.

Fig. 30: Ignition location plotted with respect to initial droplet radius. From Ref. 59.

Fig. 31: Measured ignition delay versus initial droplet diameter for different pressures. Fiber-suspended n-hexadecane droplet in an electric furnace. From Ref. 67.

Fig. 32: Measured ignition delay versus pressure for fiber-suspended n-hexadecane droplets in an electric furnace. From Ref. 67.

Fig. 33: Predicted ignition delay time as a function of droplet diameter for n-heptane and n-hexadecane droplets for different ambient pressures. The ambient gas temperature is 973 K. From Ref. 46.

Fig. 34: Radial profiles of gas temperature and fuel vapor mass fraction at the time of ignition for two different pressures. From Ref. 47.

Fig. 35: Ignition delays for homogeneous n-heptane/air mixture and for droplets (initial diameter=100 mm) plotted versus pressure for T_a=1200 K. From Ref. 59.

Fig. 36: Measured first-ignition (top) and second-ignition delay times versus ambient temperature for different compositions of ND/MN and ND/TMB blends. Droplet diameter is 0.7mm and pressure is 3 atm. Parameter Z represents the fraction of n-decane in the blend. From Ref. 61

Fig. 37: Normal-gravity ignition delay versus ambient temperature for 1.2 mm droplets of methyl decanoate, methyl dodecanoate, methyl oleate, SE-1885 soy methyl ester and commercial B99 soy methyl ester. Pressure is 1 atm. From Ref. 43.

Fig. 38: Temporal variation of the maximum gas temperature for three different droplet Reynolds numbers. Here time is normalized by the momentum diffusion time, $\tau = t\,\mu_\infty / a_o^2\,\rho_\infty$. From Ref. 71.

Fig. 39: Three flame regimes represented in ambient temperature-Reynolds number space. From Ref. 71.

Fig. 40: Normalized ignition location in the droplet wake plotted as a function of ambient temperature for different initial diameters. From Ref. 72.

Fig. 41: Measured ignition delay time versus initial diameter for n-heptane and n-hexadecane droplets. The open and filled symbols respectively indicate the times when ignition occurs and when an envelope flame forms. From Ref. 72.

Fig. 42: Measured ignition delay time versus ambient temperature for n-heptane droplets in forced and natural convection. From Ref. 72.

Fig. 43: The computed and measured ignition delay time (Fig. a) and ignition location (Fig. b) plotted versus ambient temperature for 1.55 mm n-hexadecane droplets. From Ref. 73.

Fig. 44: The computed and measured ignition delay time (Fig. a) and ignition location (Fig. b) plotted versus initial droplet diameter for n-hexadecane droplets. From Ref. 73.

Fig. 45: The effect of freestream velocity on the computed ignition delay times and ignition locations. From Ref. 73.

Fig. 46. Computed ignition delay time for a methanol droplet plotted versus the Reynolds number ($p = 7$ bar, $d_o = 400$ μm). From Ref. 74.

Fig. 47. A schematic of droplet/spray combustion regimes in terms of the non-dimensional Group number. From Ref. 75.

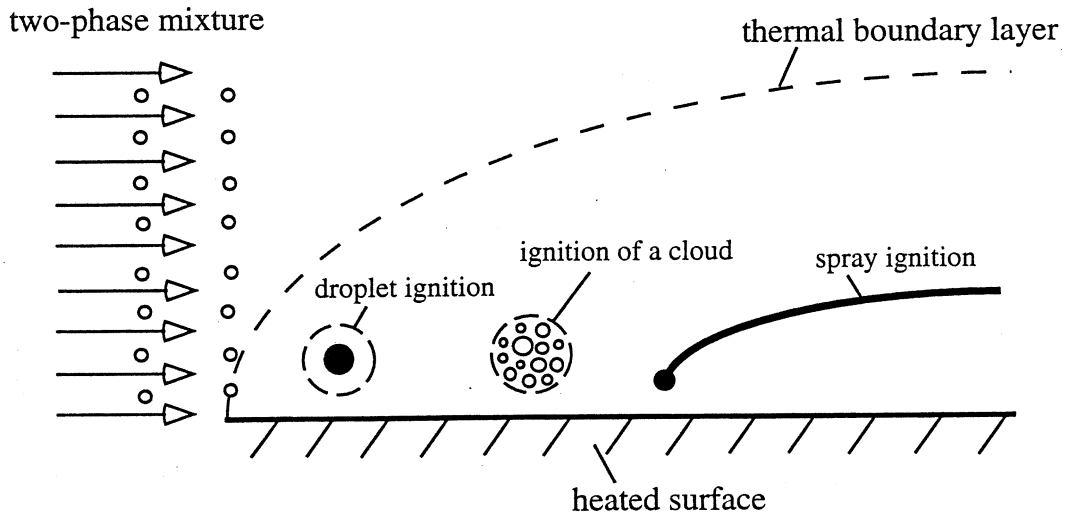
two-phase mixture
thermal boundary layer
droplet ignition
ignition of a cloud
spray ignition
heated surface

Figure 1.

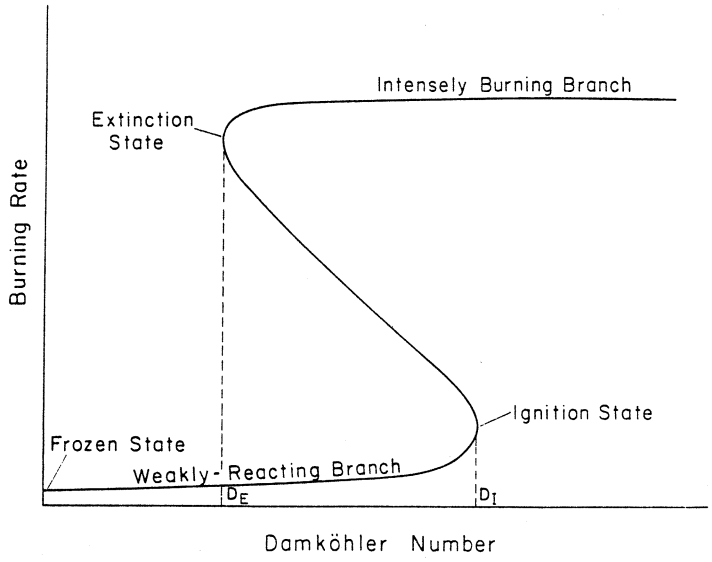
Intensely Burning Branch
Extinction State
Burning Rate
Ignition State
Frozen State
Weakly-Reacting Branch
D_E
D_I
Damköhler Number

Figure 2.

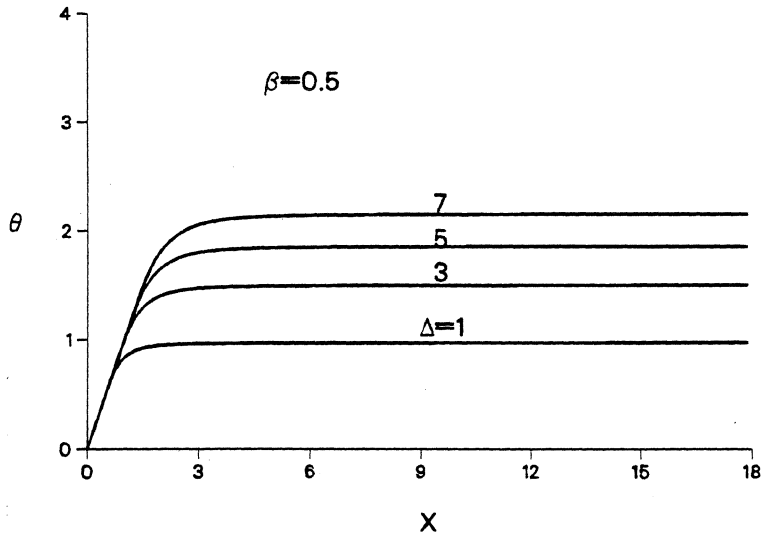

Figure 3.

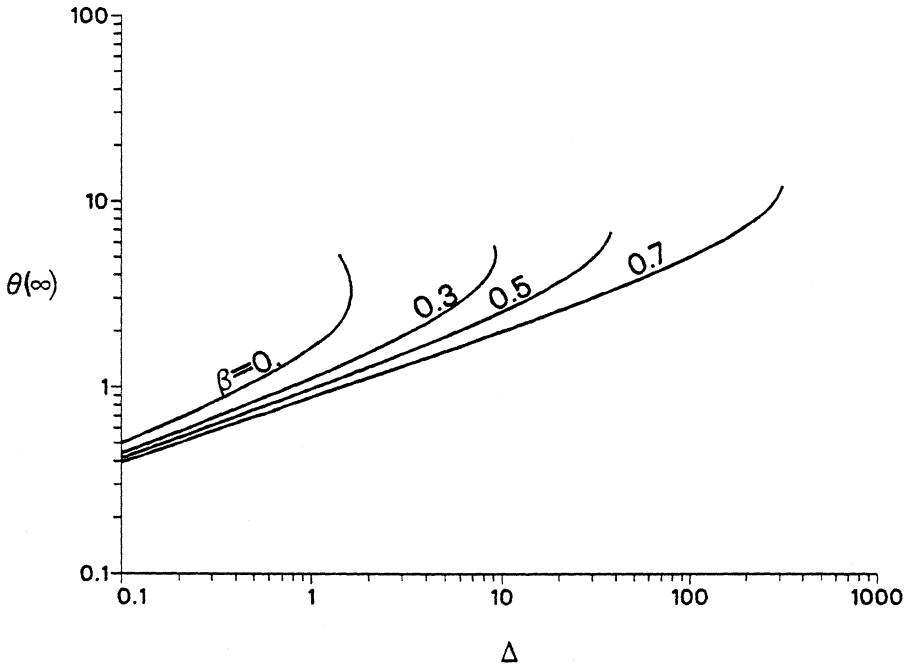

Figure 4.

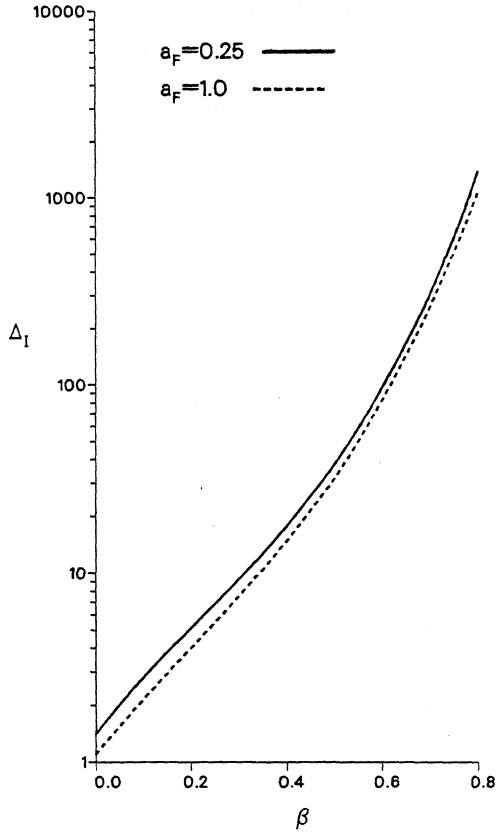

Figure 5.

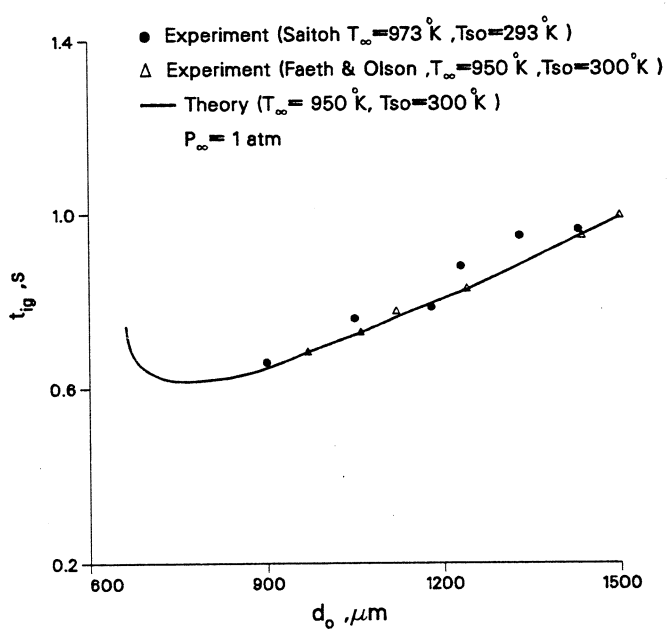
● Experiment (Saitoh T_∞=973 °K ,Tso=293 °K)
Δ Experiment (Faeth & Olson ,T_∞=950 °K ,Tso=300 °K)
—— Theory (T_∞= 950 °K, Tso=300 °K)
P_∞= 1 atm
1.4
1.0
0.6
0.2
t_{ig} ,s
600
900
1200
1500
d_o ,μm

Figure 6.

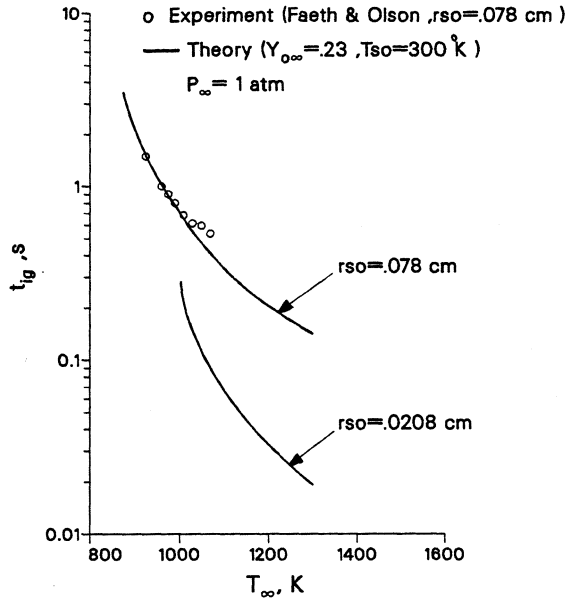
o Experiment (Faeth & Olson ,rso=.078 cm)
Theory ($Y_{O\infty}$=.23 ,Tso=300 °K)
P_∞= 1 atm
rso=.078 cm
rso=.0208 cm
t_{ig} ,s
T_∞, K
10
1
0.1
0.01
800
1000
1200
1400
1600

Figure 7.

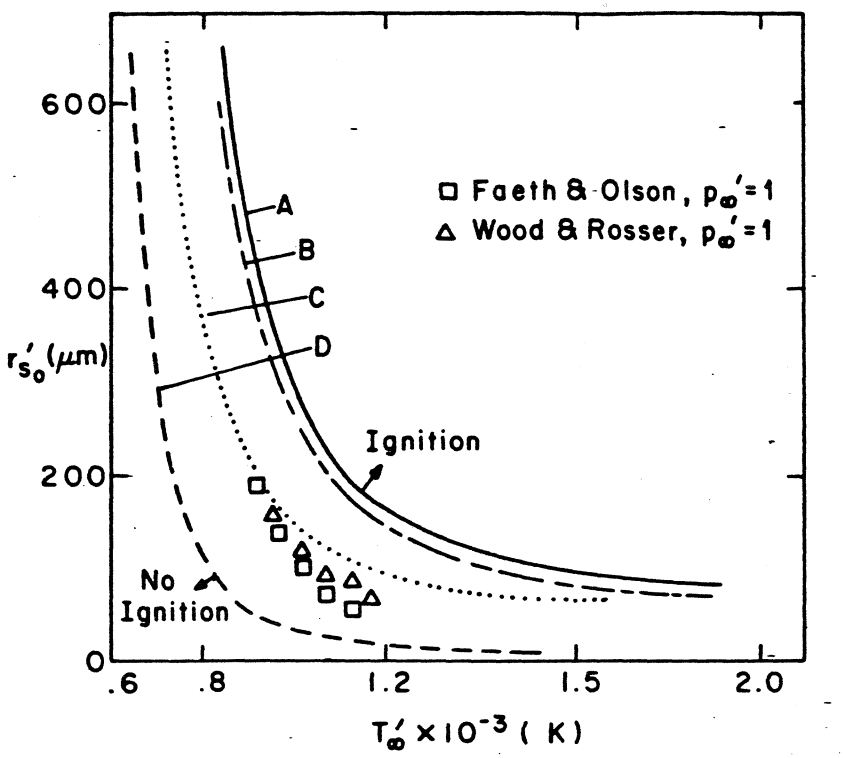
600
400
200
0
r'_{s_0} (μm)
A
B
C
D
Ignition
No Ignition
□ Faeth & Olson, $p'_\infty = 1$
△ Wood & Rosser, $p'_\infty = 1$
.6
.8
1.2
1.5
2.0
$T'_\infty \times 10^{-3}$ (K)

Figure 8.

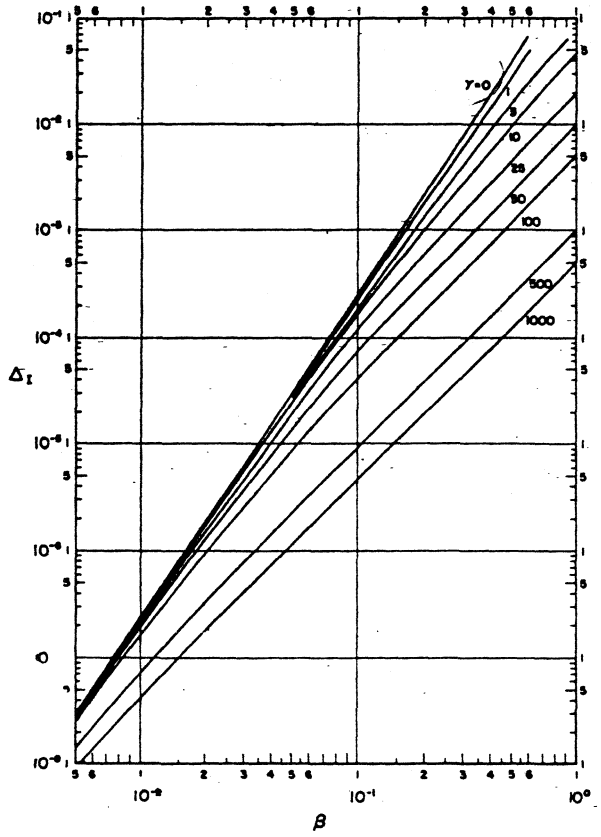

Figure 9.

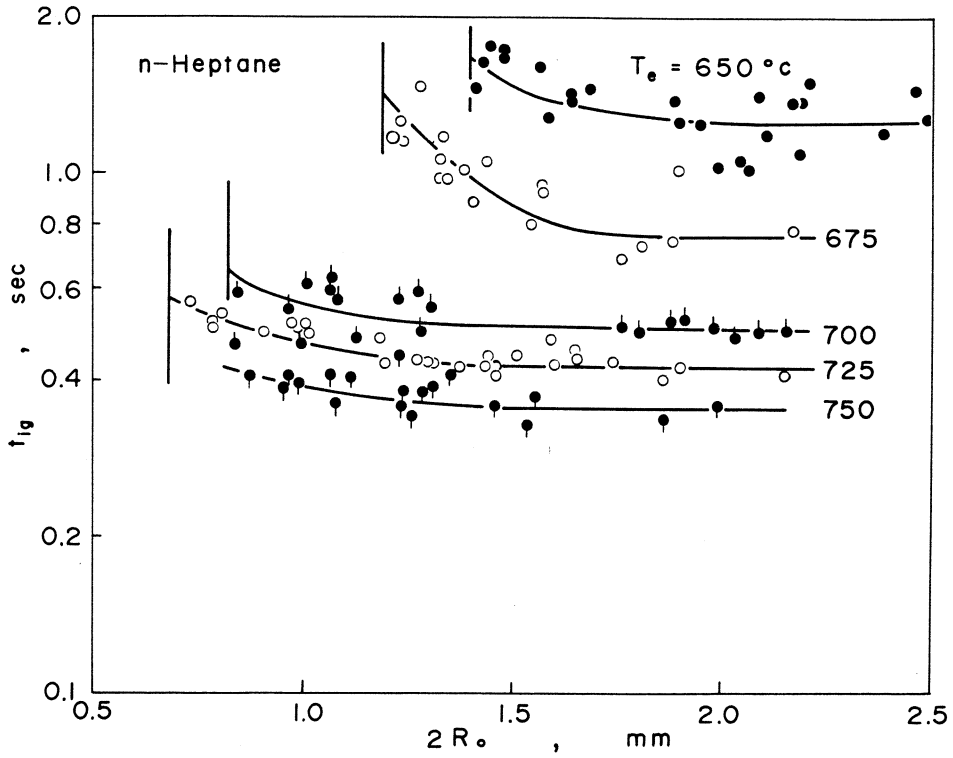
n-Heptane
T_e = 650 °c
675
700
725
750
t_{lg} , sec
2.0
1.0
0.8
0.6
0.4
0.2
0.1
0.5
1.0
1.5
2.0
2.5
2 R_o , mm

Figure 10.

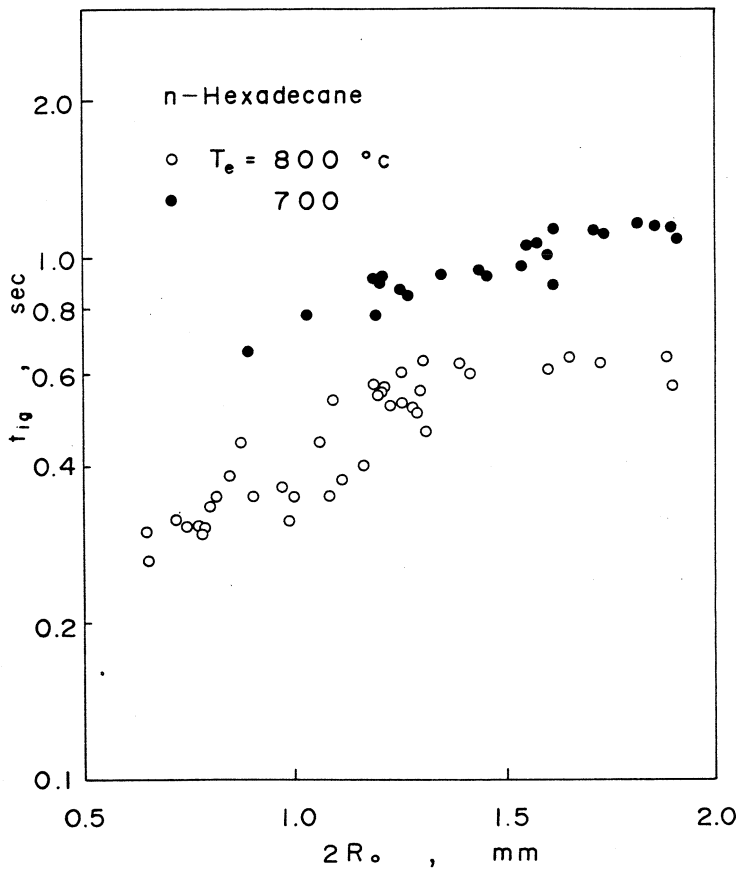
n-Hexadecane
T_e = 800 °C
700
2.0
1.0
0.8
0.6
0.4
0.2
0.1
sec
t_{ig}
0.5
1.0
1.5
2.0
$2R_o$, mm

Figure 11.

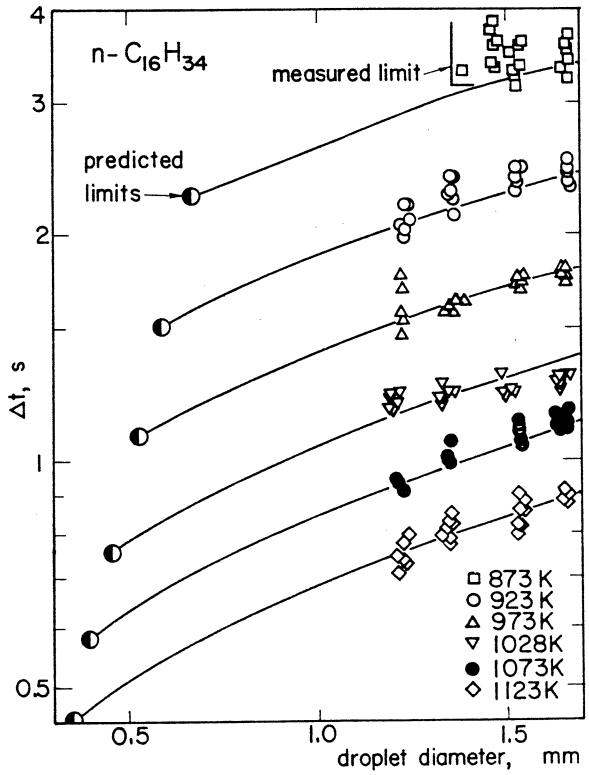
n-C16H34
measured limit
predicted
limits
Δt, s
4
3
2
1
0.5
0.5
1.0
1.5
droplet diameter, mm
873K
923K
973K
1028K
1073K
1123K

Figure 12.

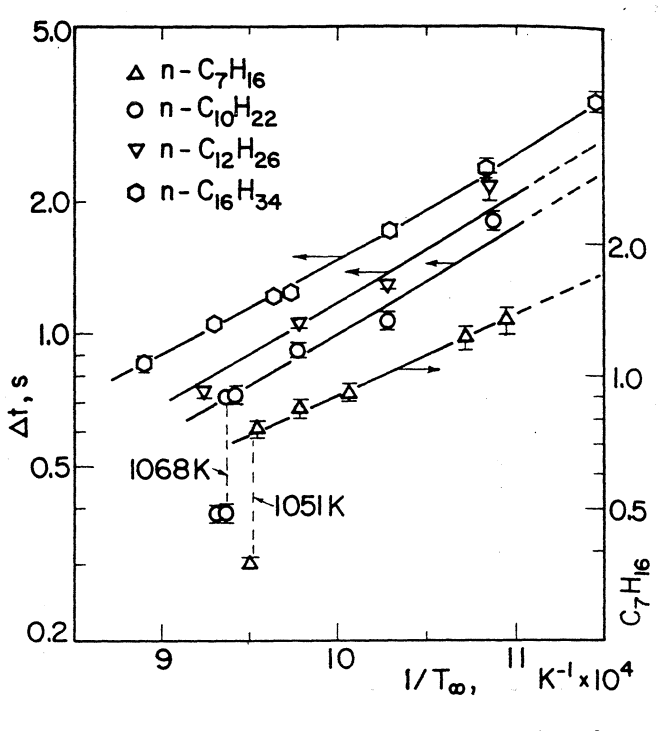
5.0
2.0
1.0
0.5
0.2
Δt, s
n - C7H16
n - C10H22
n - C12H26
n - C16H34
1068K
1051K
2.0
1.0
0.5
C7H16
9
10
11
1/T∞, K-1 x 10^4

Figure 13.

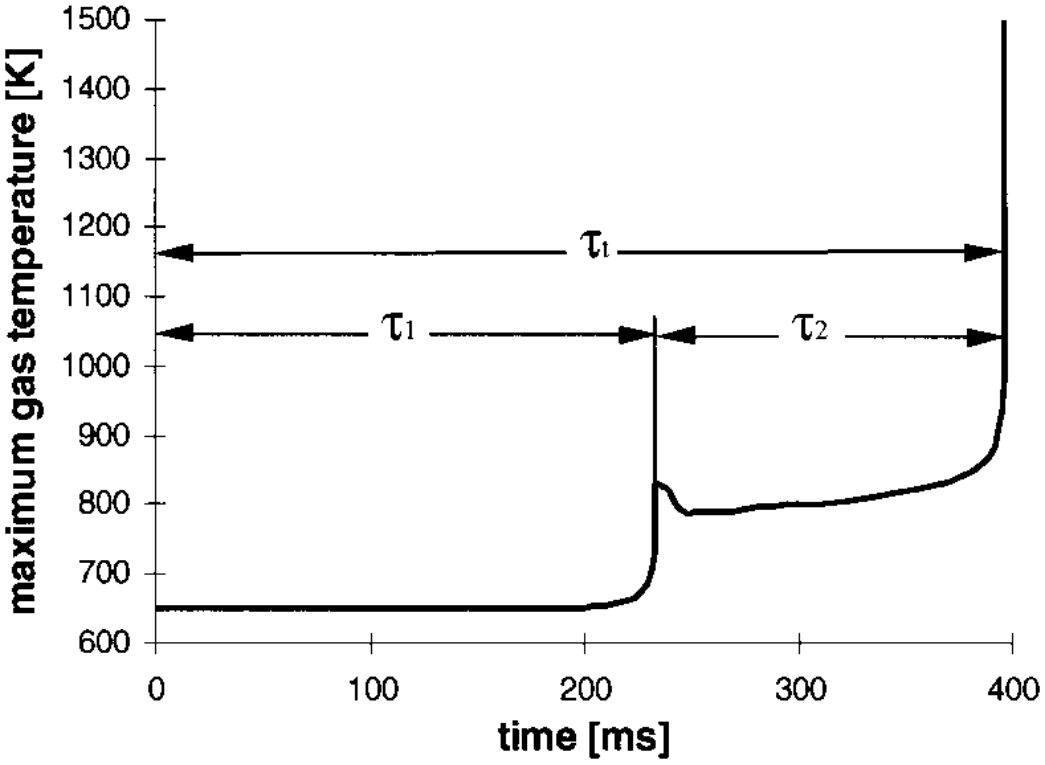
maximum gas temperature [K]
1500
1400
1300
1200
1100
1000
900
800
700
600
0
100
200
300
400
time [ms]
τt
τ1
τ2

Figure 14

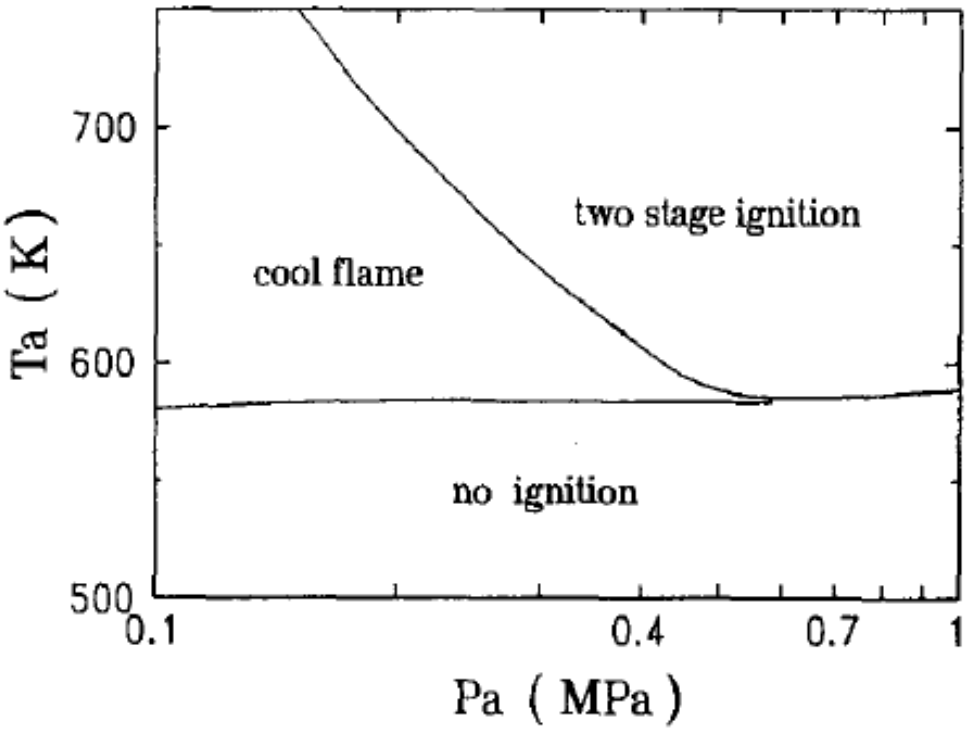
700
600
500
Ta (K)
two stage ignition
cool flame
no ignition
0.1
0.4
0.7
1
Pa (MPa)

Figure 15

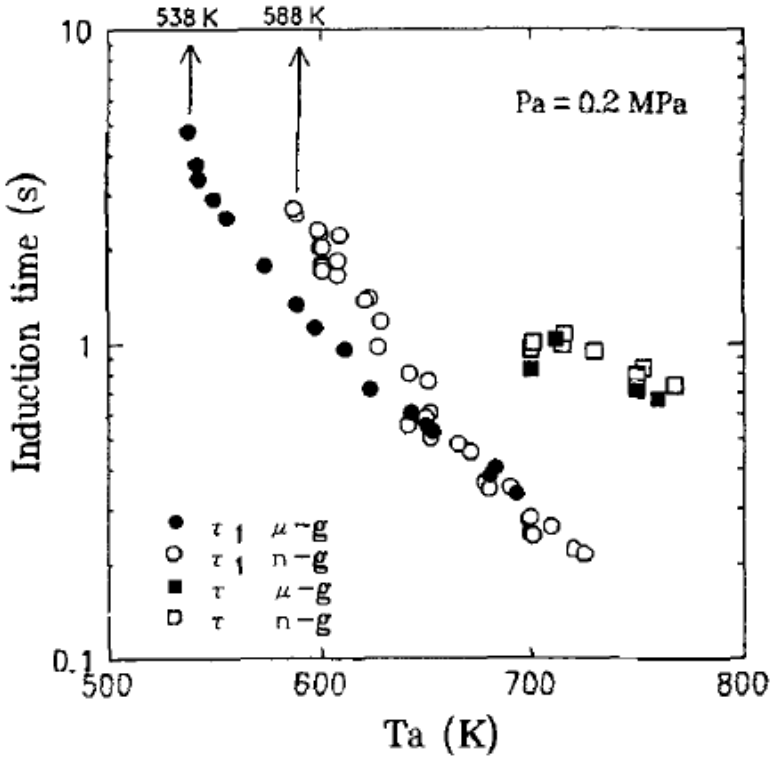
538 K
588 K
Pa = 0.2 MPa
Induction time (s)
10
1
0.1
500
600
700
800
Ta (K)
τ1 μ-g
τ1 n-g
τ μ-g
τ n-g

Figure 16

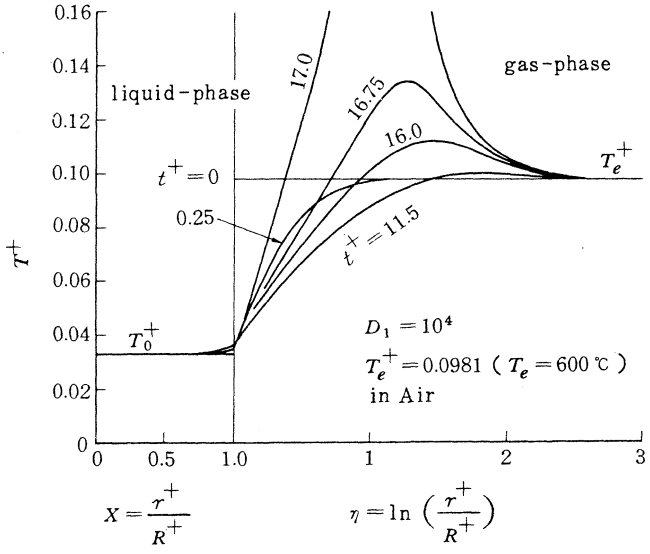
0.16
0.14
0.12
0.10
0.08
0.06
0.04
0.02
0
T^+
liquid-phase
gas-phase
17.0
16.75
16.0
T_e^+
$t^+=0$
0.25
$t^+=11.5$
T_0^+
$D_1=10^4$
$T_e^+=0.0981$ ($T_e=600$ ℃)
in Air
0
0.5
1.0
1
2
3
$X=\frac{r^+}{R^+}$
$\eta=\ln\left(\frac{r^+}{R^+}\right)$

Figure 17

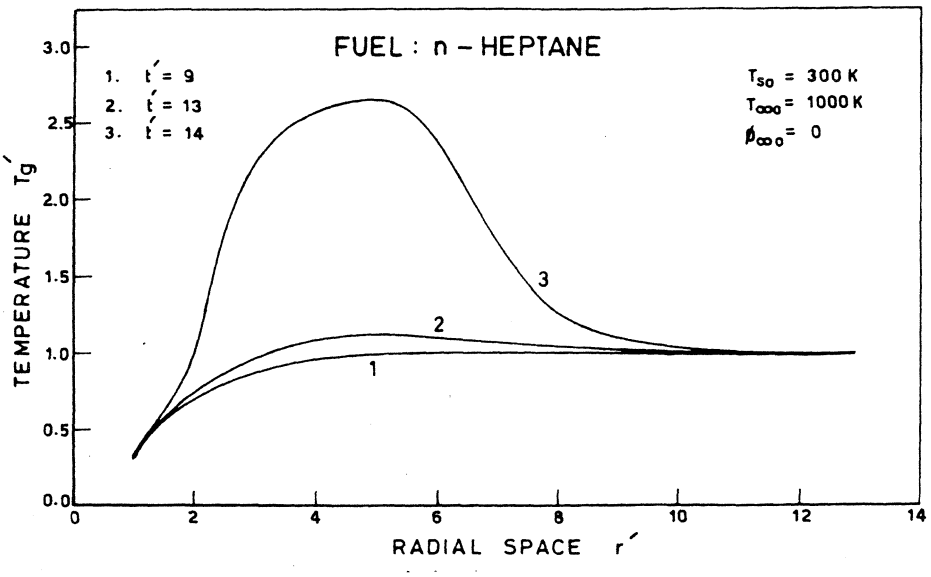
FUEL : n – HEPTANE
1. t´ = 9
2. t´ = 13
3. t´ = 14
T_{s_0} = 300 K
T_{∞_0} = 1000 K
ϕ_{∞_0} = 0
TEMPERATURE Tg´
RADIAL SPACE r´
3.0
2.5
2.0
1.5
1.0
0.5
0.0
0
2
4
6
8
10
12
14
1
2
3

Figure 18

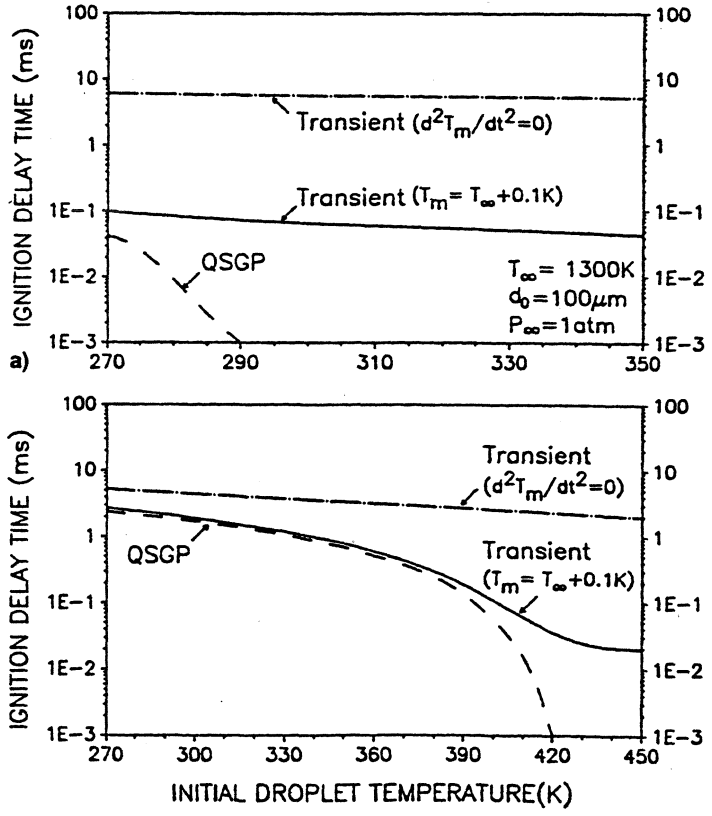
IGNITION DELAY TIME (ms)
100
10
1
1E−1
1E−2
1E−3
Transient ($d^2T_m/dt^2=0$)
Transient ($T_m = T_\infty+0.1K$)
QSGP
T_∞= 1300K
$d_0=100\mu m$
P_∞=1atm
a)
270
290
310
330
350
IGNITION DELAY TIME (ms)
Transient
($d^2T_m/dt^2=0$)
QSGP
Transient
($T_m = T_\infty+0.1K$)
300
330
360
390
420
450
INITIAL DROPLET TEMPERATURE(K)

Figure 19

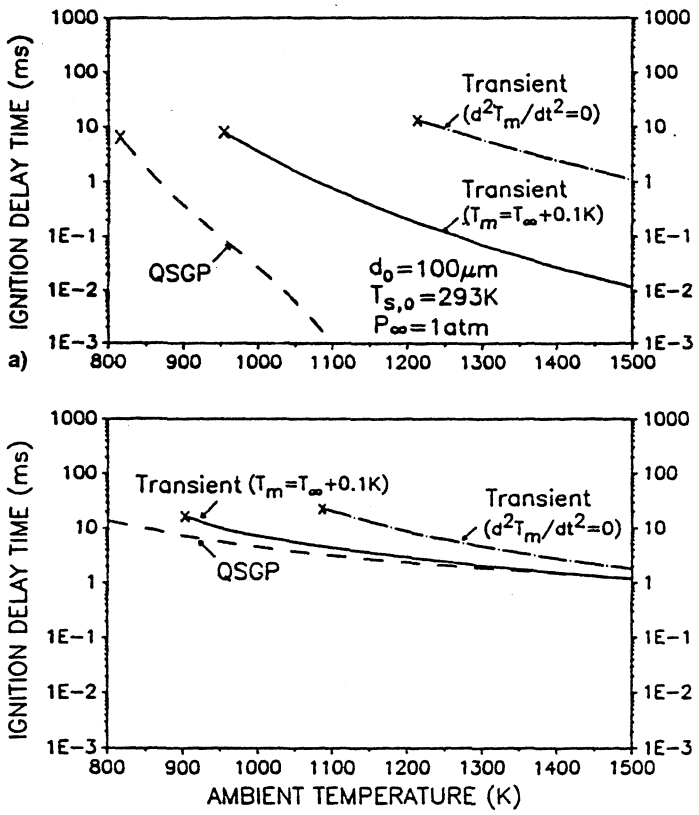
a)
IGNITION DELAY TIME (ms)
1000
100
10
1
1E−1
1E−2
1E−3
800
900
1000
1100
1200
1300
1400
1500
Transient
(d²Tm/dt²=0)
Transient
(Tm=T∞+0.1K)
QSGP
d0=100μm
Ts,0=293K
P∞=1atm
IGNITION DELAY TIME (ms)
Transient (Tm=T∞+0.1K)
Transient
(d²Tm/dt²=0)
QSGP
AMBIENT TEMPERATURE (K)

Figure 20

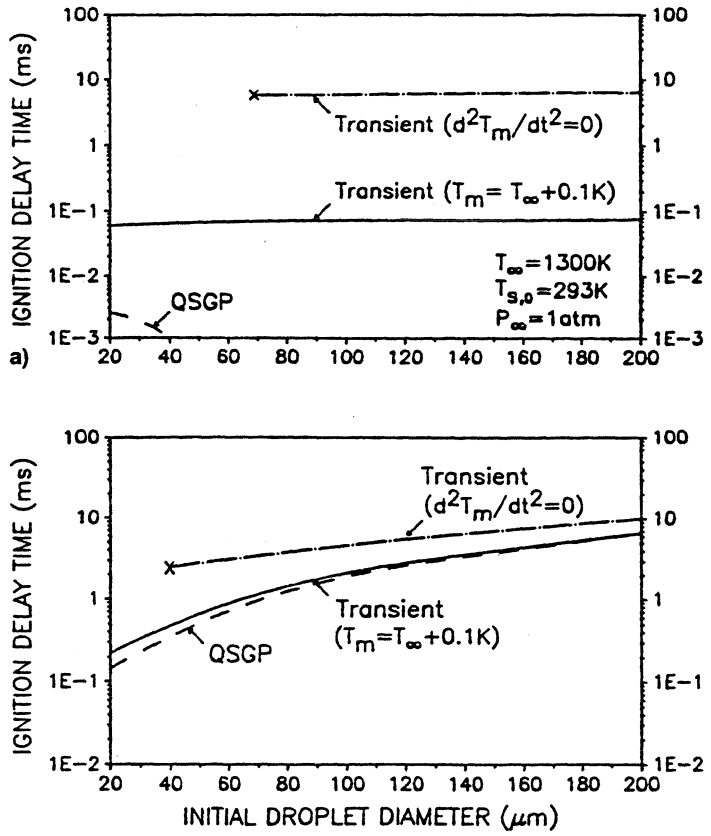
a)
IGNITION DELAY TIME (ms)
100
10
1
1E−1
1E−2
1E−3
20
40
60
80
100
120
140
160
180
200
Transient ($d^2T_m/dt^2=0$)
Transient ($T_m = T_\infty+0.1K$)
QSGP
T_∞=1300K
$T_{g,0}$=293K
P_∞=1atm
IGNITION DELAY TIME (ms)
Transient
($d^2T_m/dt^2=0$)
Transient
($T_m=T_\infty+0.1K$)
QSGP
1E−2
INITIAL DROPLET DIAMETER (μm)

Figure 21

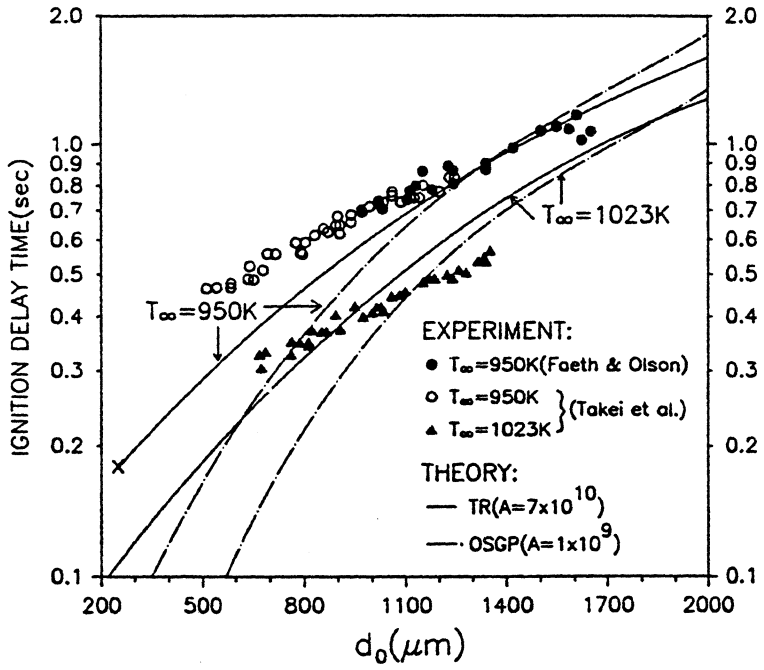
IGNITION DELAY TIME(sec)
2.0
1.0
0.9
0.8
0.7
0.6
0.5
0.4
0.3
0.2
0.1
200
500
800
1100
1400
1700
2000
$d_0(\mu m)$
T_∞=950K
T_∞=1023K
EXPERIMENT:
T_∞=950K(Faeth & Olson)
T_∞=950K
T_∞=1023K
(Takei et al.)
THEORY:
TR(A=7x10^{10})
OSGP(A=1x10^{9})

Figure 22

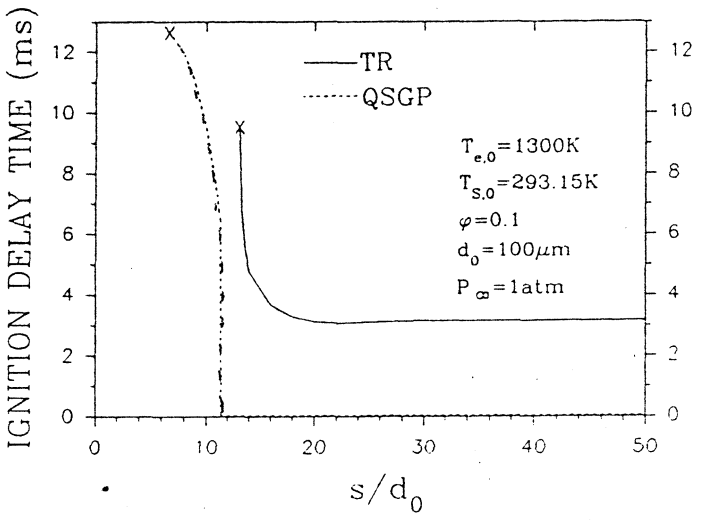
IGNITION DELAY TIME (ms)
TR
QSGP
$T_{e,0}$=1300K
$T_{S,0}$=293.15K
φ=0.1
d_0=100μm
P_∞=1atm
s/d_0
0
2
4
6
8
10
12
0
10
20
30
40
50

Figure 23

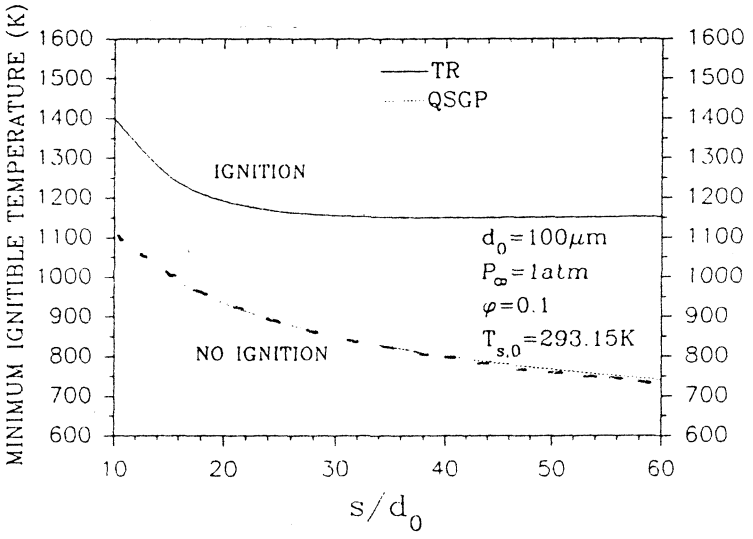
MINIMUM IGNITIBLE TEMPERATURE (K)
1600
1500
1400
1300
1200
1100
1000
900
800
700
600
TR
QSGP
IGNITION
NO IGNITION
$d_0=100\mu m$
$P_\infty=1atm$
$\varphi=0.1$
$T_{s,0}=293.15K$
10
20
30
40
50
60
s/d_0

Figure 24

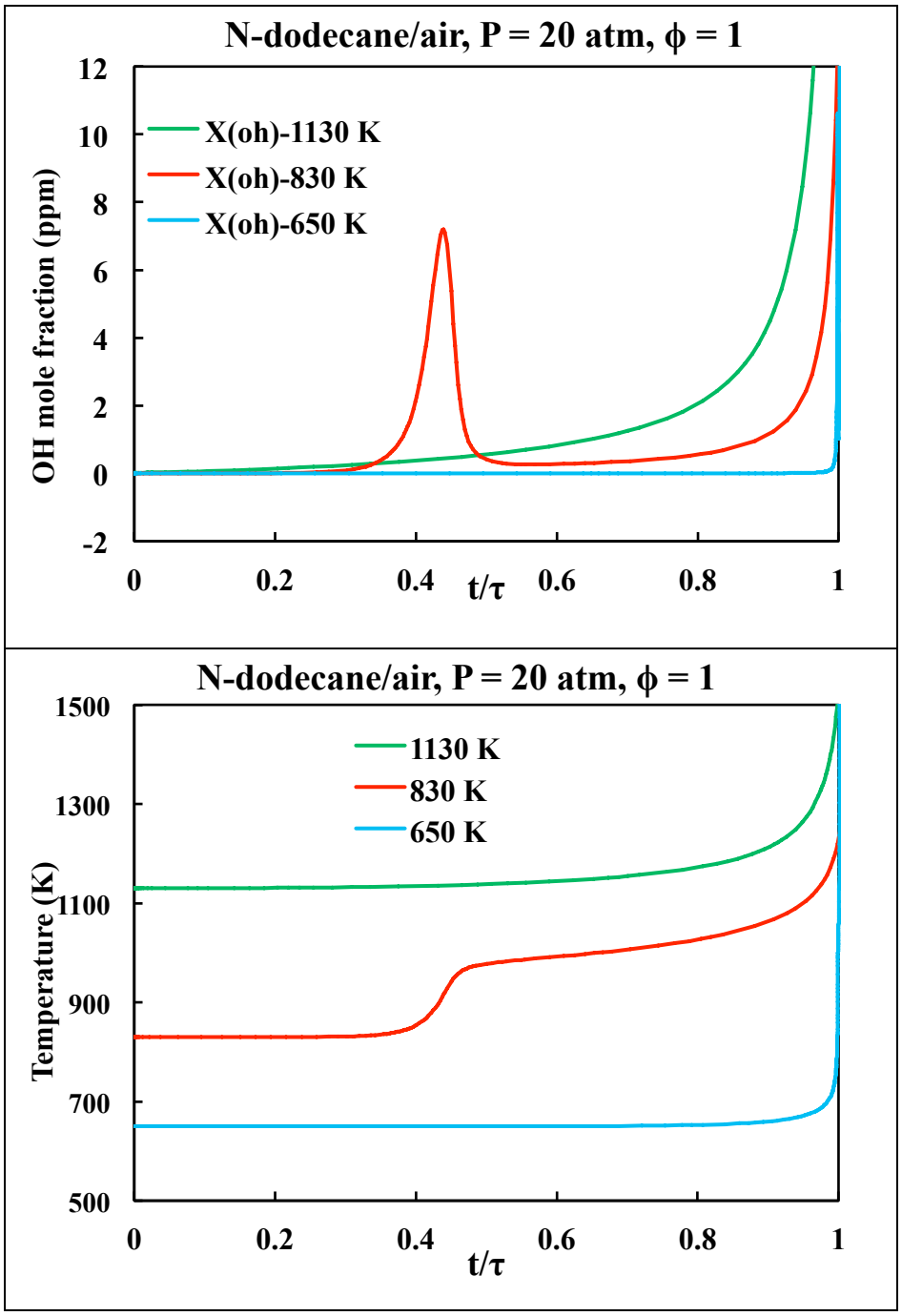
N-dodecane/air, P = 20 atm, ϕ = 1
OH mole fraction (ppm)
12
10
8
6
4
2
0
-2
X(oh)-1130 K
X(oh)-830 K
X(oh)-650 K
0
0.2
0.4
t/τ
0.6
0.8
1
N-dodecane/air, P = 20 atm, ϕ = 1
Temperature (K)
1500
1300
1100
900
700
500
1130 K
830 K
650 K
0
0.2
0.4
t/τ
0.6
0.8
1

Figure 25

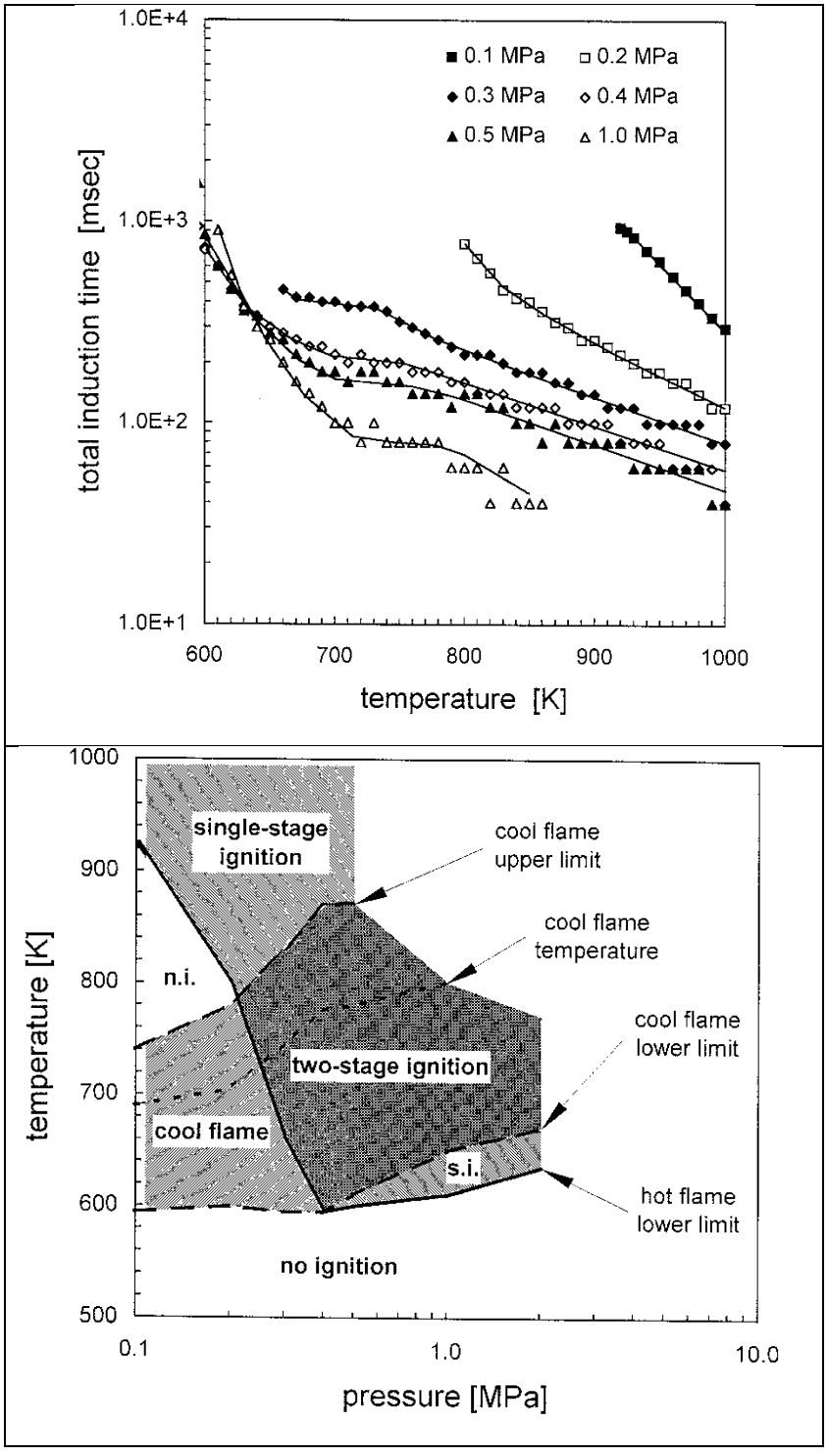
1.0E+4
1.0E+3
1.0E+2
1.0E+1
total induction time [msec]
0.1 MPa
0.2 MPa
0.3 MPa
0.4 MPa
0.5 MPa
1.0 MPa
600
700
800
900
1000
temperature [K]
1000
900
800
700
600
500
temperature [K]
single-stage ignition
cool flame upper limit
cool flame temperature
n.i.
cool flame lower limit
two-stage ignition
cool flame
s.i.
hot flame lower limit
no ignition
0.1
1.0
10.0
pressure [MPa]

Figure 26

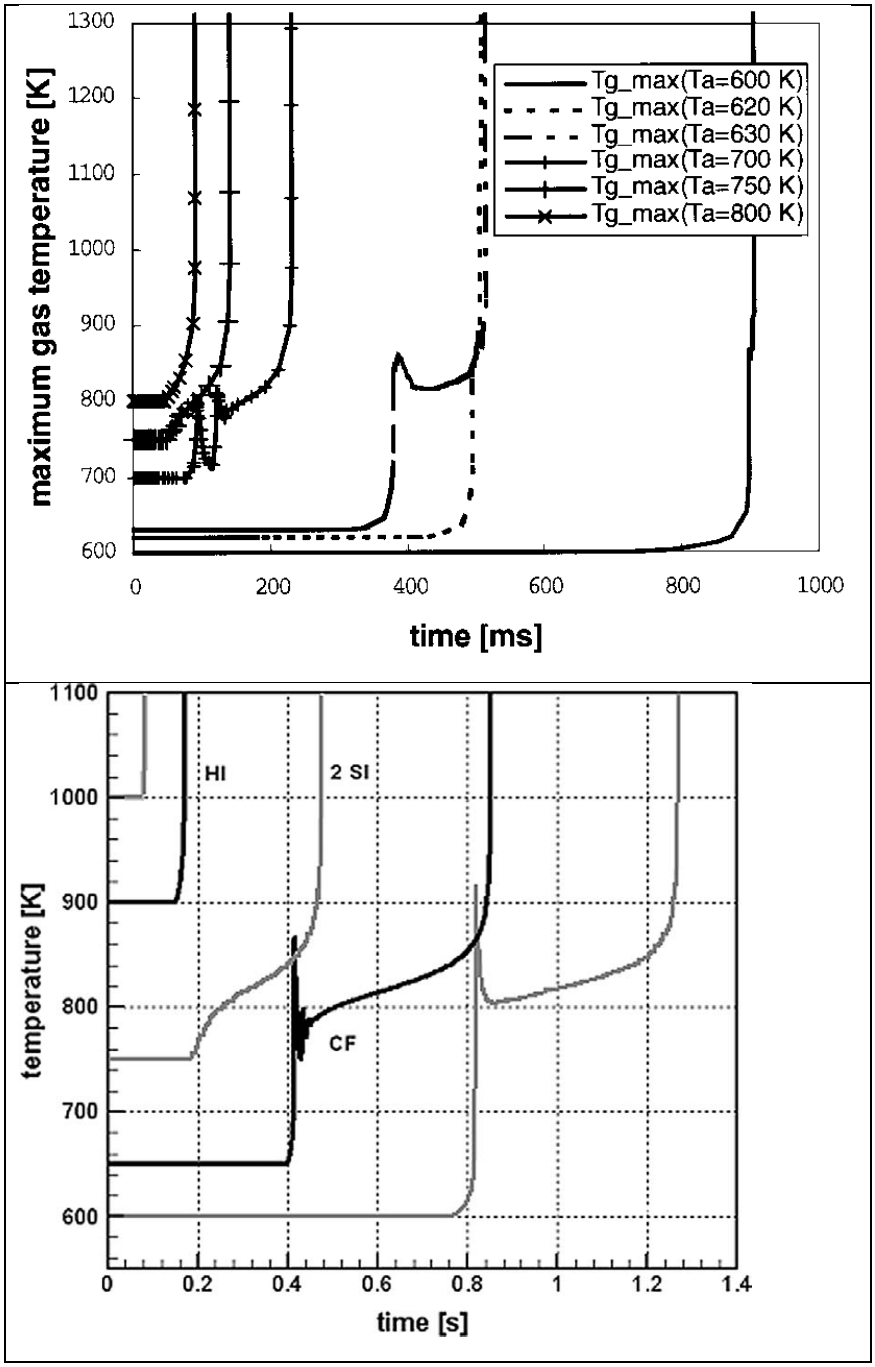
maximum gas temperature [K]
time [ms]
Tg_max(Ta=600 K)
Tg_max(Ta=620 K)
Tg_max(Ta=630 K)
Tg_max(Ta=700 K)
Tg_max(Ta=750 K)
Tg_max(Ta=800 K)
temperature [K]
time [s]
HI
2 SI
CF

Figure 27

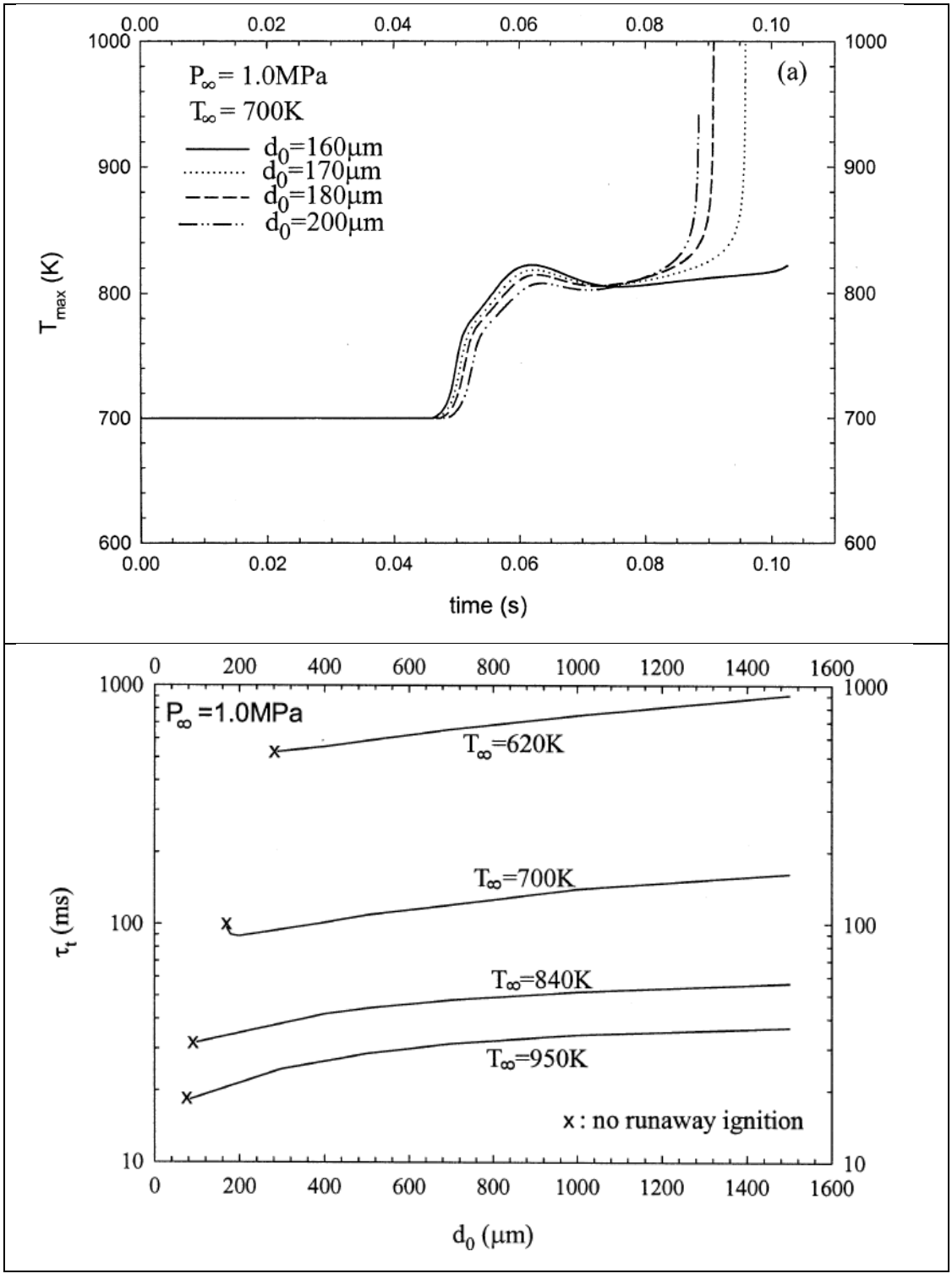
P∞= 1.0MPa
T∞= 700K
d0=160μm
d0=170μm
d0=180μm
d0=200μm
(a)
Tmax (K)
time (s)
P∞ =1.0MPa
T∞=620K
T∞=700K
T∞=840K
T∞=950K
x : no runaway ignition
τt (ms)
d0 (μm)

Figure 28

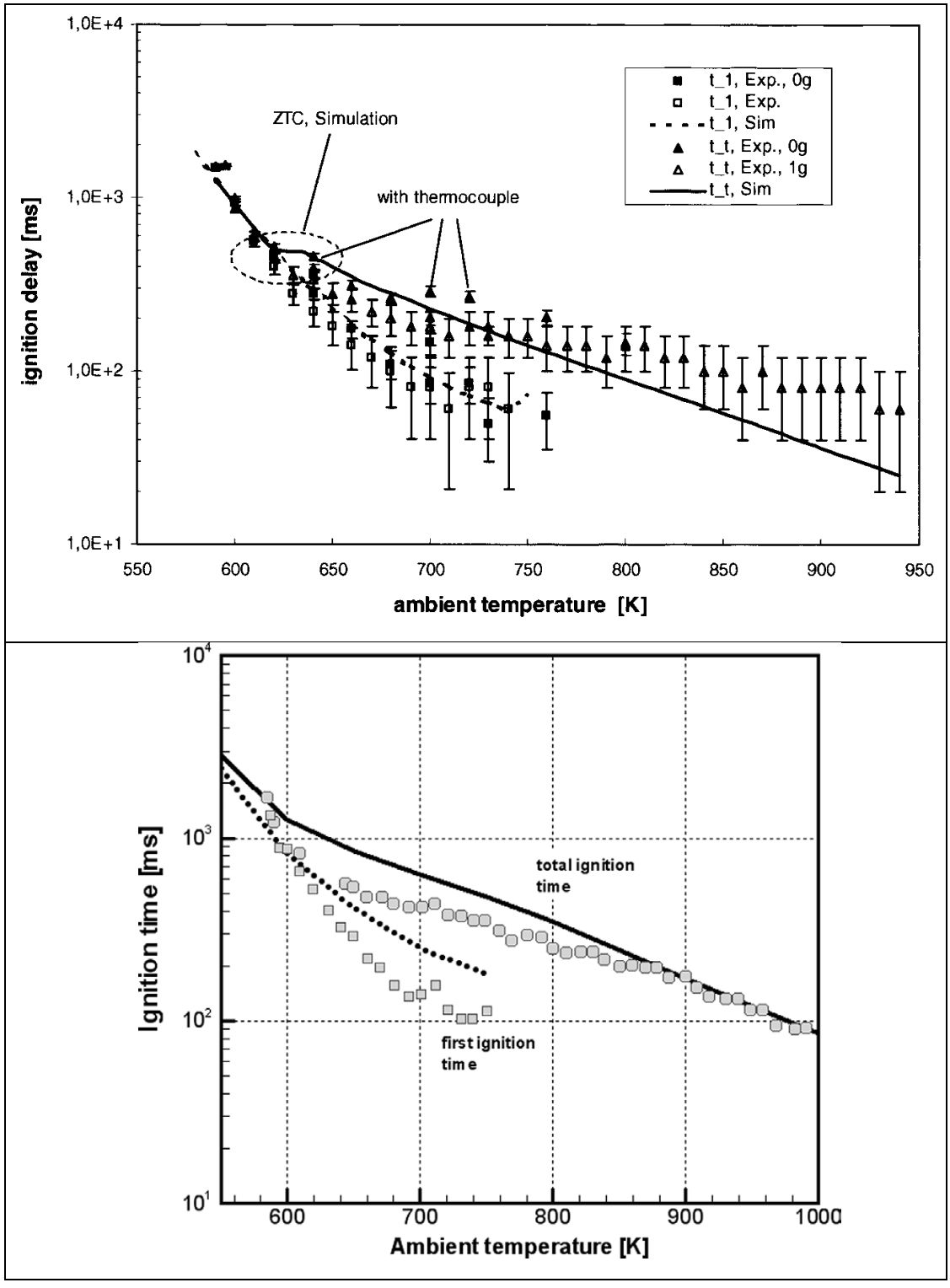
1,0E+4
1,0E+3
1,0E+2
1,0E+1
ignition delay [ms]
ZTC, Simulation
with thermocouple
t_1, Exp., 0g
t_1, Exp.
t_1, Sim
t_t, Exp., 0g
t_t, Exp., 1g
t_t, Sim
550
600
650
700
750
800
850
900
950
ambient temperature [K]
10^4
10^3
10^2
10^1
Ignition time [ms]
total ignition time
first ignition time
600
700
800
900
1000
Ambient temperature [K]

Figure 29

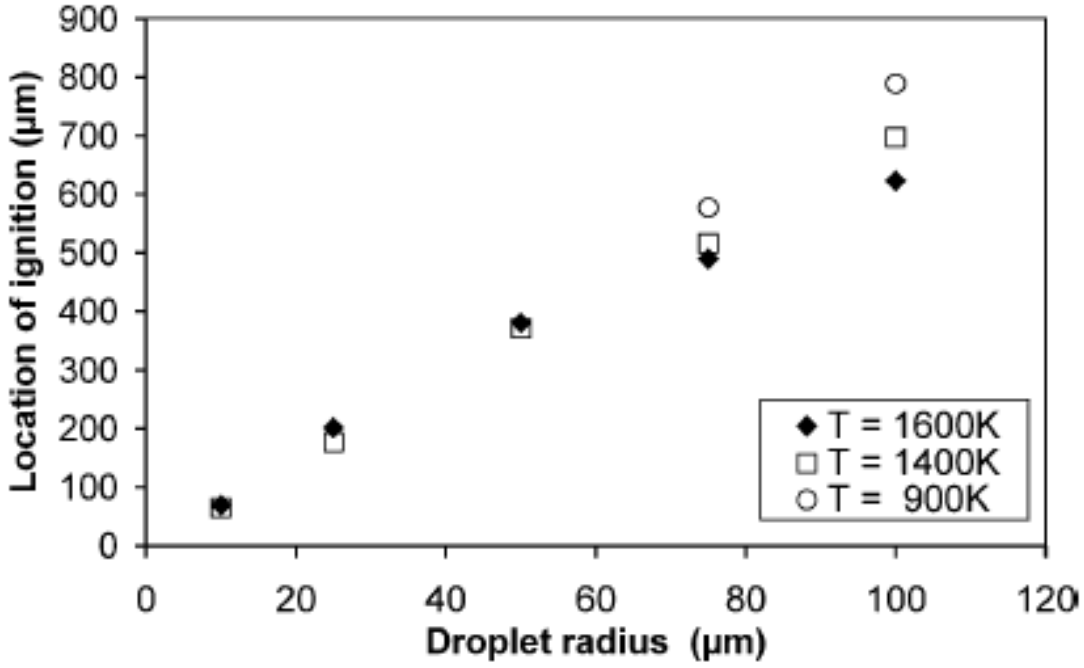
Location of ignition (μm)
900
800
700
600
500
400
300
200
100
0
0
20
40
60
80
100
120
Droplet radius (μm)
T = 1600K
T = 1400K
T = 900K

Figure 30

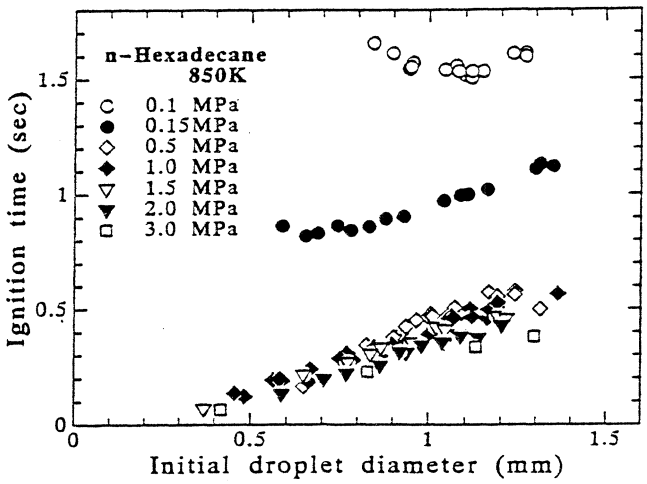
n-Hexadecane
850K
0.1 MPa
0.15MPa
0.5 MPa
1.0 MPa
1.5 MPa
2.0 MPa
3.0 MPa
Ignition time (sec)
Initial droplet diameter (mm)
0
0.5
1
1.5

Figure 31

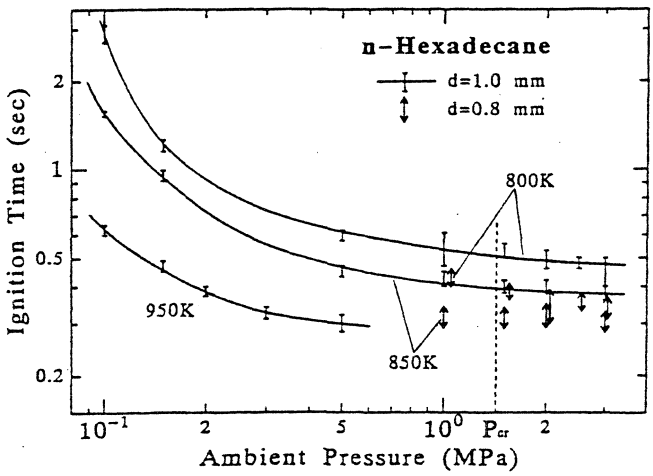
n-Hexadecane
d=1.0 mm
d=0.8 mm
800K
950K
850K
Ignition Time (sec)
2
1
0.5
0.2
10^{-1}
2
5
10^{0}
P_{cr}
2
Ambient Pressure (MPa)

Figure 32

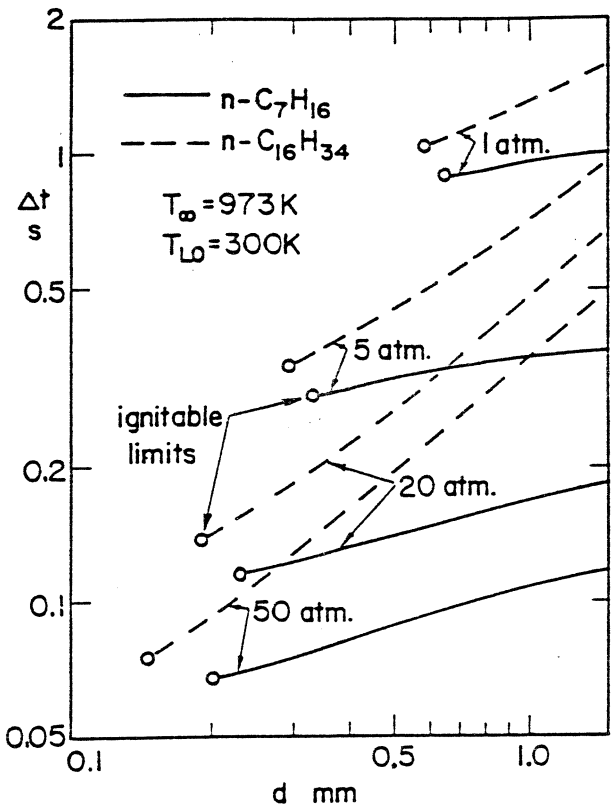
2
1
0.5
0.2
0.1
0.05
Δt
s
n-C7H16
n-C16H34
T∞=973K
TLO=300K
1 atm.
5 atm.
ignitable
limits
20 atm.
50 atm.
0.1
0.5
1.0
d mm

Figure 33

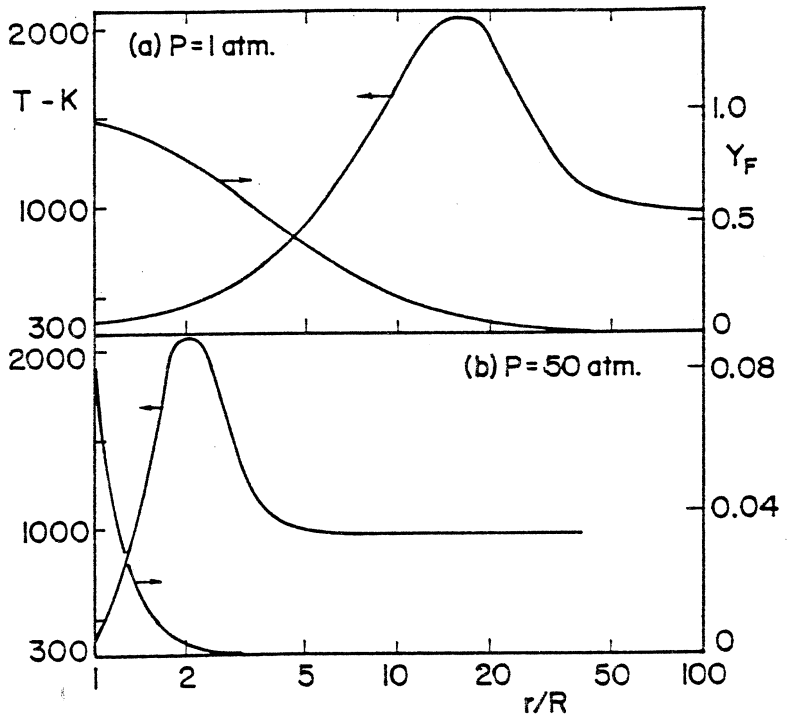
(a) P = 1 atm.
(b) P = 50 atm.
T - K
2000
1000
300
1.0
0.5
0
Y_F
0.08
0.04
0
1
2
5
10
20
50
100
r/R

Figure 34

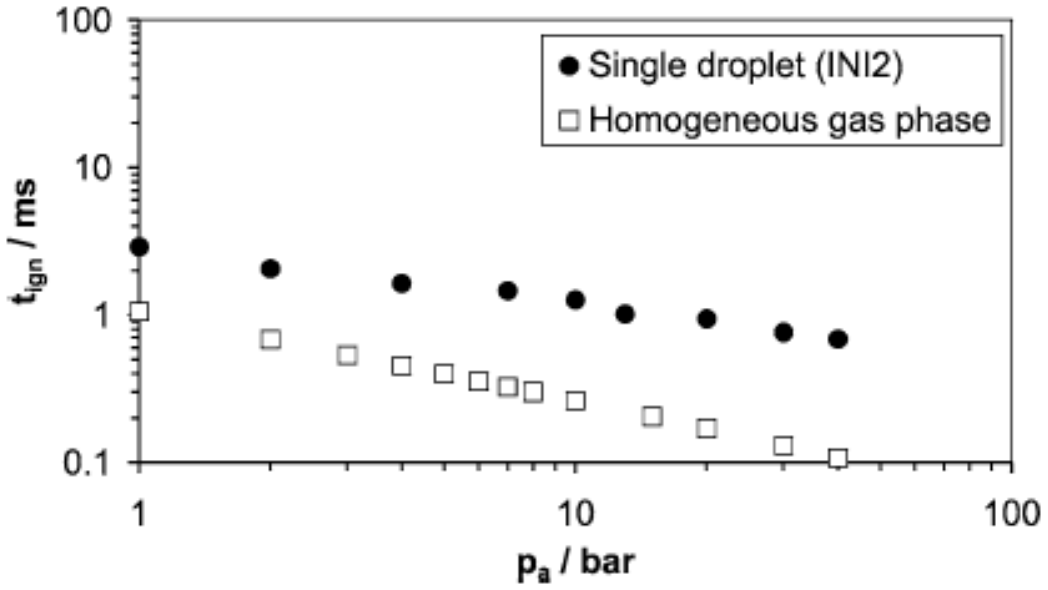
100
10
1
0.1
t_{ign} / ms
1
10
100
p_a / bar
Single droplet (INI2)
Homogeneous gas phase

Figure 35

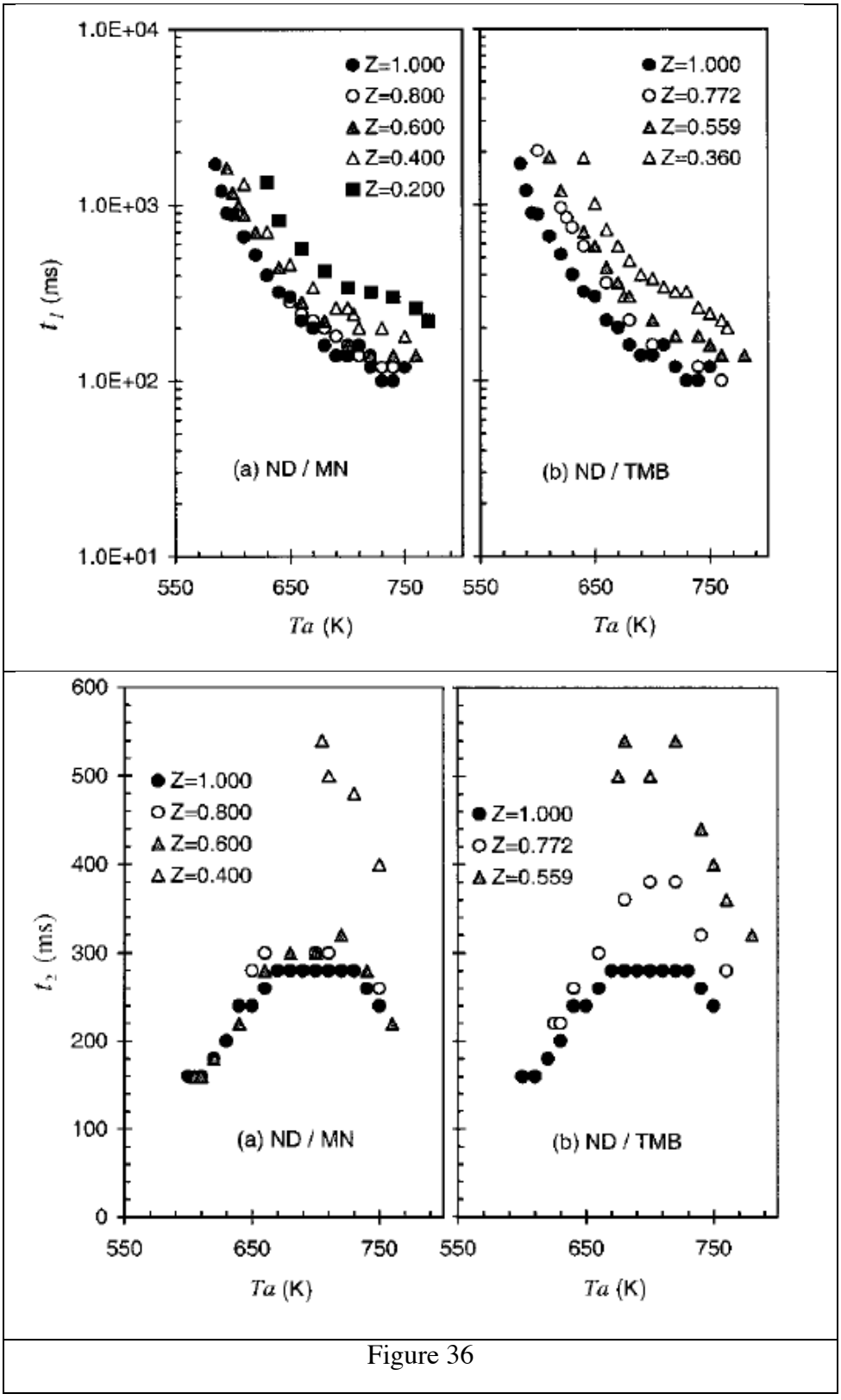
1.0E+04
1.0E+03
1.0E+02
1.0E+01
t_1 (ms)
Z=1.000
Z=0.800
Z=0.600
Z=0.400
Z=0.200
(a) ND / MN
Z=1.000
Z=0.772
Z=0.559
Z=0.360
(b) ND / TMB
550
650
750
Ta (K)
600
500
400
300
200
100
0
t_2 (ms)
Z=1.000
Z=0.800
Z=0.600
Z=0.400
(a) ND / MN
Z=1.000
Z=0.772
Z=0.559
(b) ND / TMB
550
650
750
Ta (K)

Figure 36

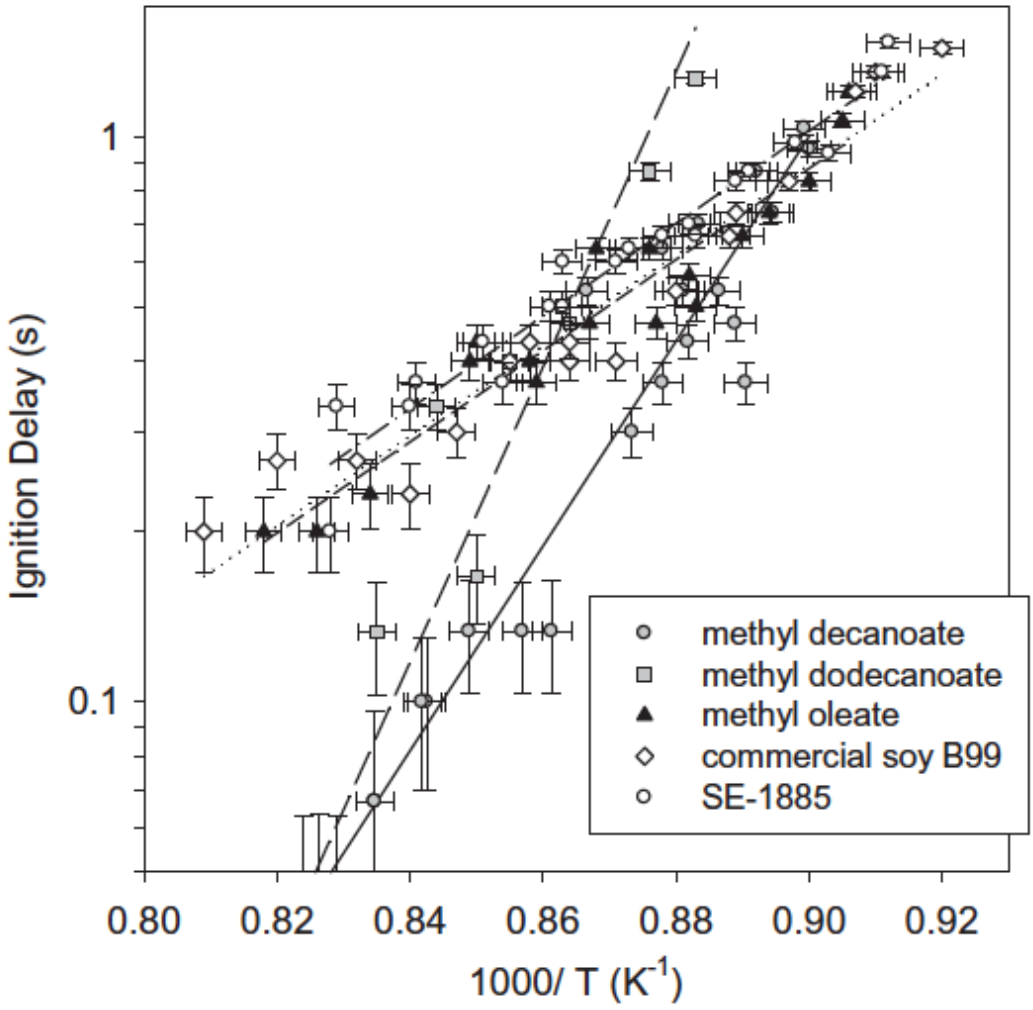
Ignition Delay (s)
1
0.1
0.80
0.82
0.84
0.86
0.88
0.90
0.92
1000/ T (K-1)
methyl decanoate
methyl dodecanoate
methyl oleate
commercial soy B99
SE-1885

Figure 37

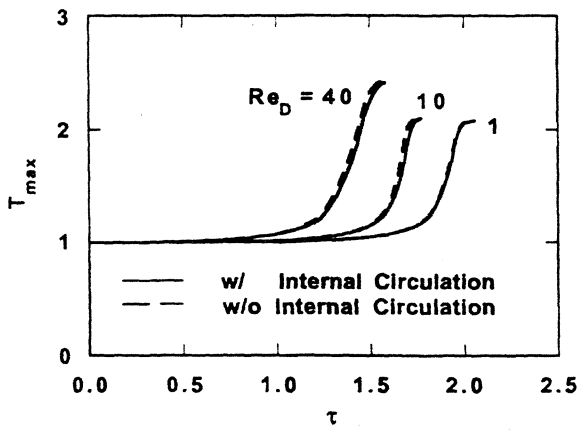
3
2
1
0
T_{max}
Re_D = 40
10
1
w/ Internal Circulation
w/o Internal Circulation
0.0
0.5
1.0
1.5
2.0
2.5
τ

Figure 38

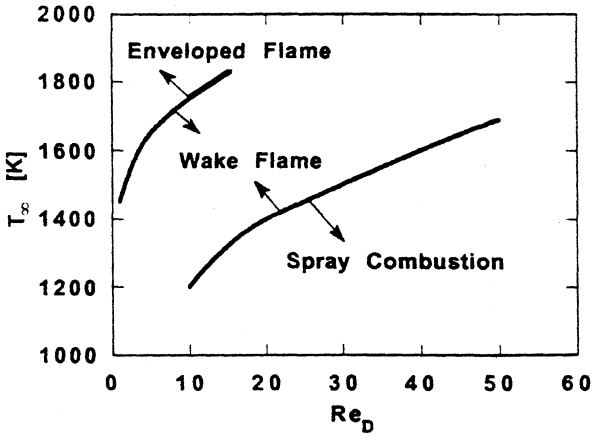
2000
1800
1600
1400
1200
1000
T_∞ [K]
Enveloped Flame
Wake Flame
Spray Combustion
0
10
20
30
40
50
60
Re_D

Figure 39

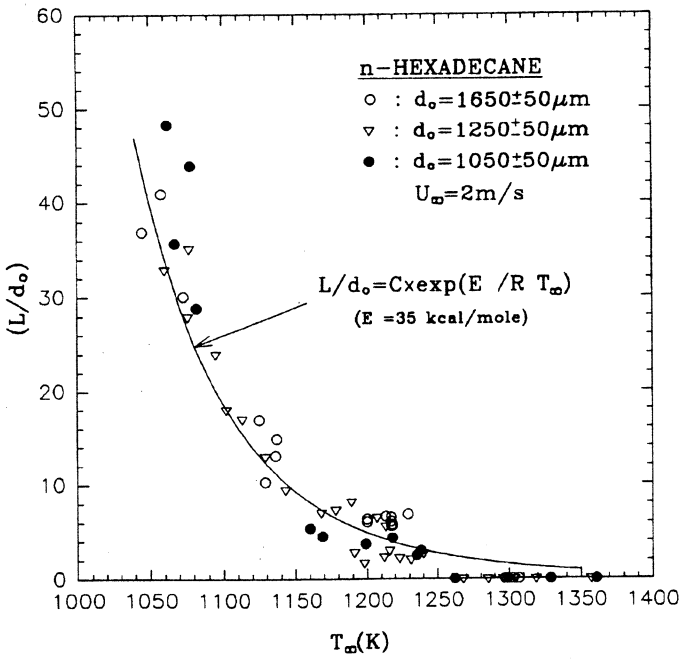
n-HEXADECANE
○ : d_o=1650±50μm
▽ : d_o=1250±50μm
● : d_o=1050±50μm
U_∞=2m/s
$L/d_o=C\times\exp(E/R\,T_\infty)$
(E =35 kcal/mole)
(L/d_o)
T_∞(K)
0
10
20
30
40
50
60
1000
1050
1100
1150
1200
1250
1300
1350
1400

Figure 40

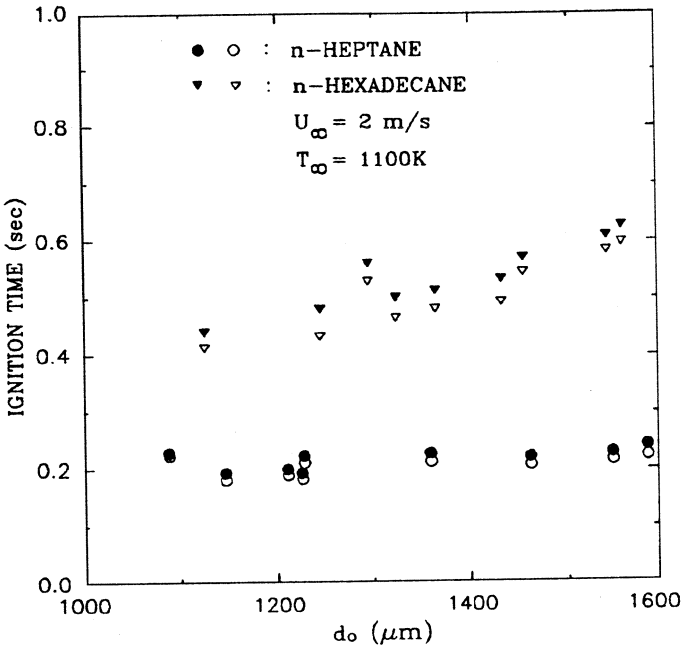
1.0
0.8
0.6
0.4
0.2
0.0
IGNITION TIME (sec)
1000
1200
1400
1600
d_o (μm)
● ○ : n−HEPTANE
▼ ▽ : n−HEXADECANE
U_∞ = 2 m/s
T_∞ = 1100K

Figure 41

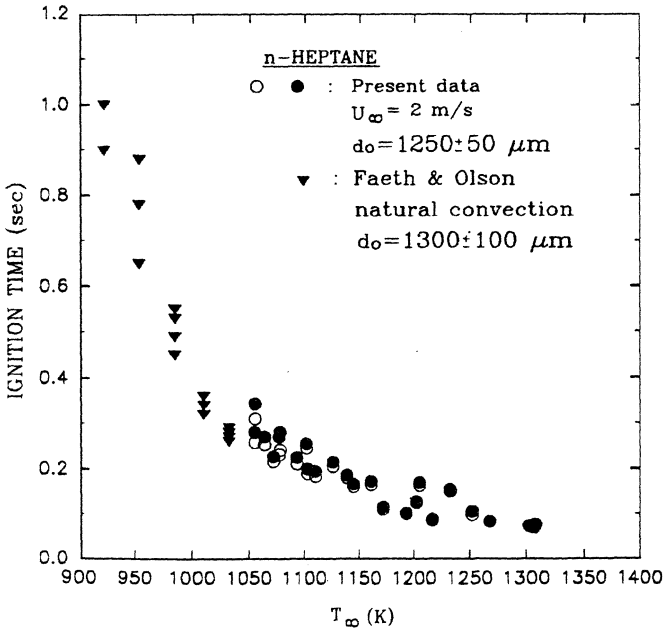
n-HEPTANE
○ ● : Present data
U_∞ = 2 m/s
d_o=1250±50 μm
▼ : Faeth & Olson
natural convection
d_o=1300±100 μm
IGNITION TIME (sec)
T_∞ (K)
0.0
0.2
0.4
0.6
0.8
1.0
1.2
900
950
1000
1050
1100
1150
1200
1250
1300
1350
1400

Figure 42

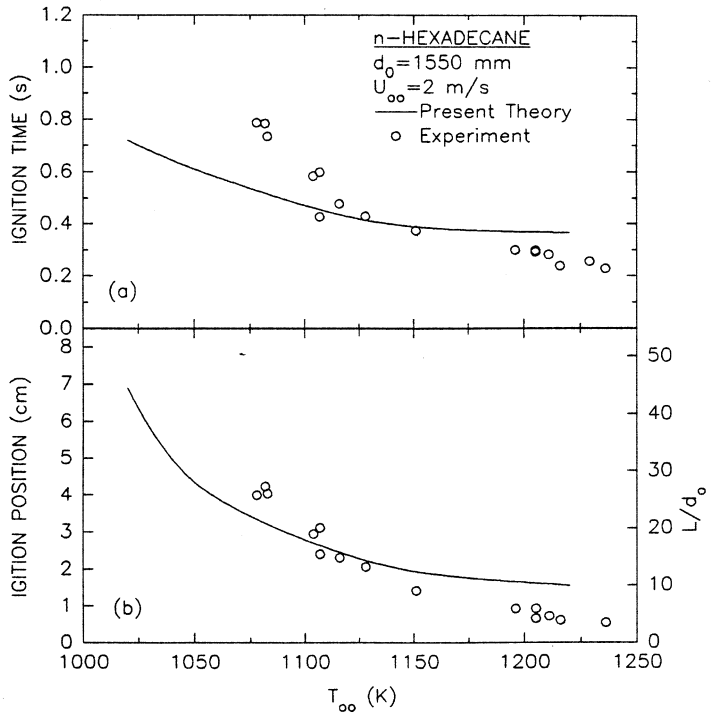
n–HEXADECANE
d_0=1550 mm
U_∞=2 m/s
Present Theory
Experiment
IGNITION TIME (s)
(a)
IGITION POSITION (cm)
(b)
L/d_o
T_∞ (K)

Figure 43

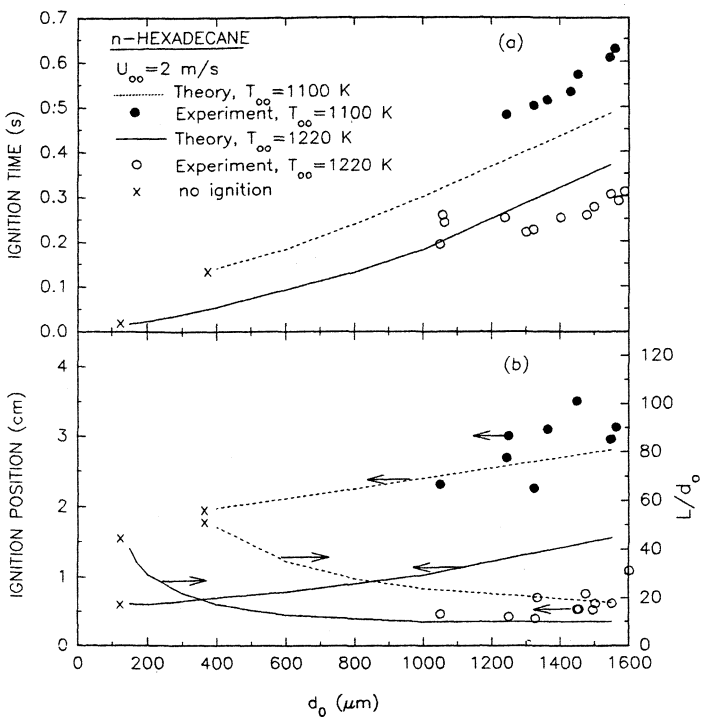
n-HEXADECANE
U_{∞}=2 m/s
Theory, T_{∞}=1100 K
Experiment, T_{∞}=1100 K
Theory, T_{∞}=1220 K
Experiment, T_{∞}=1220 K
no ignition
(a)
(b)
IGNITION TIME (s)
IGNITION POSITION (cm)
L/d_o
d_0 (μm)
0.0
0.1
0.2
0.3
0.4
0.5
0.6
0.7
0
1
2
3
4
0
20
40
60
80
100
120
0
200
400
600
800
1000
1200
1400
1600

Figure 44

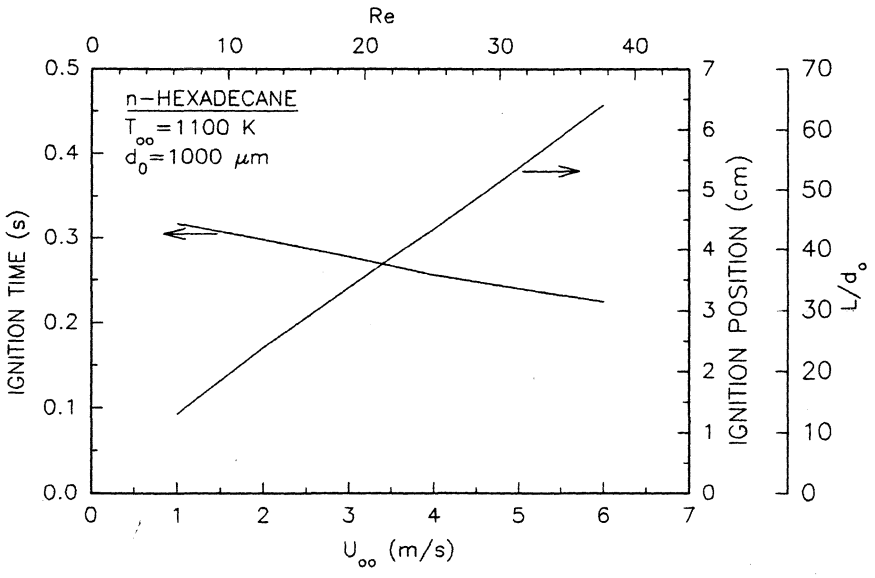
Re
0
10
20
30
40
n-HEXADECANE
T_{oo}=1100 K
d_0=1000 μm
IGNITION TIME (s)
0.0
0.1
0.2
0.3
0.4
0.5
IGNITION POSITION (cm)
0
1
2
3
4
5
6
7
L/d_o
0
10
20
30
40
50
60
70
U_{oo} (m/s)
0
1
2
3
4
5
6
7

Figure 45

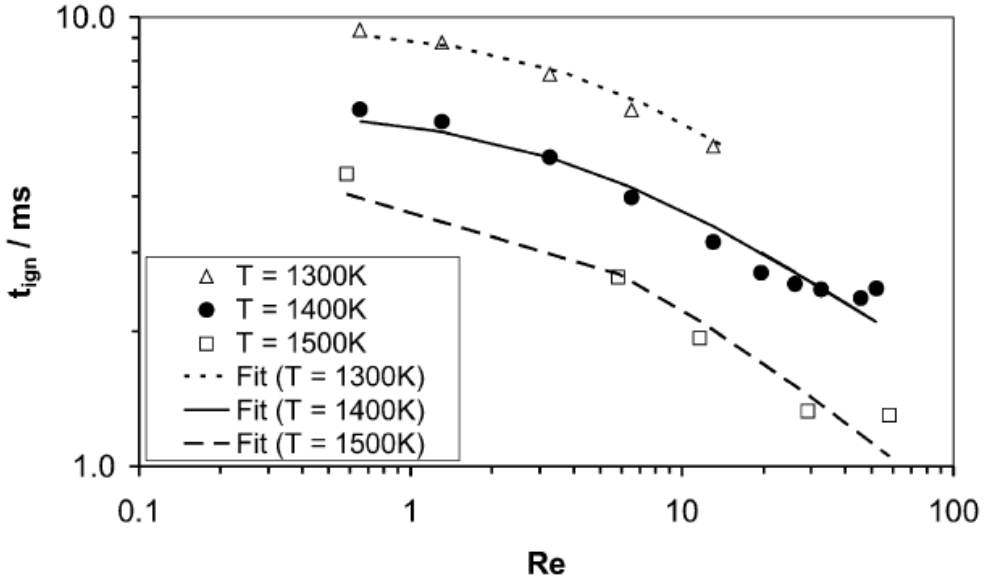
10.0
1.0
t_{ign} / ms
0.1
1
10
100
Re
T = 1300K
T = 1400K
T = 1500K
Fit (T = 1300K)
Fit (T = 1400K)
Fit (T = 1500K)

Figure 46

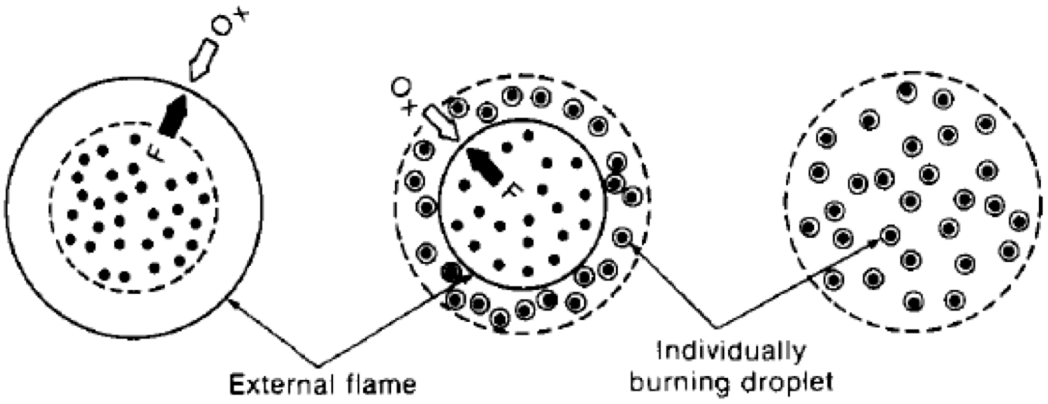

G>>1 G≈1 G<<1

Figure 47